ABSTRACT

Title of Dissertation: QUANTIFYING VARIABILITY OF BLACK CARBON TRANSPORT FROM CROPLAND BURNING IN RUSSIA TO THE ARCTIC DRIVEN BY ATMOSPHERIC BLOCKING EVENTS

Joanne V. Hall, Doctor of Philosophy, 2017

Dissertation directed by: Tatiana V. Loboda, Associate Professor, Department of Geographical Sciences

Short lived aerosols and pollutants transported from northern mid-latitudes have amplified the short term warming in the Arctic region. Specifically, black carbon is recognized as the second most important human emission in regards to climate forcing, behind carbon dioxide with a total climate forcing of $+1.1 Wm^{-2}$. Studies have suggested that cropland burning may be a large contributor to the black carbon emissions which are directly deposited on the snow in the Arctic region. However, accurate monitoring of cropland burning from existing active fire and burned area products is limited, thereby leading to an underestimation in black carbon emissions from cropland burning. This dissertation focuses on 1) assessing the potential for the deposition of hypothetical black carbon emissions from known cropland burning in Russia through low-level transport, and 2) identifying a possible

atmospheric pattern that may enhance the transport of black carbon emissions to the Arctic. Specifically, atmospheric blocking events present a potential mechanism that could act to enhance the likelihood of transport or accelerate the transport of pollutants to the snow-covered Arctic from Russian cropland burning based on their persistent wind patterns.

This research study confirmed the importance of Russian cropland burning as a potential source of black carbon deposition on the Arctic snow in the spring despite the low injection heights associated with cropland burning. Based on the successful transport pathways, this study identified the potential transport of black carbon from Russian cropland burning beyond 80°N which has important implications for permanent sea ice cover. Further, based on the persistent wind patterns of blocking events, this study identified that blocking events are able to accelerate potential transport and increase the success of transport of black carbon emissions to the snow-covered Arctic during spring when the impact on the snow/ice albedo is at its highest. The enhanced transport of black carbon has important implications for the efficacy of deposited black carbon. Therefore, understanding these relationships could lead to possible mitigation strategies for reducing the impact of deposition of black carbon from crop residue burning in the Arctic.

QUANTIFYING VARIABILITY OF BLACK CARBON TRANSPORT FROM CROPLAND BURNING IN RUSSIA TO THE ARCTIC DRIVEN BY ATMOSPHERIC BLOCKING EVENTS

by

Joanne V. Hall

Dissertation submitted to the Faculty of the Graduate School of the
University of Maryland, College Park, in partial fulfillment
of the requirements for the degree of
Doctor of Philosophy
2017

Advisory Committee:
Professor Tatiana Loboda, Chair
Professor Christopher Justice
Professor Michael Kearney
Professor Louis Giglio
Dr. Gregory McCarty

Dedication

To my loving family,

Without whom none of my success would be possible

Acknowledgements

First and foremost, I would like to thank my advisor Dr. Tatiana Loboda. Thank you for allowing me to achieve my dream. Your support and guidance has helped shape me into the researcher and person I am today. Thank you for all the opportunities you have afforded me over the course of my dissertation, but most importantly, thank you for believing in me.

I am equally grateful for the mentorship and encouragement provided by the members of my advisory committee – Dr. Louis Giglio, Dr. Gregory McCarty and Dr. Chris Justice. I am thankful to Dr. Louis Giglio for all his advice, support, and occasional laughter during the development of CRAB. I am also thankful to Dr. Gregory McCarty for providing the unique opportunities afforded to me throughout my time at the USDA. Also, thank you to Dr. Christopher Justice for all your support throughout this dissertation. And finally, I would like to thank Dr. Michael Kearney for agreeing to serve as my dean's representative.

I would also like to extend my deepest thanks to my friends and family. Thank you for supporting me through this journey. Finally, I owe my greatest thanks to my husband, Matthew. Without you, none of this would have been possible.

Table of Contents

Dedication ii
Acknowledgements iii
Table of Contents iv
List of Tables vi
List of Figures viii
List of Abbreviations xiv
Chapter 1: Introduction 1
1.1: Background and Motivation 1
1.2: Research Questions 10
1.3: Organization of the study 12
Chapter 2: A MODIS-based burned area assessment for Russian croplands: mapping requirements and challenges 14
2.1: Introduction 14
2.2: Visual assessment of fire practice in Russian croplands from VHR imagery 18
2.2.1: Archive development of field samples under various post-harvest conditions (burn, bare, standing crop residue, plowed) from VHR imagery 21
2.2.2: Visual examination of burn strategies identified in VHR imagery 25
2.2.3: Methodology for the development of post-harvest field condition archive 26
2.3: Data and Methods 28
2.3.1: Clear surface analysis 30
2.3.2: Multi-sensor clear surface composite 31
2.3.3: Burned area map and confidence level development 35
2.4: Results and Discussion 39
2.4.1: Accuracy Assessment 39
2.4.2: CRAB Analysis 41
2.4.3: Intercomparison between CRAB, MCD45A1, and MCD64A1 44
2.5: Challenges of Mapping 47
2.6: Conclusion 51
Chapter 3: Quantifying the potential for low-level transport of black carbon emissions from cropland burning in Russia to the snow-covered Arctic 53
3.1: Introduction 53
3.2: Data 59
3.3: Methods 61
3.3.1: Arctic snow cover extent 61
3.3.2: Cropland burning source locations 64
3.3.3: Transport algorithm development 64
3.4: Results 67
3.4.1: Successful transport flow patterns 67
3.4.2: *Northern reaches of Russian cropland burning emission transport* 73
3.4.3: Spatial patterns of BC transport to the Arctic snow 77
3.5: Discussion 84
3.5.1: Sources of uncertainty 84
3.5.2: Comparison with previous studies 86

3.5.3: Significance of BC deposition from cropland burning on the Arctic snow 90
3.6: Conclusion 92
Chapter 4: Quantifying the variability of potential black carbon transport from cropland burning in Russia driven by atmospheric blocking events 94
4.1: Introduction 94
4.2: Data and Methods 99
4.2.1: Low-level transport model data 99
4.2.2: Atmospheric Blocking Index 100
4.2.3: Development of daily atmospheric blocking layers 101
4.3: Results 104
4.3.1: Atmospheric Blocking Index 104
4.3.2: Cropland Burning and Atmospheric Blocking Events 108
4.3.3: Transport patterns under blocked and nonblocked conditions 110
4.3.4: Latitudinal variability 120
4.4: Discussion 127
4.4.1: Atmospheric Blocking Index uncertainty 127
4.4.2: Atmospheric Blocking Events: implications for cropland emission transport to the Arctic snow 128
4.5: Conclusion 129
Chapter 5: Conclusion 131
5.1: Major research findings 131
5.2: Contribution of this research to the broader Arctic science agenda and policy implications 135
5.2.1: Broader Arctic science agenda 135
5.2.2: Policy implications 138
5.3: Future research directions 140
Appendices 144
Bibliography 158

List of Tables

Chapter 2:

Table 2.1: Distribution of burn and non-burn samples digitized from very high resolution (< 5 m) imagery. Values in parentheses are approximate equivalent MODIS 500 m grid cells based on the size of the samples in hectares.

Table 2.2: Very high resolution (< 5 m) spring and summer samples matched to MODIS 500 m grid cells.

Table 2.3: CRAB burned area classification rules (A – G) for spring and (A2) for summer. A field is classified as burned if it satisfies each condition in any of the classification rules.

Table 2.4: Spring and summer accuracy assessment comparison between the Cropland Regional Area Burned (CRAB) product and the two official MODIS burned area products MCD45A1 and MCD64A1. The spring assessment was carried out using the full range of CRAB confidence values and greater than 60% confidence.

Table 2.5: Spring cropland burned area (units: $\times 10^4$ km^2 = Mha) comparison between CRAB, MCD45A1 and MCD64A1.

Table 2.6: Summer cropland burned area (units: $\times 10^4$ km^2 = Mha) comparison between CRAB, MCD45A1 and MCD64A1.

Chapter 3:

Table 3.1: Monthly average (2003 – 2015) successfully transported and total active fire counts within the Russian cropland.

Chapter 4:

Table 4.1: Monthly average transport time (μ, hours) and associated n value (n) between 2003 and 2015 under blocked (B and nonblocked (NB) conditions for all injection heights.

Table 4.2: Monthly average success rate (μ, %) and associated n value (n) between 2003 and 2015 under blocked (B and nonblocked (NB) conditions for all injection heights.

Table 4.3: Welch's two-sided t-test results comparing the difference in the mean transport time (hours) under blocked and nonblocked conditions for all injection heights (pressure levels). P values: < 0.05 (blue); < 0.1 (green); > 0.1 (grey; null hypothesis accepted). The dashes (-) indicate there was either no data for either one or both scenarios.

Table 4.4: Difference in mean transport time to the snow-covered Arctic. Negative values indicate transport to the snow-covered Arctic was on average quicker under blocking conditions, whereas the positive values indicate nonblocked conditions were quicker.

List of Figures

Chapter 1:

Figure 1.1: Average monthly MODIS active fire counts (2003 – 2015) within grassland, shrubland, forest and cropland as defined by the International Geosphere-Biosphere Programme (IGBP) land cover type data layer (MCD12Q1; Friedl et al., 2010).

Figure 1.2: Russian cropland area as defined by the IGBP cropland/ natural vegetation mosaic.

Figure 1.3: Flow diagram illustrating the major outcomes for the three phases of the doctoral research project.

Chapter 2:

Figure 2.1: Very high resolution (< 5 m) field state examples: burned field (a), residue field (b), freshly plowed field (c) and bare field (d). Images are displayed using the true color composite.

Figure 2.2: MODIS active fire (MCD14ML; Giglio et al., 2003) counts within the Russian cropland area as defined by the crop mask (see Figure 2.3) between 2003 and 2012.

Figure 2.3: Very high resolution (< 5 m) samples (2003 – 2012) acquired from DigitalGlobe's high resolution commercial satellites, QuickBird and World View-2 overlaid over the Russian cropland.

Figure 2.4: Burn sample area (above) and field area (below) frequency distributions and cumulative area ($\times 10^3$ ha) for all VHR polygon samples before the matching process. The vertical dashed line indicates a change in area size categories along the horizontal axis.

Figure 2.5: Visual burning practices found in available very high resolution (< 5 m) imagery: complete field burn (a), partial field burn (b), partial field burn (c), and pile burn (d).

Figure 2.6: Cropland Regional Area Burned pre-algorithm development and methodological framework.

Figure 2.7: Solar (Ts, As) and sensor (Tv, Av) azimuthal and zenith angles for Terra and Aqua over 16 – 19 August 2006. The verified active burn occurred on 17 August 2006. The zenith angles are represented by the radius of the black line. Zenith angles scaled between 0° and 50° for visualization. The near infrared reflectance (NIR) values are located in the lower right boxes.

Figure 2.8: Methodological framework for the combination of Aqua and Terra clear surface datasets into one BRDF adjusted time series.

Figure 2.9: Summer 2012 CRAB product output. A subset of Russia (red circle, top insert) is shown for display purposes. Colors represent Julian Date of burn. Grey area denotes the Russian crop mask.

Figure 2.10: Temporal distribution of the average fractional burned area by month between 2003 and 2012 for the Russian cropland region partitioned by Federal Districts (okrugs).

Figure 2.11: Daily burned area (km^2) left axis and MODIS active fire counts right axis during spring 2012 for all Russian cropland MODIS tiles. All confidence values greater than 60% were included for the CRAB product.

Figure 2.12: Daily burned area (km^2) left axis and MODIS active fire counts right axis during summer 2005 for all Russian cropland MODIS tiles. All confidence values were included for the CRAB product.

Figure 2.13: Spring and summer cropland burned area (units: $\times 10^4$ km^2 = Mha) comparison between CRAB (all confidence in fall and > 60% confidence in spring), MCD45A1 and MCD64A1.

Figure 2.14: Mean number of cropland clear surface days per year between 1 March and 30 September (2003 and 2012) as defined by the 1 km MODIS quality assessment bit thresholds as set out in Section 2.3.1. This image corresponds to the combined Aqua and Terra dataset for the Russian cropland region.

Figure 2.15: MODIS grid cell area masks (light grey squares) and field boundary area (dark grey shapes) overlay analysis.

Chapter 3:

Figure 3.1: Russian cropland area as defined by the IGBP cropland/ natural vegetation mosaic.

Figure 3.2: Directional criteria for the calculation of the following grid cell based on wind direction.

Figure 3.3: Transport trajectory line maps for successful events for October 2007 at five different pressure levels: 900mb (a); 925mb (b); 950mb (c); 975mb (d); 1000mb (e). For illustration purposes only October 2007 is shown, but the pattern is representative of the generally observed decrease in the number of successful events with shallower injection heights across all months and years.

Figure 3.4: 900mb (a) and 1000mb (b) October 2003 successful trajectories highlighting the curved pattern evident in 900mb maps.

Figure 3.5: 925mb monthly successful trajectory counts (2003 – 2015).

Figure 3.6: Monthly snow extent maps. The values represent the number of years each 0.75° grid cell contained snow between 2003 and 2015.

Figure 3.7: Total number of successful events (monthly) between 2003 and 2015 that reach snow cover between 60° – 65°N (a), 65° – 70°N (b), 70° – 75°N (c), 75° – 80°N (d), 80° – 90°N (e) as their northern-most extent per pressure level. The inset table represents the contribution from the lower latitude bands (40° – 45°N, 45° – 50°N, 50° – 55°N, 55° – 60°N) for March, April and May.

Figure 3.8: 900mb (a) and 1000mb (b) March 2003 – 2015 average transport (hours), percent successful and active fires potentially contributing to BC deposition on snow in the Arctic. The grey color in the percent successful maps (middle) represents the starting fire locations which were unsuccessful at reaching the snow in the Arctic within 96 hours.

Figure 3.9: 900mb (a) and 1000mb (b) April 2003 – 2015 average transport (hours), percent successful and active fires potentially contributing to BC deposition on snow in the Arctic. The grey color in the percent successful maps (middle) represents the starting fire locations which were unsuccessful at reaching the snow in the Arctic within 96 hours.

Figure 3.10: 900mb (a) and 1000mb (b) May 2003 – 2015 average transport (hours), percent successful and active fires potentially contributing to BC deposition on snow in the Arctic. The grey color in the percent successful maps (middle) represents the starting fire locations which were unsuccessful at reaching the snow in the Arctic within 96 hours.

Figure 3.11: USFS AirFire Arctic Potential Transport Climatology maps (data source: https://www.airfire.org/data/arctic-transport-clim/). The figure was generated by the author using the USFS AirFire online data analysis system.

Chapter 4:

Figure 4.1: (a) Average wind direction (arrows) and MODIS active fire (MCD14ML; red points) cropland fires and (b) Aerosol Optical Depth (MOD08; Hubanks et al., 2008) between 25th July and 10th August 2010. The persistent anticyclonic wind pattern transported the emissions from the southern regions of European Russia and pooled them over Moscow and surrounding regions. (Aerosol Optical Depth data source: Giovanni, 2013).

Figure 4.2: Illustration representing the selection of a pure blocked grid cell (A) and a pure nonblocked grid cell (B). The two mixed scenarios (C and D) are also represented. Hypothetical blocking events (grey) are shown over a five day period.

Figure 4.3: Monthly counts of weak, moderate and strong blocking events between 2003 and 2015.

Figure 4.4: Monthly counts of blocking events duration between 2003 and 2015.

Figure 4.5: Total monthly count (grey) and March, April and May (yellow, blue, and green respectively) between 2003 and 2015 for all blocking events. Blocking events are defined sharply at different longitudes causing the observed exaggerated effect on this graph.

Figure 4.6: Monthly active fire detections normalized by cropland area and number of days under blocked (a) and nonblocked (b) conditions between March and November (2003 – 2015). The data was normalized to account for the larger number of nonblocked grid cells.

Figure 4.7: 900mb March 2003 – 2015: The average transport time (top), percent success (middle) and successful active fires (bottom) are highlighted for All Blocks (a), Nonblocks (b) and Difference (c) maps. Only grid cells which contained values in both block and nonblock maps were differenced. The difference map color bars have been created so that red grid cells indicate transport under blocked conditions was either quicker, more successful or contained higher fire loads compared to the blue color indicating that transport was quicker, more successful or had higher fuel load under nonblocked conditions.

Figure 4.8: 900mb April 2003 – 2015: The average transport time (top), percent success (middle) and successful active fires (bottom) are highlighted for All Blocks (a), Nonblocks (b) and Difference (c) maps. Only grid cells which contained values in both block and nonblock maps were differenced. The difference map color bars have been created so that red grid cells indicate transport under blocked conditions was either quicker, more successful or contained higher fire loads compared to the blue color indicating that transport was quicker, more successful or had higher fuel load under nonblocked conditions.

Figure 4.9: 900mb May 2003 – 2015: The average transport time (top), percent success (middle) and successful active fires (bottom) are highlighted for All Blocks (a), Nonblocks (b) and Difference (c) maps. Only grid cells which contained values in both block and nonblock maps were differenced. The difference map color bars have been created so that red grid cells indicate transport under blocked conditions was either quicker, more successful or contained higher fire loads compared to the blue color indicating that transport was quicker, more successful or had higher fuel load under nonblocked conditions.

Figure 4.10: 900mb April 2006 blocking event transport time to the snow-covered Arctic within 96 hours of burning (a) and corresponding trajectories (b).

Figure 4.11: March average (2003 – 2015) transport time under blocked and nonblocked conditions at 900mb (a) and 1000mb (b) for latitude bands: 45° – 50°N, 50° – 55°N, and 55° – 60°N.

Figure 4.12: April average (2003 – 2015) transport time under blocked and nonblocked conditions at 900mb (a) and 1000mb (b) for latitude bands: 45° – 50°N, 50° – 55°N, and 55° – 60°N.

Figure 4.13: May average (2003 – 2015) transport time under blocked and nonblocked conditions at 900mb (a) and 1000mb (b) for latitude bands: 45° – 50°N, 50° – 55°N, and 55° – 60°N.

List of Abbreviations

ABoVE - Arctic-Boreal Vulnerability Experiment

AMAP - Arctic Monitoring and Assessment Programme

BC - Black carbon

BRDF - Bidirectional reflectance distribution function

CRAB - Cropland Regional Area Burned

GFED - Global Fire Emissions Database

GPH - Geopotential height

HYSPLIT - Hybrid Single Particle Lagrangian Integrated Trajectory

IGBP - International Geosphere-Biosphere Programme

MODIS - Moderate Resolution Imaging Spectroradiometer

NASA - National Aeronautics and Space Administration

NBR - Normalized Burn Ratio

NCEP/NCAR - National Centers for Environmental Prediction – National Center for Atmospheric Research Global Reanalysis

NDVI - Normalized Difference Vegetation Index

NDWI - Normalized Difference Water Index

NH - Northern hemisphere

NIR - Near infrared reflectance

NOAA - National Oceanic and Atmospheric Administration

NSIDC - National Snow and Ice Data Center

PACES - air Pollution in the Arctic: Climate Environment and Societies

QA - Quality assessment

SA - Solar azimuth

SWIR - Shortwave infrared reflectance

SZ - Solar zenith

USDS - United States Department of Agriculture

USFS - United States Forest Service

UTC - Coordinated Universal Time

VA - View azimuth

VHR - Very high resolution

VI - Vegetation Index

VZ - View zenith

Chapter 1: Introduction

1.1: Background and Motivation

Understanding how the Earth system responds to natural and human-induced changes and how these consequences impact society is a key priority in Earth System Science. The complex nature of the Earth system creates a diverse range of feedbacks in response to both long-term forcing and short-term perturbations. These feedbacks can either act to amplify or diminish the initial response of the Earth system; however, due to the complex interconnectivity of the Earth system, these perturbations have consequences far beyond their geographic scope and have pronounced impacts on the earth as a whole. In particular, the remote Polar Regions have garnered increasing attention due to the acute responses to outside influence (Lenton, 2012). Although Antarctica and the Arctic are both remote frigid regions, they contain two fundamentally different landscapes with unique roles in the environmental and climate systems. The Arctic region is primarily comprised of the Arctic Ocean surrounded by land, whereas Antarctica is a continent surrounded entirely by the Southern Ocean. These differing geographic characteristics lead to variations in their sea ice extent, climates, landscapes, fauna, flora, and human populations.

Both Antarctica and the Arctic have important functions within the Earth system and each have responded differently to the various natural and anthropogenic activities that have impacted the Polar Regions. However, the Arctic has received increased scientific attention as the region's surface air temperature has risen at rates more than double of those anywhere else on Earth (Screen and Simmonds, 2010). This accelerated warming has resulted from the disproportionate influences from both natural and human-

induced changes (Arnold et al., 2016; Pettus, 2009). The Arctic landscape is a complex environment dominated by tundra, permafrost, lakes, rivers, and sea ice. Changes in one component, such as in the distribution and extent of sea ice, can lead to significant regional and global impacts. For example, the very low Arctic temperatures (amplified by the presence of snow and sea ice which reduces the fraction of the incoming solar radiation that can be absorbed by the surface resulting in surface heating) drive the poleward transfer of heat effectively creating a global heat sink. This constant heat flux helps regulate the global temperature through atmospheric and oceanic circulation (NSIDC, 2017). Furthermore, the presence of sea ice also helps insulate the cold Arctic air from the warmer ocean temperatures thus preserving the heat sink circulation.

Perturbations in the Arctic climate can often lead to feedback processes which ultimately have larger implications for both the regional and global climate. According to the National Snow and Ice Data Center (NSIDC) the Arctic sea ice area has decreased by approximately 13.3% per decade since 1979, while ice sheets in Iceland and Greenland have lost approximately 281 billion metric tons of ice per year since 2002 (NSIDC, 2017). Unfortunately, these substantial changes within the Arctic ecosystem are leading to a phenomenon known as Arctic amplification: due to the large scale reduction in snow and ice extent, a change in the net radiation balance can lead to additional positive feedback effects which further drives warming in an already vulnerable region. Although there are interannual and regional variations in the observed warming in the Arctic, the magnitude of this warming has led scientists to firmly believe anthropogenic warming is now surpassing the natural variability of the climate system (Gillet et al., 2008; Najafi et al., 2015). Anthropogenic activities have been implicated in the amplified warming of the

Arctic, including the release of long-lived greenhouses gases from burning fossil fuels and the release of short-lived pollutants from open biomass burning.

The Arctic is known as a pollutant receptor region as the majority of pollution is transported via ocean and air circulation from outside source regions; however, there are also important local sources such as pollution from gas and oil exploration, shipping, and emissions from boreal forest fires (Arnold et al., 2016; Law and Stohl, 2007). The release of long-lived greenhouses gases, such as carbon dioxide, are responsible for the longer-term warming of the Earth, however, emitted short-lived aerosols and pollutants are key drivers impacting the Arctic climate. Specifically, short-lived pollutants, such as methane and black carbon (BC) primarily emitted from open-source biomass burning, have a large influence on regional warming (EPA, 2016). Despite the presence of other emitted aerosols and particulates, BC has received a lot of attention due to its absorptive efficiency (Quinn et al., 2011). BC is the absorptive byproduct of the incomplete combustion of carbonaceous fuels. New estimates place BC as the second most important human emission in regards to climate forcing, behind carbon dioxide (+1.82 Wm^{-2}; Stocker et al., 2013) with a total climate forcing of +1.1 Wm^{-2} with 90% uncertainty bounds of +0.12 to +2.1Wm^{-2} (Bond et al., 2013). The influence of BC on the climate is fairly complex as it has both direct (increased absorption of shortwave radiation in the atmosphere) and indirect (changes in the surface albedo; changes in emissivity; and impacts on the distribution and properties of clouds) effects.

Most notably, the deposition of BC on Arctic snow and sea ice leads to a decrease in the snow/ice albedo, resulting in decreased reflection of incoming solar radiation. Due to the absorptive properties of BC, the incoming solar radiation is absorbed, thus

warming the surface and melting the snow and ice. As the snow and ice melt, the snow/ice albedo continues to decrease, eventually leading to a positive feedback cycle. The accelerated surface warming from the increased snow and sea ice melt results in increased influxes of freshwater entering the oceans which contributes to rising sea levels and potential weakening of the Atlantic Meridional Overturning Circulation (Swingedouw et al., 2006). Furthermore, with the increased deposition of BC on snow and ice and the subsequent melting, there has been recent interest in understanding the impacts of increased runoff of dissolved BC levels in Arctic rivers and the Arctic Ocean. While dissolved organic carbon influx estimates to the Arctic Ocean have been well constrained, quantifying dissolved BC and understanding the impacts on the oceanic carbon cycle are still at very early stages (Fang et al., 2016; Stubbins et al., 2015).

The complex environmental and atmospheric feedback effects in this vulnerable ecosystem has prompted a surge of scientific research in the last few decades. Over the past two years, a new international initiative PACES (air Pollution in the Arctic: Climate Environment and Societies) under the partnership of the International Global Atmospheric Chemistry Project and the International Arctic Science Committee has been developed with a focus on improving the scientific knowledge on processes controlling Arctic air pollution and the subsequent impacts on human health and ecosystems (Arnold et al., 2016). Accurately identifying the potential BC source locations and the relative contributions to the potential deposition on the Arctic snow is essential to provide a solid foundation on which to base policy decisions and develop future adaptive and mitigation strategies.

Previous BC source contribution studies have identified East- and South Asia and Russia as the largest contributors of BC in the Arctic (e.g. AMAP, 2015; Klonecki et al,. 2003). Specifically, biomass burning (forests, grassland, and croplands) and gas flaring within Russia were identified as dominant BC sources (e.g. Evangeliou et al., 2016; Hegg et al., 2009; Koch and Hansen, 2005; Pettus, 2009; Stohl et al., 2006). The relative importance of the various BC sources are dependent on their seasonal patterns as the timing of the burning plays a key role in determining the efficacy of BC in the Arctic (Doherty et al., 2015). The highest concentration of BC in the Arctic occurs in winter/spring (December – May) with the lowest concentrations occurring during summer/fall (June – November) (Sharma et al., 2004). Sharma et al., (2004) found the average difference in BC concentrations during these two time periods to be almost ten times greater during the winter/spring. This is a key finding as the largest impact on the snow/ice albedo in the Arctic from BC deposition occurs during spring when the solar energy is increasing while still retaining the maximum snow cover extent (Quinn et al., 2011). Despite the vast circumpolar extent of the boreal forest, the majority of forest fires occur during the summer months (Groisman et al., 2007); whereas cropland burning in Russia predominantly occurs within spring and fall months – related to the harvest cycles (Figure 1.1).

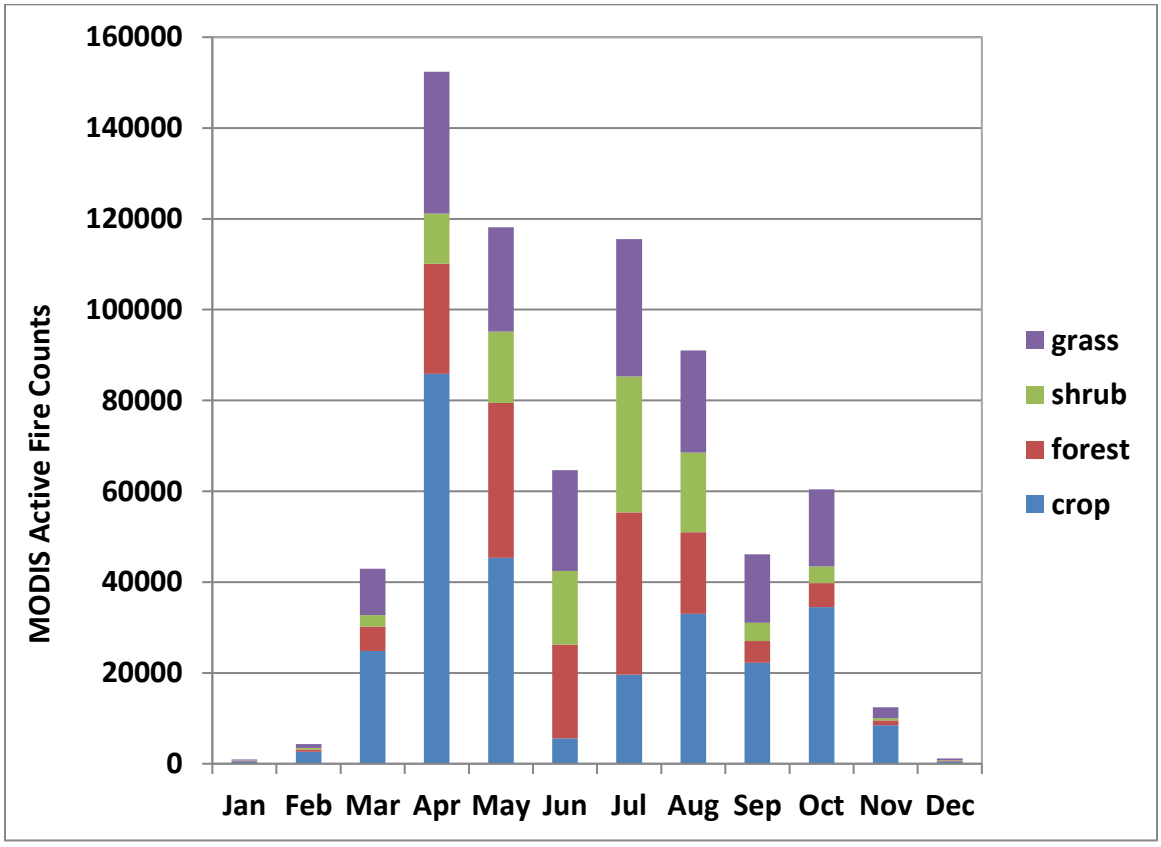

Figure 1.1: Average monthly MODIS active fire counts (2003 – 2015) within Russian grassland, shrubland, forest and cropland as defined by the International Geosphere-Biosphere Programme (IGBP) land cover type data layer (MCD12Q1; Friedl et al., 2010).

Crop residue fires are typically low intensity, short-lived events and even with low injection heights (ranging between 500 m and 1500 m; Soja et al., 2012; Martin et al., 2010; Ichoku and Kaufman, 2005), several studies have identified cropland burning in northern mid-latitudes as a contributor to BC deposited in the Arctic (Hegg et al., 2009; Koch and Hansen, 2005; Pettus, 2009; Stohl et al., 2006). Although federal laws banning open burning are established in Russia, it is still a common practice; however, there is

little consensus amongst the available data on the magnitude of the burning. Studies have identified that Russia and Kazakhstan area responsible for the largest portions of BC emissions from biomass burning, followed by China, the United States, and Canada (Pettus, 2009). With the majority of the Russian cropland region located between 40°N and 55°N and the prevalence of crop residue burning, Russia makes a good case study for quantifying the potential impact from crop residue burning on the snow in the Arctic (Figure 1.2).

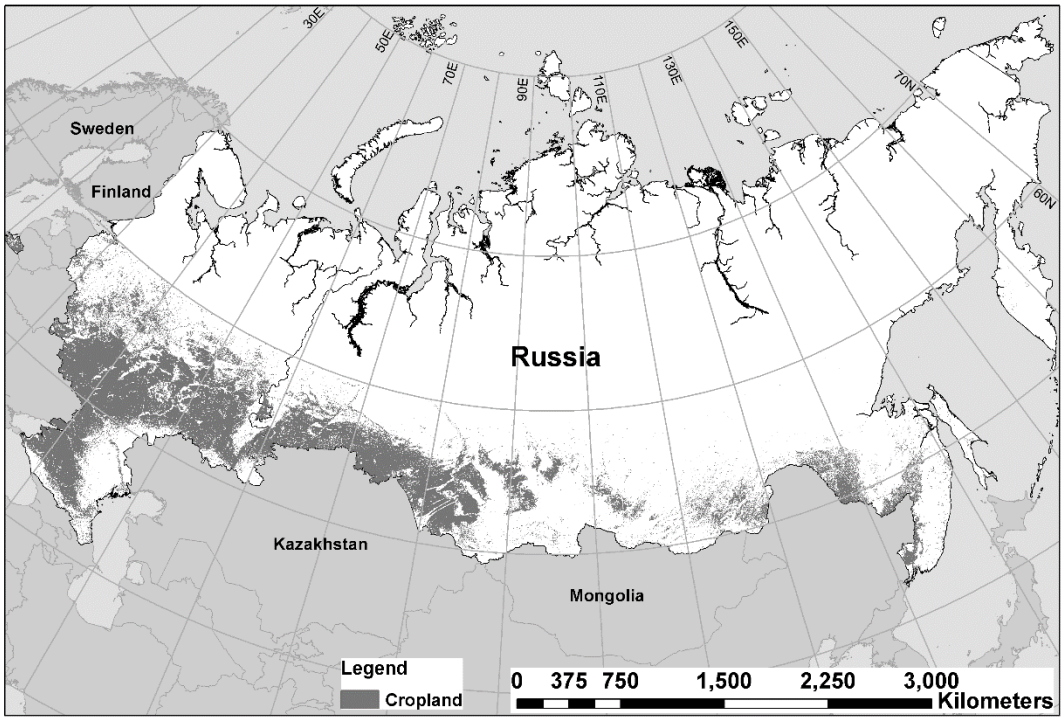

Figure 1.2: Russian cropland area as defined by the IGBP cropland/ natural vegetation mosaic.

Several long-distance transport mechanisms have been identified in the scientific literature; however, these mechanisms are primarily associated with transport during the northern hemisphere winter and early spring (Stohl, 2006; Warneke et al, 2010). The mid-latitude weather patterns are primarily driven by the movement of frontal boundaries from west to east along the storm tracks. The development of mid-latitude cyclones arise

from baroclinic instability along the polar front boundary (Bjerknes and Solberg, 1922). These migratory cyclones are essential in regulating the Earth's energy balance as they are responsible for moving heat, moisture, and energy poleward (Hare, 1968). With rising temperatures driven by the increase in greenhouse gases in the atmosphere, a poleward shift in these mid-latitude storm tracks has been observed (Wu et al., 2011). In addition, there is mounting evidence that the extreme persistent weather events – atmospheric blocking events - impacting the high and mid-latitudes are linked to the changing characteristics of atmospheric Rossby Waves, responsible for the production of cyclones (low pressure system) and anticyclones (high pressure system) (e.g. Nakamura et al., 1997; Screen and Simmonds, 2013; Vargin et al., 2012). More recently, studies have suggested that Arctic amplification, driven by the loss of snow and sea ice, may be linked to the increase in mid-latitude extreme events (e.g. Francis and Vavrus, 2012); however, this relationship is still under debate (Barnes and Screen, 2015; Cohen et al., 2014).

Atmospheric blocking events are synoptic-scale patterns in the atmospheric pressure field that are nearly stationary and act to block migratory cyclones. Blocks are most commonly associated with anticyclones; however, there are instances of blocked cyclones preventing the westerly flow of migratory cyclones. They are often associated with prolonged periods of dry weather which can lead to extreme droughts in the summer or extreme temperature fluctuations in the winter; however, their impacts are dependent on the location, magnitude and seasonality of the blocking event. The temporal persistence and large spatial scale of these systems affect both natural and managed ecosystems. Several studies have focused on the ability of these blocking events to transport pollutants to regions outside of the emission source (Raatz and Shaw, 1984;

Witte et al., 2011). Primarily focusing on blocking highs (an atmospheric block associated with a stagnant high pressure system) the persistent anticyclonic wind field leads to either the accumulation of air pollutants within the circulating wind field or leads to the accelerated transport of pollutants along the periphery where the pressure gradients are relatively strong. The identification of a potential transport mechanism that can enhance the transport of BC emissions to the Arctic has important implications for its absorptive efficacy and subsequent snow/ice albedo impacts.

The presence of air pollution in the Arctic environment has both local and global consequences and these impacts have spurred a surge of research studies. Despite the ongoing scientific progress, a key motivation in the PACES initiative is to improve the predictive capabilities of the current earth-system and chemical-transport models. Some of the major challenges lie in the inability to accurately simulate the temporal and spatial variations in Arctic air pollution and to accurately quantify the contribution of air pollution from the source regions (e.g. Monks et al., 2015). To help address these issues, this dissertation research study is focused on assessing the potential for the deposition of BC emissions from cropland burning in Russia through low-level transport, and to identify a possible transport mechanism that may enhance the transport of BC emissions to the Arctic. Furthermore, this study also sets out to address several key deficiencies in both current estimates of BC emissions from Russian cropland burning, and the misleading outcomes from complex chemical-transport models. The overall framework of this dissertation study is highlighted in section 1.2.

1.2: Research Questions

The major scientific goal of this research is to answer the overarching question: *How does crop residue burning in Russia contribute to the BC deposition on snow in the Arctic from low-level transport?* To achieve this goal, three integrated studies were undertaken which were designed to address the following research questions (Figure 1.3).

Question 1: What are the interannual and seasonal patterns of cropland burning in Russia?

This question examines cropland burning in Russia to identify the spatial and temporal burning patterns with a particular focus on the key time periods for impacts of BC deposition on the Arctic snow/ice albedo. This question is centered on the development of a custom burned area product with the aim of improving the current cropland residue emission estimates.

Question 2: What fraction of cropland burning in Russia potentially contributes to the deposition of BC on snow in the Arctic?

This question examines the potential low-level transport from cropland burning in Russia to the snow in the Arctic. It focuses on identifying the spatial and temporal patterns of cropland burning that are likely to contribute to BC deposition in the Arctic. This question also examines the northern-most extent for potential transport of crop residue BC emissions since cropland fires are low intensity and have low injection heights.

Question 3: How does the seasonality and magnitude of blocking event occurrence enhance the potential transport of BC emissions from cropland residue burning in Russia?

This question examines if the persistent wind patterns associated with atmospheric blocking events enhance the transport of cropland emissions to the Arctic. Furthermore, this question also examines the relationship between managed cropland burning fire occurrences and blocking events as the relationship between forest fires and blocking events is well established in the literature.

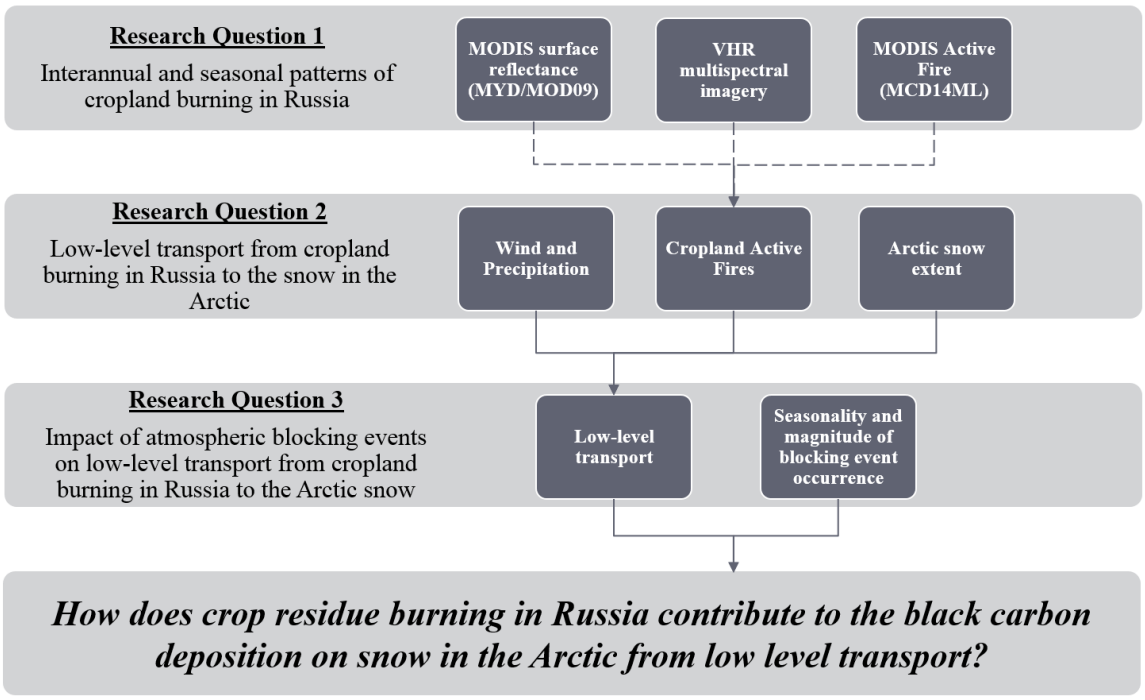

Figure 1.3: Flow diagram illustrating the major outcomes for the three phases of the doctoral research project.

1.3: Organization of the study

The remainder of the dissertation is organized into three research chapters, conclusion, supplementary material, and reference list. Chapter 2 addresses research question 1 through the development of an independent estimate of cropland burning in Russia through assessing the capabilities of global burned area products (MCD45A1; Roy et al., 2008 and MCD64A1; Giglio et al., 2009) and a custom Moderate Resolution Imaging Spectroradiometer (MODIS) based Cropland Regional Area Burned (CRAB) product. An archive of cropland field state samples was generated from very high resolution (< 5 m) imagery allowing a unique perspective into the challenges of mapping cropland burned area through detailed analysis of the Russian agricultural practices. This chapter has been peer-reviewed and published in Remote Sensing of Environment (Hall et al., 2016). Although this was a multi-author paper, I was responsible for the data collection and creation of the algorithm under the advisement of Dr. Loboda. Dr. McCarty was the project principle investigator and Dr. Giglio provided valuable expertise during the later stages of the algorithm development.

Chapter 3 corresponds to research question 2 and highlights the development of a long-range, low-level transport model based on wind direction, wind speed, and precipitation to identify potential BC source regions within the Russian cropland between 2003 and 2015. Due to the extensive limitations of the crop residue burning estimates, this model does not attempt to quantify the magnitude of BC emissions which could potentially deposit on the Arctic snow. Instead, this model attempts to quantify the fraction of cropland burning that is likely to contribute to BC deposition in the Arctic.

Chapter 4 extends the methodology developed in Chapter 3 through the integration of atmospheric blocking event occurrence data to answer research question 3. This chapter identifies if the persistent winds are able to enhance the transport of potential BC emissions from the Russian croplands to the snow on the Arctic.

Chapter 5 presents the major conclusion of the doctoral dissertation through summarizing the overall findings of three research chapters (2 – 4). It also provides a discussion of the overall contribution of this work to the broader Arctic science agenda, and finally, provides recommendations for future research directions.

Chapter 2: A MODIS-based burned area assessment for Russian croplands: mapping requirements and challenges[1]

2.1: Introduction

Anthropogenic transformations of the terrestrial biosphere have greatly altered the earth's land surface. By 2011, approximately 40% of the ice-free land surface had been modified for agricultural activities (FAOSTAT, 2015). These managed areas have replaced forests, natural grasslands and savannas and have led to a range of impacts on the planet's ecosystem structures and functions (Ramankutty et al., 2008). The impacts of these activities vary greatly due to the differing management practices applied throughout the various global agricultural regions. The use of fire in agricultural management for removal of excess residue and the control of diseases and pests is a common practice across different regions from developing to developed countries (EPA, 2012; McCarty et al., 2012). Although prescribed burning is a useful agricultural management tool, concern is growing in the scientific community regarding the negative consequences on regional climates and air quality due to associated emissions of gases and particulates (Foley et al., 2005).

Impacts from agricultural activities are not limited to areas within these managed ecosystems. Chemical studies of particles deposited on Arctic snow indicate that northern mid-latitude agricultural burning and forest fires are the dominant sources of black carbon (BC) deposition above the Arctic Circle (Hegg et al., 2009; Koch and Hansen, 2005; Pettus, 2009; Stohl et al., 2006). BC is a product of incomplete combustion of

[1] This chapter has been published as a multi-authored paper in the Remote Sensing of Environment as Hall, J.V., Loboda, T.V., Giglio, L., & McCarty, G.W. (2016). A MODIS-based burned area assessment for Russian croplands: Mapping requirements and challenges. Remote Sensing of Environment, 184, 506-521. Joanne Hall was the primary developer of the training and validation data sets and the primary mapping algorithm developer. She conducted all mapping and validation activities with advisory input from other authors of the manuscript.

carbonaceous fuels and new estimates place BC as the second most important human emission in regards to climate forcing, behind carbon dioxide (+1.82 Wm^{-2}; Stocker et al., 2013) with a total climate forcing of +1.1 Wm^{-2} with 90% uncertainty bounds of +0.12 to +2.1Wm^{-2} (Bond et al., 2013). Unlike the mid- and low latitudes, the Arctic has a unique role in the earth climate system through increased surface reflectance created by the region's high snow and ice albedo. Both natural and human-induced changes to the region's albedo have resulted in the accelerated warming of the Arctic. Specifically the deposition of BC, transported from northern mid-latitudes, is a significant contributor to observed short term warming trends in the Arctic (Bond et al., 2013; Hansen and Nazarenko, 2004; Jacobson et al., 2007; Ramanathan and Carmichael, 2008; Quinn et al., 2008, 2011).

The identification of BC emissions from fires as a contributor to Arctic warming has led to a surge of interest in limiting or eliminating prescribed burning, particularly in spring, to reduce the warming effect of BC (Zender, 2007). There are large uncertainties in the current estimates of the sources, source regions, and transport and transformation pathways of BC transported to the Arctic region (Hegg et al., 2009; Shindell et al., 2008; Quinn et al., 2008) and many of these uncertainties stem from the current inaccurate estimates of cropland burned area. In this paper, we aim to develop an independent estimate of cropland burning in Russia through assessing the capabilities of global burned area products and our own custom Moderate Resolution Imaging Spectroradiometer (MODIS) based burned area product to quantify cropland burning in Russia. Russian agriculture is of global importance, however, relatively little is known about the crop management strategies and in particular the burning practices in rural areas (Pettus,

2009). Russia is the world's fifth-largest wheat exporter and impacts on the wheat harvest can have large implications on global markets (FAOSTAT, 2015b; Grumm, 2011; Kramer, 2010). Although federal law banned open burning, Russia and Kazakhstan are responsible for the largest portions of BC emissions from biomass burning that reach the Arctic, followed by China, the United States and Canada (Pettus, 2009).

Accurate monitoring of the temporal dynamics of prescribed burning is crucial as studies have found that the timing of the burning plays an important role in determining the magnitude of the BC impact on the Arctic (Stohl, 2006; Warneke et al., 2010). In particular, early springtime cropland burning has a surprisingly large impact on the Arctic considering cropland fire injection heights are lower than forest fires and they have a much shorter duration of burning. Even with low injection heights, under the right atmospheric conditions, BC particles can be transported long distances. One such method of low-level transport is related to surfaces of constant potential temperature (Stohl et al., 2007). During the spring, Arctic temperatures are higher, thus reducing the temperature contrast between the northern mid-latitude source regions (40°N and above) and the Arctic (Law and Stohl, 2007). This reduction in the temperature contrast leads to the creation of efficient pollution pathways that facilitate low-level transport of BC from northern mid-latitudes to beyond the Arctic Circle; hence it is imperative to understand both the spatial and temporal patterns of cropland residue burning in the northern mid-latitudes.

Currently, accurate monitoring of cropland burning from existing active fire and burned area products is limited. The transient nature and non-contiguous patches of cropland fires requires a tailored mapping algorithm that is designed to capture the subtle

nuances of the cropland spectral signature. Many existing burned area algorithms are focused on mapping hotter and larger wildfire events and several have global extents (MCD45A1; Roy et al., 2008 and MCD64A1; Giglio et al., 2009). Even with regional burned area algorithms (Loboda et al., 2007; McCarty et al., 2008), the inclusion of the MODIS active fire Product (MCD14ML; Giglio et al., 2003) as a driver of the mapping algorithm will inhibit the ability to capture the full extent of burning in the cropland regions. For example, McCarty et al., (2008) found that MODIS active fire detections contributed to less than 4% of the total burned area estimated in the United States croplands within MODIS tile h10v05, which encompasses a large portion of the Mississippi River Delta and the southern Great Plains. In addition, burned area algorithms which do not address small fires, defined as fires smaller than the spatial resolution of the surface reflectance imagery, potentially underestimate the total burned area particularly in cropland regions where fires are both small and transient (McCarty et al., 2009; Randerson et al., 2012; Wu et al., 2015). Recent studies have found that utilizing the MODIS active fire product helped identify crop residue burning, particularly in small fields which are not able to be detected through traditional difference Normalized Burn Ratio (dNBR) threshold methodologies (McCarty et al., 2009; Randerson et al., 2012).

In this paper, we focus on the creation of a customized MODIS-based burned area product for the Russian cropland area and the comparison with the existing MCD45A1, MCD64A1 and MCD14ML products to highlight the challenges in mapping cropland burning. In section 2.2, we highlight the various agricultural practices using a unique archive of samples extracted from multispectral very high resolution (VHR, defined as

less than 5 m resolution) imagery. Section 2.3 focuses on the development of a customized MODIS-based burned area product, including the creation of a multi-sensor clear-surface compositing algorithm (section 2.3.2). Section 2.4 focuses on the accuracy assessment, results and intercomparison between the burned area products, followed by challenges of mapping cropland burned area (section 2.5) and concludes with recommendations for future cropland burned area studies.

2.2: Visual assessment of fire practice in Russian croplands from VHR imagery

Multispectral VHR imagery was acquired from DigitalGlobe's high resolution commercial satellites, QuickBird and World View-2. The high spatial resolution (< 5 m) is a much needed element for the identification and discrimination of various cropland field states, including, active fire verified burn, visually identified burn, plow, residue and bare fields (Figure 2.1). A particular challenge with cropland burned area mapping is the difficulty in distinguishing burned from plowed fields (McCarty et al., 2009; Roy et al., 2005). The VHR imagery allows for more accurate identification of field condition through visual interpretation and from the incorporation of the MODIS active fire (MCD14ML) dataset as a means of independent validation for the selection of burned training and validation samples (see section 2.2.3).

For our archive, dark, smooth textured fields were digitized as plowed. Typically these fields were fairly homogenous and the dark uniform color filled the entire field area (Figure 2.1c), whereas burns without the flaming front were identified by the rough texture and natural fingerlike patterns created from the moving flaming front (Figure 2.1a).

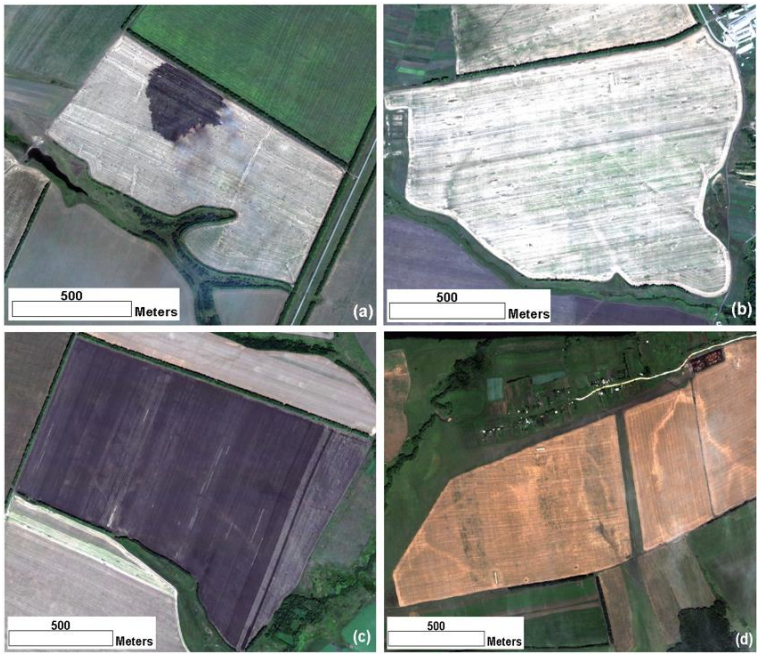

Figure 2.1: Very high resolution (< 5 m) field state examples: burned field (a), residue field (b), freshly plowed field (c) and bare field (d). Images are displayed using the true color composite.

Quantifying the extent and magnitude of cropland burning is a challenging task as there is little consensus amongst the available data. Visual analysis of the VHR imagery reveals a larger proportion of cropland burned area than what is indirectly detected through the MODIS active fire product and what has been reported by farmers through telephone surveys undertaken as part of a USDA Black Carbon Initiative project (SovEcon, 2013). According to the survey results, farmers have noticed a significant reduction in agricultural burning, with some respondents claiming agricultural burning has not been observed in the Rostov region for at least the last 10 years, the Stavropol region for 5 – 7 years, the Krasnodar region for 2 – 5 years, the Saratov region for 3 years, and the Altai region for 2 years (see supplementary material Figure S1). However, the survey results also claim that mainly small agricultural enterprises in these regions

still burn for a variety of reasons which include the reduction of soil harbored plant diseases in the Rostov region and the removal of straw for the improved crop planting and germination success in areas of the Saratov and Voronezh regions.

Analysis of the MODIS active fire product between March and September 2003 to 2012 revealed an interannual range of approximately 60,000 – 166,000 active fire counts within the Russian cropland region. Specifically addressing the aforementioned regions from the survey, analysis of the active fire product found burning in all areas; however, the magnitude and temporal distribution varied across all regions. The variation in the distribution is related to the agricultural practices of the different regions. In particular, a common pattern relates to the spring and winter wheat cycles. Typically the winter wheat campaign begins in mid-August in the Volga District and advances southward. The crops enter dormancy in late October/ early November, whereby in an average year, approximately 13% of winter grains are lost over the course of winter due to severe frost damage and other winter weather-related impacts (USDA FAS, 2013a). Harvesting of the remaining winter wheat crops begins in late June and concludes in late August. On the other hand, the spring wheat campaign begins in April and the harvest commences in August and is finished by late October. Analysis of the active fire burning distribution, within the Russian cropland region, found that there were generally two distinct burning seasons (Figure 2.2), thus the VHR samples were divided into spring (1 March – 30 June) and summer (1 July – 30 September). The MODIS instrument acquires daily observations of fire activity from two satellites – Terra, launched in late 1999, and Aqua, launched in 2002. Only active fire detections acquired between 2003 and 2012 were included in the analysis to ensure the temporal consistency of the dataset.

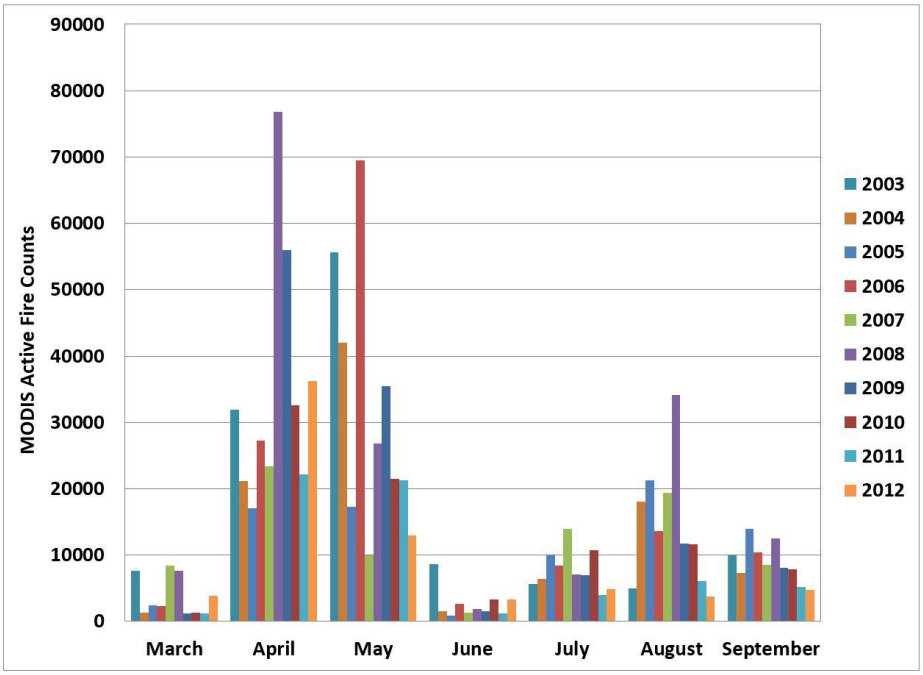

Figure 2.2: MODIS active fire (MCD14ML; Giglio et al., 2003) counts within the Russian cropland area as defined by the crop mask (see Figure 2.3) between 2003 and 2012.

2.2.1: Archive development of field samples under various post-harvest conditions (burn, bare, standing crop residue, plowed) from VHR imagery

We have created an archive of various field state samples within the Russian cropland region from VHR imagery (Figure 2.3). The VHR samples were visually identified and digitized by several image analysts (for details see section 2.2.3). The low repeat frequency of VHR satellites and their small footprint size (e.g., ~360 km × 18 km for QuickBird) leads to an opportunistic acquisition strategy and therefore the archive does not cover the full extent of the Russian cropland region.

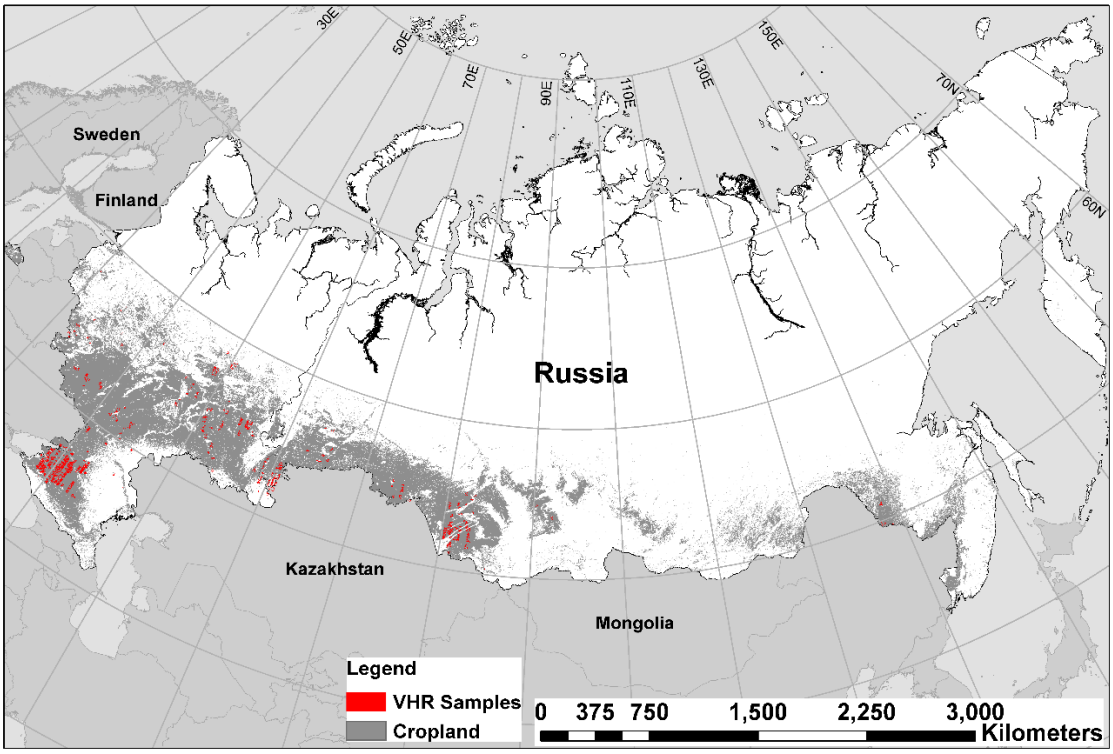

Figure 2.3: Very high resolution (< 5 m) samples (2003 – 2012) acquired from DigitalGlobe's high resolution commercial satellites, QuickBird and World View-2 overlaid over the Russian cropland.

From the analysis of the active fire counts, it is clear there is a substantial amount of burning within Russian cropland. Using the archive of VHR data, we examined these burns in greater detail than can be accomplished through the current MODIS products. This archive allows us a unique perspective into the challenges of mapping cropland burned area through the detailed analysis of the Russian agricultural practices. Table 2.1 below presents the size distribution of the entire VHR sample archive. Analysis of the size distribution of the cropland burns and field samples found a large proportion of the burn and non-burn samples occupying less than 21 ha, which is the approximate equivalent of one 463 m MODIS grid cell.

Table 2.1: Distribution of burn and non-burn samples digitized from very high resolution (< 5 m) imagery. Values in parentheses are approximate equivalent MODIS 500 m grid cells based on the size of the samples in hectares.

	Burn Samples	**Field Samples**
Minimum, ha (~grid cell)	0.5 (< 1)	2.4 (< 1)
Maximum, ha (~grid cell)	411 (20)	656 (31)
Mean, ha (~grid cell)	57 (3)	88 (4)
Median, ha (~grid cell)	40 (2)	71 (3)
Standard Deviation, ha (~grid cell)	56 (3)	68 (3)
Skewness	2.3	1.9
Kurtosis	7.8	5.6
Total Number of Samples	782	6037

Depending on the exact configuration of the field relative to the 500 m MODIS sinusoidal grid, the actual relationship between the MODIS grid cells and the sizes of burned or total field areas can be substantially smaller. Here we are presenting the best case estimates. Furthermore, in general the burned area samples are smaller than the field area as only the burned portion of the field was digitized when creating the burn sample. The distribution of field sizes and burned area both have a positively skewed relationship (Figure 2.4) with the majority of burns occupying less than 50 ha.

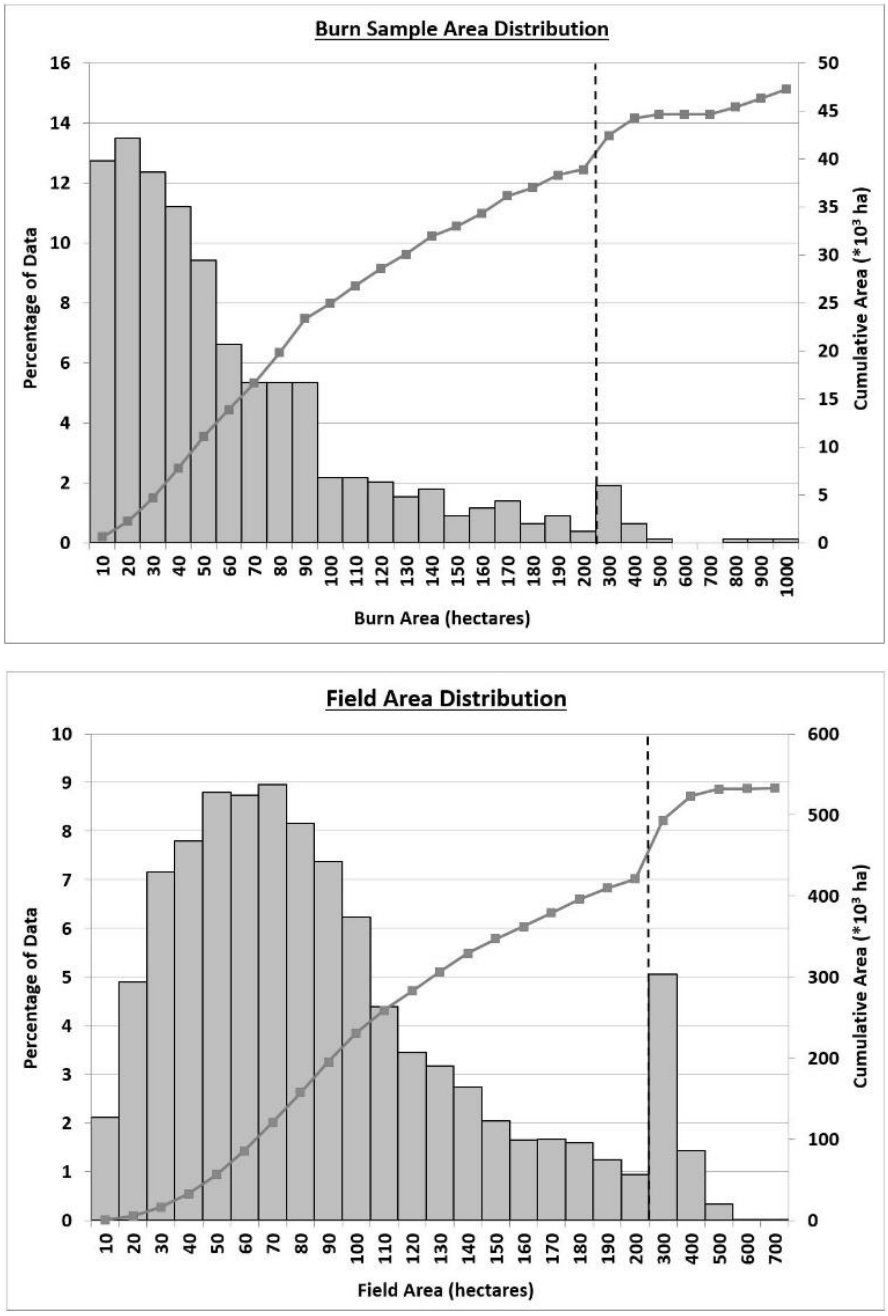

Figure 2.4: Burn sample area (above) and field area (below) frequency distributions and cumulative area ($\times 10^3$ ha) for all VHR polygon samples before the matching process. The vertical dashed line indicates a change in area size categories along the horizontal axis.

2.2.2: Visual examination of burn strategies identified in VHR imagery

Further analysis was carried out on the burn samples to identify any additional potential challenges. Visual examination of burning practices in the available VHR imagery found a variety of burning strategies including, complete field burns, partial field burns and pile burning (Figure 2.5).

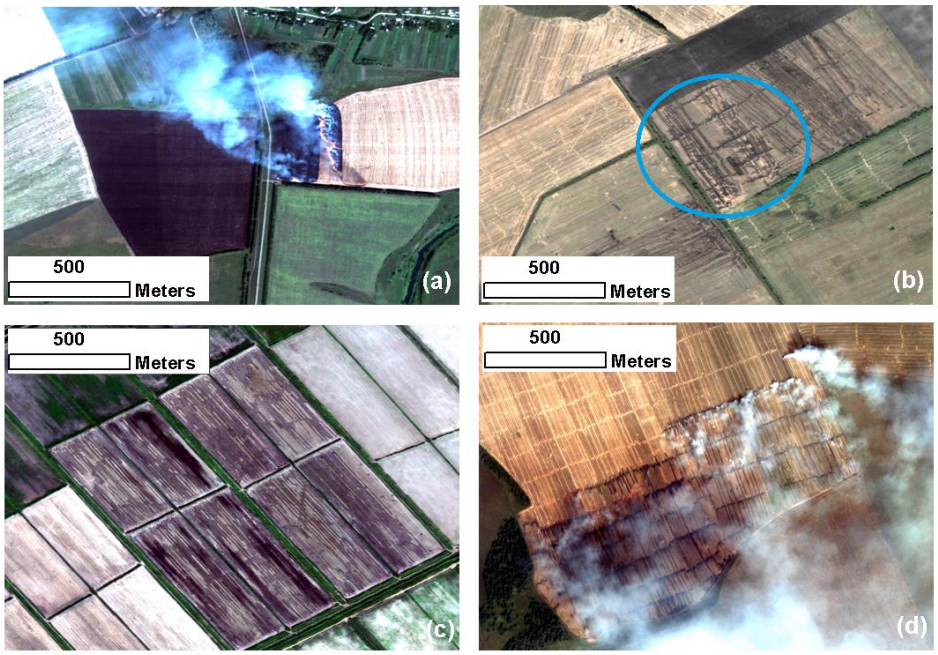

Figure 2.5: Visual burning practices found in available very high resolution (< 5 m) imagery: complete field burn (a), partial field burn (b), partial field burn (c), and pile burn (d).

From visual analysis, the full burns (Figure 2.5a) are associated with the burns that leave little to no unburned residue in the burn extent that can be seen in the VHR image, whereas the partial burns (Figure 2.5b and 2.5c) include varying degrees of unburned residue within the burn extent. Depending on a number of factors including the amount of biomass within the field and local burn conditions, these partial burns can

cover the entire field extent (Figure 2.5c) or can only begin to burn in a small section of the field (Figure 2.5b – blue circle). Finally pile burns (Figure 2.5d) are associated with setting fire to piles of residue. Analysis of the VHR burn samples revealed that the practice of pile burning has an impact on the burn spectral signature due to the larger percentage of non-burned residue within the burned area extent. Although excluding both pile and partial burn samples would improve the purity of the burn spectral signature, the majority of the burn samples are not full burns and do not give a good representation of the agricultural burn practices within Russia (as seen in the VHR archive). Furthermore, visual analysis of the VHR archive found additional nuances in the agricultural practices including fields which were not burned before plowing (see supplementary material Figure S2). These variations in agricultural practices and the hesitancy of farmers to disclose their burning methods leads to further hindrances on the ability to accurately map cropland burned area.

2.2.3: Methodology for the development of post-harvest field condition archive

To assist the image analysts in the initial sorting of the VHR images, the MODIS active fire product was incorporated to highlight any VHR images with a potential active fire within ten days of the image date. Each VHR image was then examined and any burns within approximately a 1 km radius, to account for off nadir viewing angle geolocation inaccuracies, of the active fire point were manually digitized and classified as an active fire verified burn. Any burns which were not highlighted by the active fire dataset, but were visually identified by the analyst, were classed as a burn and not an active fire verified burn. Visually identifiable burned fields constituted a very small

fraction of all fields in the processed VHR imagery. For each processed image, the analysts were instructed to digitize all burns and collect 5 samples per non-burn field state (plow, bare and residue) whether the image contained any burned fields or not. Following the manual digitization of the VHR imagery by an image analyst and subsequent collection of the various field type samples (burn, plow, bare and residue), the samples were georegistered to orthorectified Landsat imagery and then geometrically matched through the rasterization of the VHR polygons to the 500 m Level 2G MODIS imagery (MOD/MYD09GA; Vermote et al., 2011 – see section 2.3). Approximately 4% of the burn samples (average size $\leq$ 1 MODIS grid cell) were lost during the matching process as the configuration of the field sample relative to the 500 m MODIS grid cell led to the splitting of the sample between adjacent grid cells and therefore the smaller samples were unable to be rasterized to the coarser MODIS resolution based on the 50% majority aggregation rule. Upon completion of the matching process, the field samples were temporally stratified by typology based on a randomized sampling scheme to separate the samples into training or validation categories based on the dates and field type. The final totals of VHR spring and summer samples are highlighted in Table 2.2.

Table 2.2: Very high resolution (< 5 m) spring and summer samples matched to MODIS 500 m grid cells.

	Training	
	Spring	**Summer**
Burn	480 grid cells	1312 grid cells
Bare	835 grid cells	3171 grid cells
Residue	693 grid cells	3401 grid cells
Plow	662 grid cells	2491 grid cells
	Validation	
	Spring	**Summer**
Burn	369 grid cells	762 grid cells
Bare	762 grid cells	1872 grid cells
Residue	527 grid cells	1996 grid cells
Plow	579 grid cells	1616 grid cells

2.3: Data and Methods

The Cropland Regional Area Burned (CRAB) algorithm was designed to improve quantification of the spatial and temporal variability of burned area from Russian cropland residue burning between 2003 and 2012. The CRAB algorithm maps daily burned area over the Russian cropland at 500 m resolution. The generated outputs include seasonal burned area maps, containing the Julian Date for the mapped burn date for each burn pixel, and confidence layers. The CRAB algorithm is divided into two seasons based on the assumption that croplands can burn more than once a year (e.g. before planting and/or after harvest) thus resulting in two distinct burning seasons: spring (1 March – 30 June) and summer (1 July – 30 September). These were defined based on the analysis of the frequency distribution of the MODIS active fire product (MCD14ML) (Figure 2.2) and the general planting and harvesting practices (described earlier, USDA FAS, 2013a). It is further assumed that a given pixel can burn only once during one of the burning seasons (cumulatively no more than twice during a year).

Figure 2.6 shows the overall framework of CRAB. The algorithm ingests the daily surface reflectance 500 m Level 2G MODIS imagery acquired from Terra and Aqua (MOD/MYD09GA; Vermote et al., 2011) satellites between 2003 and 2012. A combination of the 1 km quality assessment layers and angle geometry layers were extracted from the Aqua (MYD09GA) and Terra (MOD09GA) datasets and were composited using a multivariate decision making approach to select the best quality observations with intent to minimize false detections (see section 2.3.2 for more detail). To ensure the algorithm only processed observations over the Russian cropland region, a crop mask was created using the cropland and cropland/natural vegetation mosaic layers from the 2011 500 m Level 3 International Geosphere-Biosphere Programme (IGBP) classification scheme within the MODIS land cover dataset (MCD12Q1; Friedl et al., 2010). After analyzing the variability in the IGBP cropland and cropland/natural vegetation layers, we are satisfied with utilizing this product in the CRAB algorithm (see supplementary material S3 for more details). In addition, the MODIS 250 m land-water mask (MOD44W; Carroll et al., 2009) was aggregated to 500 m using a strict aggregation rule to avoid water contamination and applied to the IGBP crop mask. The 500 m grid cell was flagged as water if any of the four 250 m grid cells were identified as water. Since wet soil can often trigger a response in the SWIR bands we opted to reduce any confusion with small water bodies.

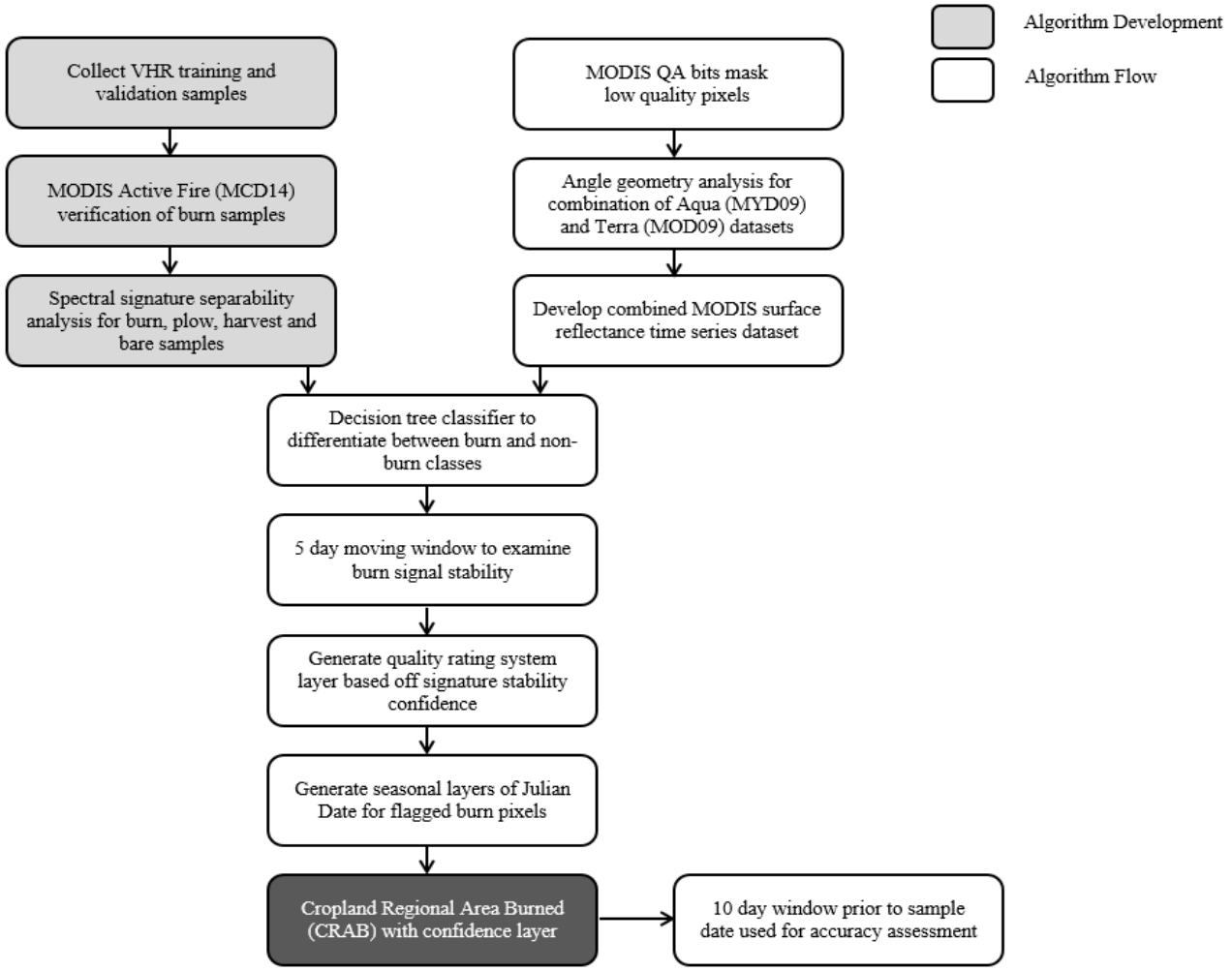

Figure 2.6: Cropland Regional Area Burned pre-algorithm development and methodological framework.

2.3.1: Clear surface analysis

Accurate mapping of cropland burned area requires multiple subsequent daily observations to alleviate one of the largest sources of error being the inability to distinguish burned from plowed fields. This is particularly relevant in the Mollisol regions of southern Russia (McCarty et al., 2009; Roy et al., 2005). Although MODIS imagery is acquired daily, the time series is not continuous as periods of prolonged

clouds, aerosols and snow can limit the number of available clear surface days. A new compositing algorithm has been developed to combine Aqua and Terra data to improve the availability of clear surface views and to avoid forward scattering which results in artificial darkening of the spectral signature. The 1 km MODIS quality assessment (QA) data layers were extracted from the MOD09GA and MYD09GA products for use in the clear surface analysis over the Russian cropland region as defined by the crop mask. Each image contains a corresponding QA layer which holds 16 bit flags that summarize 11 different parameters. For this analysis, only bits related to clouds, aerosols and snow were chosen (see supplementary material Table S1). The QA bits were extracted into daily binary layers, representing the clear surface days for both Aqua and Terra.

2.3.2: Multi-sensor clear surface composite

Due to the non-Lambertian nature of cropland fields, the bidirectional reflectance characteristics varies considerably, leading to large differences in the observed reflectance (Rahman et al., 1999, Ranson et al., 1985; Schaaf et al., 2002). Analysis from a sample field's spectral output illustrates the impact on the burn spectral signature (Figure 2.7). Reflectance values are expected to decrease in the visible and near infrared bands following a burn due to the deposition of char on the brighter soil surface (Zhang et al., 2003). This decrease is visible in Terra's output following the burn on Julian Date 229 (17 August 2006, 10:04:20 MSK; Figure 2.7b), whereas there is a clear increase in reflectance in the spectral output of Aqua (17 August 2006, 12:11:09 MSK; Figure 2.7c). Further analysis on the solar and view zenith and azimuthal angles found the discrepancies in reflectance values between the two datasets were related to the differing

solar and viewing angle geometries and it is clear that the higher reflectance values correspond to a back scatter scenario with zenith angles far off nadir (Figure 2.7c). This same pattern is seen in a number of studies whereby the reflectance values generally decrease from the backward to the forward scattering direction (e.g. Galvao et al., 2009, Rahman et al., 1999).

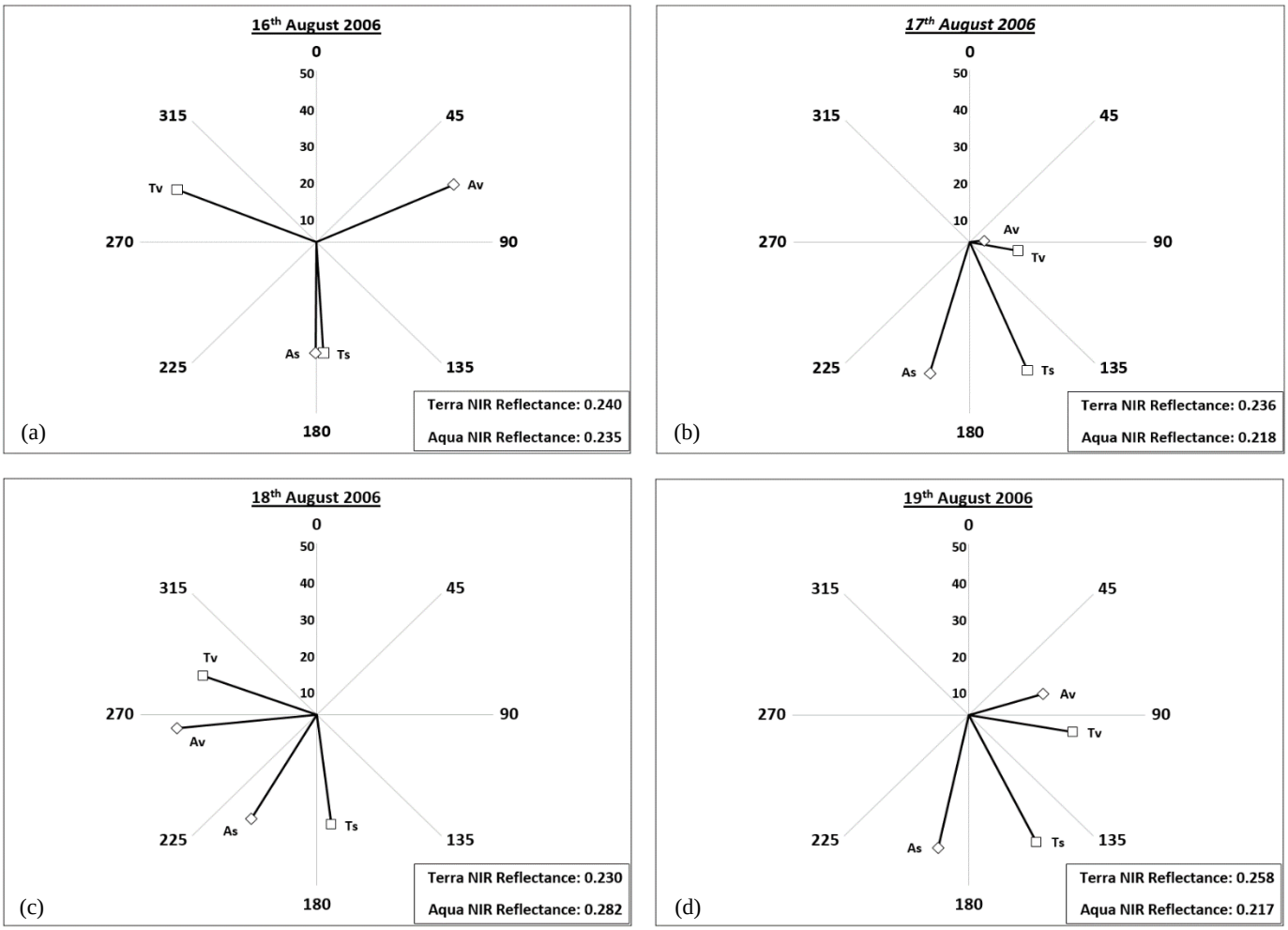

Figure 2.7: Solar (Ts, As) and sensor (Tv, Av) azimuthal and zenith angles for Terra and Aqua over 16 – 19 August 2006. The verified active burn occurred on 17 August 2006. The zenith angles are represented by the radius of the black line. Zenith angles scaled between 0° and 50° for visualization. The near infrared reflectance (NIR) values are located in the lower right boxes.

The following method outlining the combination of Aqua and Terra daily observations aims to minimize the impact of bidirectional reflectance distribution function (BRDF) related decreases in surface reflectance with the general aim to lower the commission error of the CRAB product (Figure 2.8).

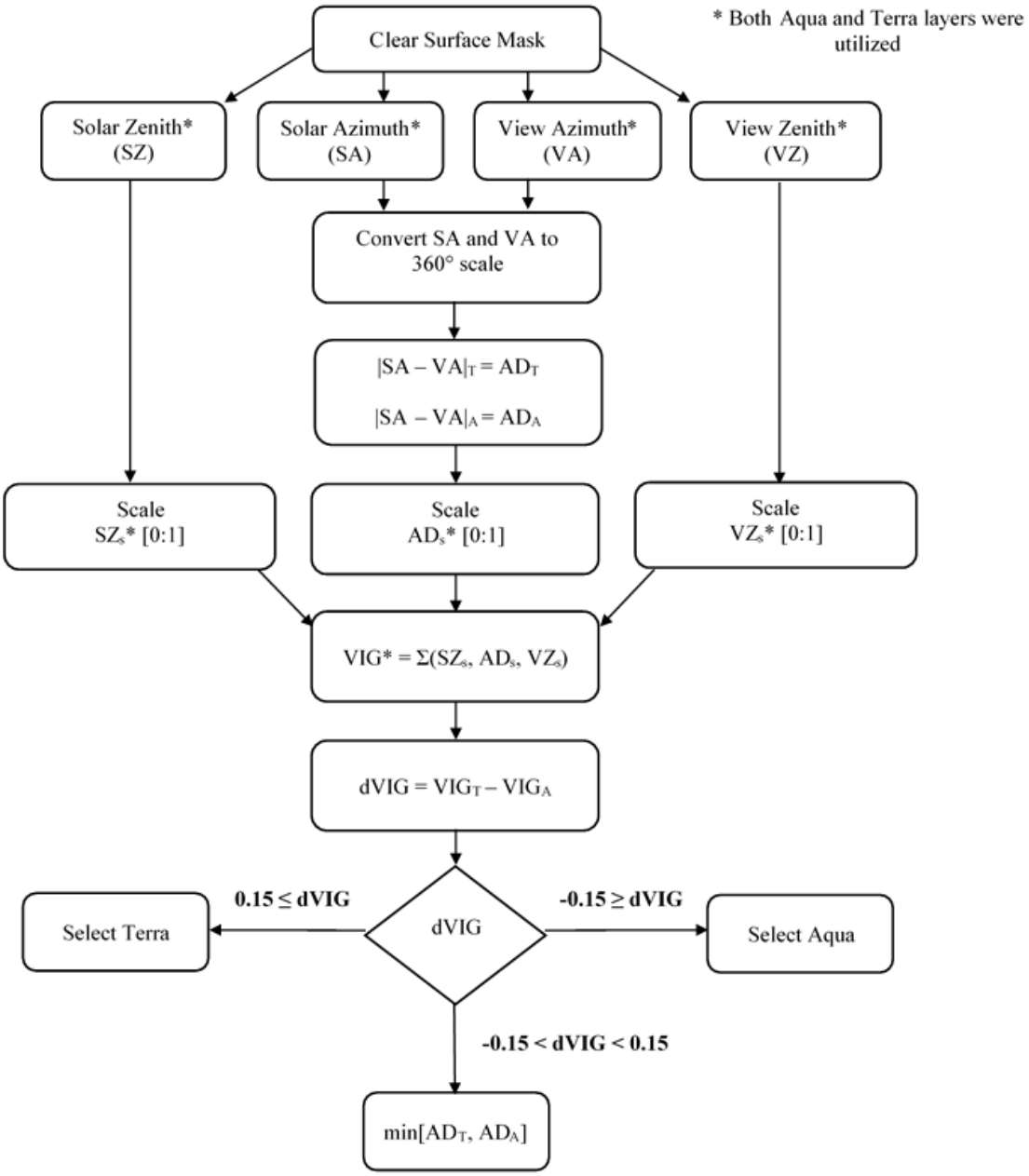

Figure 2.8: Methodological framework for the combination of Aqua and Terra clear surface datasets into one BRDF adjusted time series.

In the combination of the two datasets, the solar zenith (SZ), view zenith (VZ), solar azimuth (SA) and view azimuth (VA) angles were extracted from the MOD09GA and MYD09GA products. Following the outline in Figure 2.8, the angle geometry algorithm ingested the four angles for the creation of the three variables used in the calculation of the Viewing Indicator Geometry (VIG) index:

Variable 1: Linearly scaled solar zenith angle (SZ_s) for both Aqua and Terra between 0 (90° off nadir = undesired) and 1 (nadir = desired).

Variable 2: Linearly scaled absolute azimuthal difference (AD_s) for both Aqua and Terra between 0 (0° or 180° diff = undesired) and 1 (90° diff = desired). We preferred to avoid forward scattering (artificial darkening) and backward scattering (artificial brightening) and rather considered values between both situations.

Variable 3: Linearly scaled view zenith angle (VZ_s) for both Aqua and Terra between 0 (90° off nadir = undesired) and 1 (nadir = desired).

The three variables were summed and weighted equally in the calculation of VIG. The difference between VIG Aqua and VIG Terra (dVIG) was evaluated against our chosen threshold. If the difference was less than -0.15 Aqua was chosen; whereas if the difference was greater than 0.15 then Terra was chosen. If the value lay between these two thresholds then the smallest azimuthal difference, corresponding to a back scatter scenario, as calculated in variable 2 was chosen. The composition process can be seen in Figure 2.7. On 16 August 2006, the VIG values are almost identical, leading to a small dVIG (-0.03). According to the threshold criteria, the low dVIG requires the lowest AD_s

value to be chosen. In this instance Terra was slightly closer to 90°, whereas on 17 August 2006 Aqua's geometry was preferred as Terra was closer to a more intense backscatter scenario. In this instance Aqua was preferred as Aqua's VZ angle was also closer to nadir. The combination angle geometry and clear surface layers created a combined multi-sensor clear surface composite which was subsequently utilized in the CRAB algorithm (Figure 2.6).

2.3.3: Burned area map and confidence level development

Upon completion of the clear surface composite, a single daily image of clear surface observations combined from Terra and Aqua is evaluated for burned area detection. The CRAB algorithm uses a decision tree classifier that differentiates between burn and non-burn (residue, plow and bare) classes and assigns a probability to each of the burn terminal nodes. A total of 690 training fields (116 burned and 574 unburned) were utilized in the spring classification tree and 2249 training fields (326 burned and 1923 unburned) were utilized in the summer tree. A set of 12 metrics was created as an input into the decision tree for each burn and unburned training sample split between the two mapping seasons, spring and summer. These inputs were a combination of spectral reflectance bands (ρ); band 1 (620 – 670 nm), band 2 (841 – 876 nm), band 3 (459 – 479 nm), band 4 (545 – 565 nm), band 5 (1230 – 1250 nm), band 6 (1628 – 1652 nm) and band 7 (2105 – 2155 nm), and derived spectral indices, including; Normalized Burn Ratio ($[\rho_2 - \rho_7]/ [\rho_2 + \rho_7]$; Key and Benson, 1999), Normalized Difference Vegetation Index ($[\rho_2 - \rho_1]/ [\rho_2 + \rho_1]$; Rouse et al., 1974), Vegetation Index ($[\rho_5 - \rho_7]/ [\rho_5 + \rho_7]$; Giglio et al., 2009) and Normalized Difference Water Index (Gao, 1996) for both band 5 ($[\rho_2 - \rho_5]/ [\rho_2 + \rho_5]$) and band 6 ($[\rho_2 - \rho_6]/ [\rho_2 + \rho_6]$).

An output decision tree was generated for each of the two seasons. The spring tree has 29 terminal nodes of which seven classify burned fields and 22 classify unburned fields with an overall misclassification rate of 11%. The summer tree has six terminal nodes of which one classifies burned fields and five classify unburned fields with an overall misclassification rate of 14%. The spring tree utilized all input metrics for the classification of the burned fields while the summer tree only utilized ρ_1, ρ_3, ρ_6, NBR and NDWI5 in the classification of the burned fields. The classification rules for each season's tree are reported in Table 2.3.

Table 2.3: CRAB burned area classification rules (A – G) for spring and (A2) for summer. A field is classified as burned if it satisfies each condition in any of the classification rules.

Rule	**Classification Rule (AND)**
A	ρ_4 (< 0.081); NDVI (< 0.302); NDWI6 (< -0.230); NBR (> -0.291); NBR (< -0.236); NDWI6 (> -0.302)
B	ρ_4 (< 0.081); NDVI (< 0.302); NDWI6 (< -0.230); NBR (> -0.291); NBR (< -0.236); NDVI (< 0.284); NDWI5 (< -0.131)
C	ρ_4 (< 0.081); NDVI (< 0.302); NDWI6 (< -0.230); NBR (> -0.291); NBR (< -0.236); NDVI (> 0.284)
D	ρ_4 (< 0.081); NDVI (> 0.302); ρ_1 (< 0.034); ρ_5 (< 0.291); ρ_3 (> 0.016)
E	ρ_4 (< 0.081); NDVI (> 0.302); ρ_1 (> 0.034); NDWI5 (< 0.007); NDWI6 (> -0.317); ρ_5 (< 0.261); ρ_7 (> 0.179); ρ_7 (< 0.134)
F	ρ_4 (< 0.081); NDVI (> 0.302); ρ_1 (> 0.034); NDWI5 (< 0.007); NDWI6 (> -0.317); ρ_5 (< 0.261); ρ_7 (> 0.179); ρ_7 (> 0.134); ρ_2 (< 0.198); ρ_4 (<0.765); NDVI (> 0.404); ρ_6 (< 0.239); VI (> 0.196)
G	ρ_4 (< 0.081); NDVI (> 0.302); ρ_1 (> 0.034); NDWI5 (< 0.007); NDWI6 (> -0.317); ρ_5 (< 0.261); ρ_7 (> 0.179); ρ_7 (> 0.134); ρ_2 (< 0.198); ρ_4 (> 0.765)
A2	ρ_6 (< 0.325); NDWI5 (> -0.156); ρ_1 (< 0.113); ρ_3 (> 0.041); NBR (< -0.194)

The algorithm is designed to monitor the spectral signature and look for a persistent burn signal over a five day moving window. The CRAB product is generated

for each season between 2003 and 2012; however, the algorithm is computed on a daily time step. Each seasonal output has a corresponding confidence layer, which was determined through using a five day weighting scheme (Conf. = 0.4 day_1 + 0.2 day_2 + 0.1 day_3 + 0.1 day_4 + 0.1 day_5) over five consecutive days to check for signal stability (here day_i represents the original confidence values assigned from the decision tree nodes for the *i*'th day within the five day window). The final output records the date of burn detection, which was assigned on the first day that the spectral thresholds were crossed, within the season and the confidence of burning.

The CRAB product is comprised of two separate decision trees because the biophysical conditions are vastly different between spring and summer. The spring burning conditions are extremely challenging as the excess moisture in the soil from the snow melt lowers the surface reflectance across the full visible – SWIR range with a particularly strong impact on the SWIR range resulting in further diminished spectral separability between burned and unburned fields. In contrast, in the summer soils are substantially drier as compared to the post snow melt period in the spring and fields are typically covered in either crop residue or regrowth of weeds, both detectable in the NIR range. However, even in the summer plowed and wet fields can still be easily confused with burns because of the small difference in reflectance across all bands. Due to these differences, we empirically determined that burned grid cells below a confidence of 60% for the CRAB spring product are not as reliable as in the CRAB summer product and therefore we have applied a mapping confidence threshold of greater than 60% for the CRAB spring product in the subsequent analysis.

Figure 2.9 illustrates an example of the CRAB output for summer 2012 for all confidence values. The grey denotes the cropland region. The inset highlights the grid cell based Julian Date of burn detection.

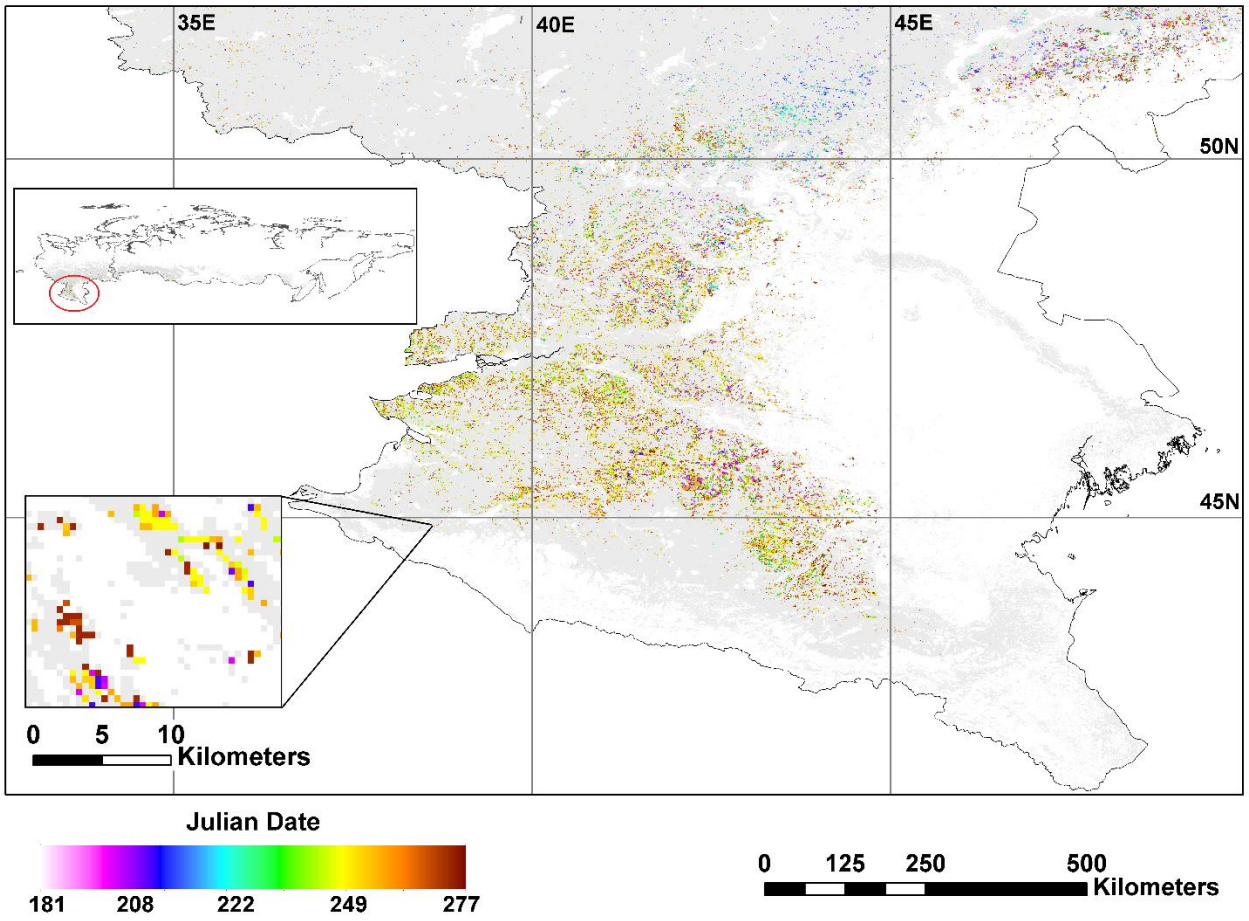

Figure 2.9: Summer 2012 CRAB product output. A subset of Russia (red circle, top insert) is shown for display purposes. Colors represent Julian Date of burn. Grey area denotes the Russian crop mask.

Upon creation of the CRAB seasonal burned area maps and corresponding confidence layers, the product's accuracy was assessed using the VHR validation samples and compared to the MCD45A1, MCD64A1 and MCD14ML products. All three burned

area products (MCD45A1, MCD64A1 and CRAB) are designed to map burned area and are based on differing principles. MCD45A1 is based on the deviation from the anticipated reflectance change due to burning with applied corrections for BRDF. MCD64A1 is based on the dynamic spectral thresholds generated from a burn sensitive vegetation index coupled with the inclusion of the MODIS active fire observations and a measure of the change in temporal texture following a potential burn. CRAB is a decision tree based algorithm constructed from a suite of spectral bands and indices with corrections for BRDF.

2.4: Results and Discussion

2.4.1: Accuracy Assessment

An accuracy assessment was carried out on CRAB using a ten day window prior to the date of the validation samples. Due to cloud obscuration of the land surface, a ten day window is required to enhance the probability of mapping the cropland burns. Our decision to use a window of this duration was based on the transient nature of cropland fires and the potential of plowing or reseeding soon after a burn. The persistence of these low biomass burn scars varies as a function of climate, fuel load and crop management practices. Several studies focusing on grass dominated systems such as cropland, savanna and grasslands have found that the persistence of the burn scars is short lived (days to weeks) and therefore long temporal windows are likely to lead to an increase in burn area omission errors (Korontzi et al., 2012; Trigg and Flasse 2000). In addition, for regions with double cropping, such as in the Mississippi River Valley, a field can go from harvest to burning and reseeding in a few days to two weeks (Korontzi et al., 2012). This quick turnover and short burn-scar persistence justifies the use of a comparatively short

temporal window. While the optimal duration of this value is debatable, it is evident that a 30 day window is too long as the burn signals are virtually always lost to weathering and/or plowing within this period of time (Chuvieco et al., 2008).

Here the samples were applied to the Julian Date of burn detection as described by the CRAB product. If the pixels associated with the validation samples were flagged as burned within a ten day window prior to the date of the image, then it was counted in the accuracy assessment. An assessment using the VHR spring and summer validation samples was carried out between CRAB, MCD45A1 and MCD64A1 (Table 2.4). Additionally MCD14ML was assessed to identify the number of CRAB burn pixels that were intersected by a 1 km radius buffered active fire point within ten days of the burn detection date.

Table 2.4: Spring and summer accuracy assessment comparison between the Cropland Regional Area Burned (CRAB) product and the two official MODIS burned area products MCD45A1 and MCD64A1. The spring assessment was carried out using the full range of CRAB confidence values and greater than 60% confidence.

		Commission Error			**Omission Error**
		Residue	**Bare**	**Plow**	**Burn**
Spring	**CRAB (all conf.)**	9.11	9.97	10.36	86.98
	CRAB (> 60%)	0.00	0.00	0.00	99.42
	MCD45A1	0.00	0.00	0.86	97.30
	MCD64A1	0.00	0.00	0.00	99.19
Summer	**CRAB (all conf.)**	0.45	1.28	4.27	96.86
	MCD45A1	0.60	0.91	2.66	92.65
	MCD64A1	0.00	0.00	0.00	96.73

All four products (MCD45A1, MCD64A1, MCD14ML and CRAB) were unable to map approximately 95% of the burn validation samples during summer (93%, 97%, 90% and 97% omission errors, respectively), while in spring there was an improvement using the CRAB product with full confidence values (97%, 99%, 92% and 87% omission error, respectively); however, applying a confidence of greater than 60% led to a CRAB omission error of 99%. The reduced commission error in the MCD45A1 and MCD64A1 products as compared to the CRAB product are due in part to the restrictiveness of their algorithm's spectral mapping thresholds. The mapping thresholds for CRAB can be constrained further to reduce commission error; however, this causes an increase in omission error.

2.4.2: CRAB Analysis

The total Russian cropland area as defined by the crop mask totals approximately 215×10^4 km^2. Using the full range of confidence values, our estimated annual burned area from CRAB within the Russian cropland ranged from approximately 121×10^4 km^2 (2007) to approximately 144×10^4 km^2 (2010), which equates to roughly 57 – 67% of the total cropland area. Applying a mapping confidence value of greater than 60% on the spring output and using the full range of confidence values on the summer output, the annual burned area estimate decreased to between approximately 3.54×10^4 km^2 (2003) and 7.92×10^4 km^2 (2010), which equates to roughly 1 – 4% of the total Russian cropland area. The majority of the burned area occurred in spring (defined 1 March – 30 June) as compared to summer (defined 1 July – 30 September). Table 2.5 and Table 2.6 summarize the seasonal burned area estimates for CRAB (full confidence and greater

than 60% confidence values), MCD45A1 and MCD64A1 (see section 2.4.3 for intercomparison between the three BA products).

Table 2.5: Spring cropland burned area (units: $\times 10^4$ km^2 = Mha) comparison between CRAB, MCD45A1 and MCD64A1.

	Spring: Total Burned Area in Russian Croplands			
	CRAB (all conf.)	**CRAB (> 60%)**	**MCD45A1**	**MCD64A1**
2003	126	1.91	6.87	4.78
2004	133	2.70	2.74	0.98
2005	121	1.36	1.41	0.49
2006	128	3.19	4.90	1.45
2007	118	2.70	3.09	1.05
2008	135	2.31	7.79	6.18
2009	139	2.17	5.74	3.00
2010	138	1.86	2.32	0.64
2011	132	2.20	3.27	1.12
2012	131	1.40	3.66	1.32

Table 2.6: Summer cropland burned area (units: $\times 10^4$ km^2 = Mha) comparison between CRAB, MCD45A1 and MCD64A1.

	Summer: Total Burned Area in Russian Croplands			
	CRAB (all conf.)	**CRAB (> 60%)**	**MCD45A1**	**MCD64A1**
2003	1.63	0.00075	2.04	0.54
2004	2.34	0.0022	2.12	1.08
2005	3.43	0.0014	3.61	1.64
2006	3.38	0.0041	3.40	1.35
2007	3.92	0.0049	4.47	1.89
2008	3.60	0.0020	5.49	2.12
2009	4.86	0.0012	3.21	1.27
2010	6.06	0.0029	4.32	1.21
2011	3.70	0.0025	2.68	0.62
2012	5.63	0.0015	4.01	0.66

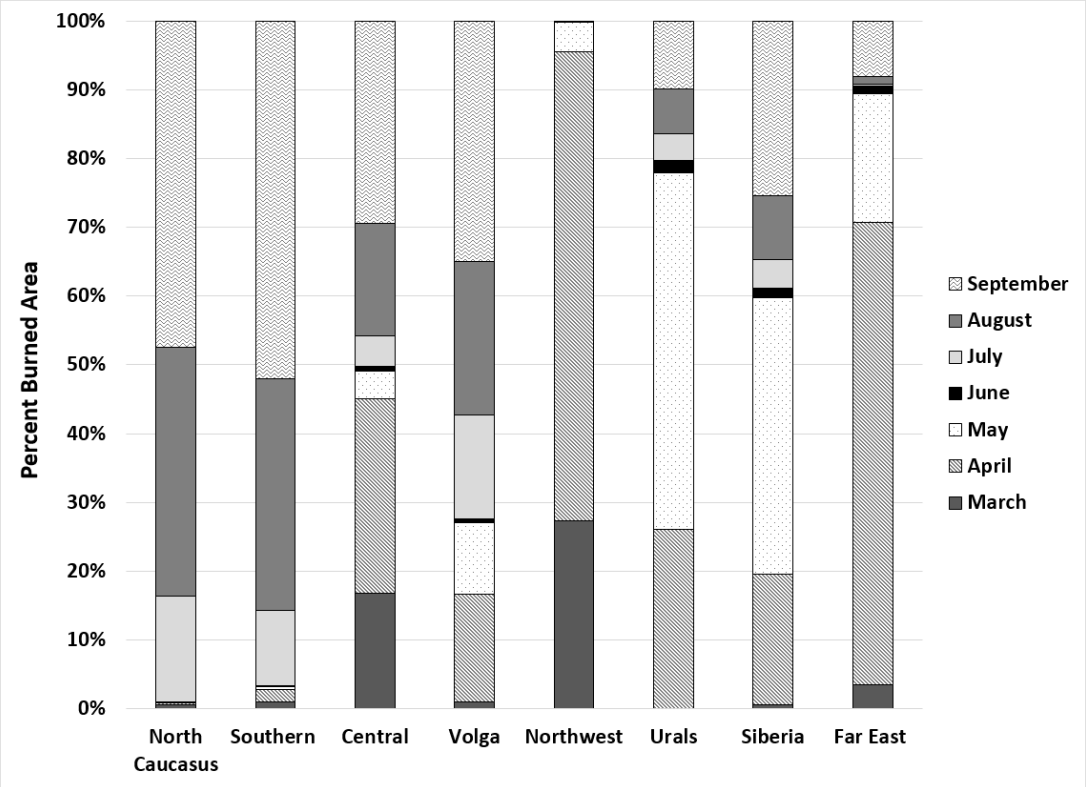

Figure 2.10: Temporal distribution of the average fractional burned area by month between 2003 and 2012 for the Russian cropland region partitioned by Federal Districts (okrugs).

Subdividing Russia into administrative units (oblasts) and Federal Districts (okrugs) revealed further information on the spatial and temporal patterns of burning. Analysis on the average fractional burned area per oblast between 2003 and 2012 (see supplementary material Table S2) revealed the general patterns of burned area produced by CRAB correspond with the known winter wheat and spring wheat oblasts. Additionally temporal analysis of the average fractional burned area between 2003 and 2012 revealed information about the relative contribution of spring and summer burning between the various okrugs (Figure 2.10, supplementary material Table S3). CRAB reported larger contributions of spring burning in the eastern okrugs whereas the southern

and western okrugs contained a higher contribution of burning in the summer and early fall. This pattern is consistent with the winter and spring wheat agricultural practices in the region.

2.4.3: Intercomparison between CRAB, MCD45A1, and MCD64A1

When comparing the magnitude of mapped burned area for each of the three burned area products within the Russian cropland region it is clear that MCD64A1 and CRAB follow similar patterns of burned area frequency in the spring, while MCD45A1 contains considerable spikes (Figure 2.11). Whereas in the summer, MCD45A1 and CRAB show considerable spikes throughout the season with MCD64A1 fairly muted in comparison (Figure 2.12). The similarity in mapped burned area between MCD45A1 and CRAB may be related to external factors such as missed clouds or BRDF effects. For illustration purposes one example is shown for each season but the relative patterns are consistent over all years (2003 – 2012).

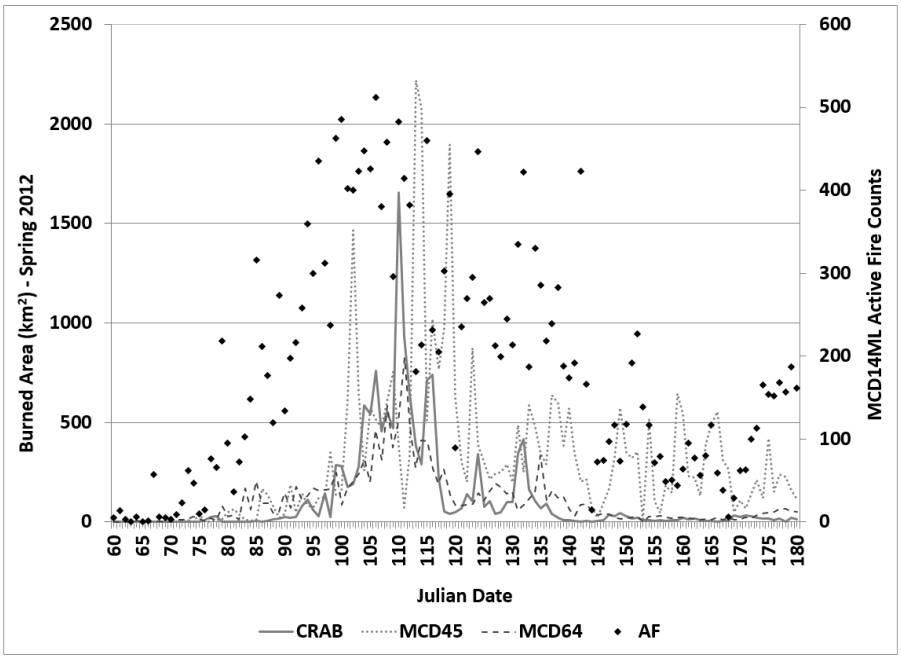

Figure 2.11: Daily burned area (km^2) left axis and MODIS active fire counts right axis during spring 2012 for all Russian cropland MODIS tiles. All confidence values greater than 60% were included for the CRAB product.

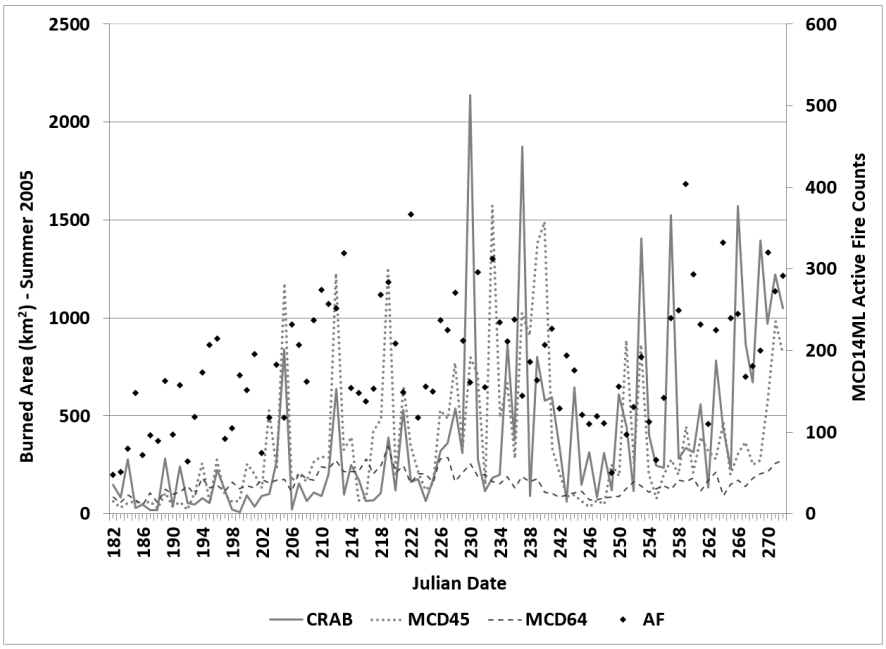

Figure 2.12: Daily burned area (km^2) left axis and MODIS active fire counts right axis during summer 2005 for all Russian cropland MODIS tiles. All confidence values were included for the CRAB product.

When comparing the three burned area products' seasonal totals (Figure 2.13), MCD45A1 generally has the higher magnitude of burning in the summer; however, there are a few years where CRAB and MCD45A1 have very similar magnitudes. Interestingly CRAB, and to some extent MCD45A1, saw a large spike of burned area in summer 2010 which was the season of extreme drought in Russia where widespread fires in forests and cropland in European Russia were reported.

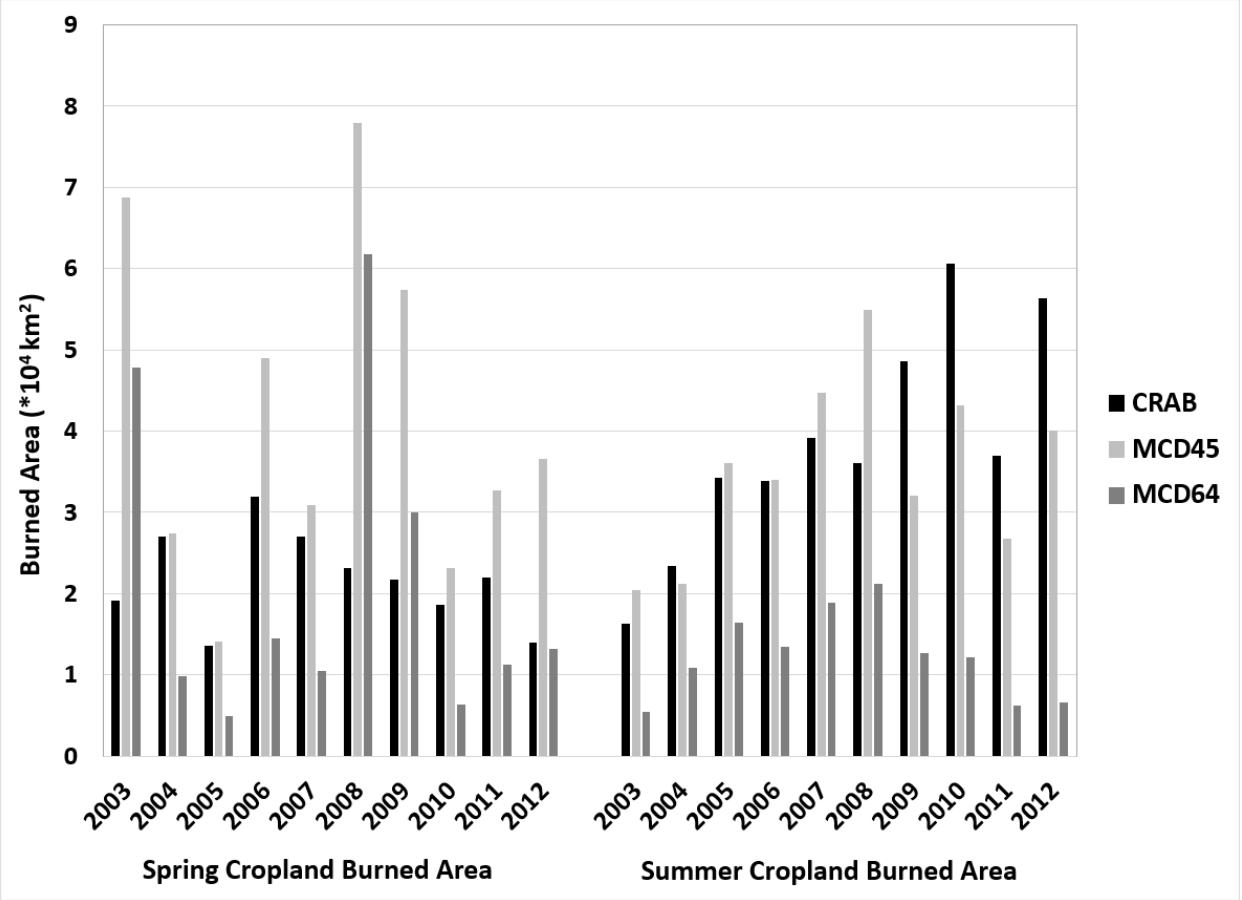

Figure 2.13: Spring and summer cropland burned area (units: × 10^4 km^2 = Mha) comparison between CRAB (all confidence in fall and > 60% confidence in spring), MCD45A1 and MCD64A1.

Although based on different mapping algorithms, the similarities in the general burned area patterns between the three BA products reveals that using MODIS to map cropland burned area in Russia is not the solution as all three products contain large omission errors (Table 2.4) thus are not representing the true burned area within Russian croplands well.

2.5: Challenges of Mapping

Successfully developing an accurate estimate of cropland burning in Russia is a difficult task due to the inherent challenges in meeting the particular mapping requirements. Cropland fires are transient in nature in comparison to grassland or forest fires. The short duration of the cropland burn scars, matched with the subsequent plowing of the fields, makes it difficult to capture the entirety of the cropland burned area without daily clear observations of moderate (10 – 50 m) spatial resolution over agricultural areas. Analysis carried out on the Russian cropland region between 2003 and 2012 (see section 2.3.1 for additional details) shows that on average early afternoon observations from Aqua provided 51 clear views per growing period (defined as 1 March – 30 September) with a range from 6 to 113 clear views; whereas Terra provided 61 clear views per growing period with a range from 14 to 114 clear views. Upon combination of the Aqua and Terra clear view time series, the analysis found an increase in the number of clear views with an average of 106 clear views per growing period with a range from 24 to 199 clear views (Figure 2.14).

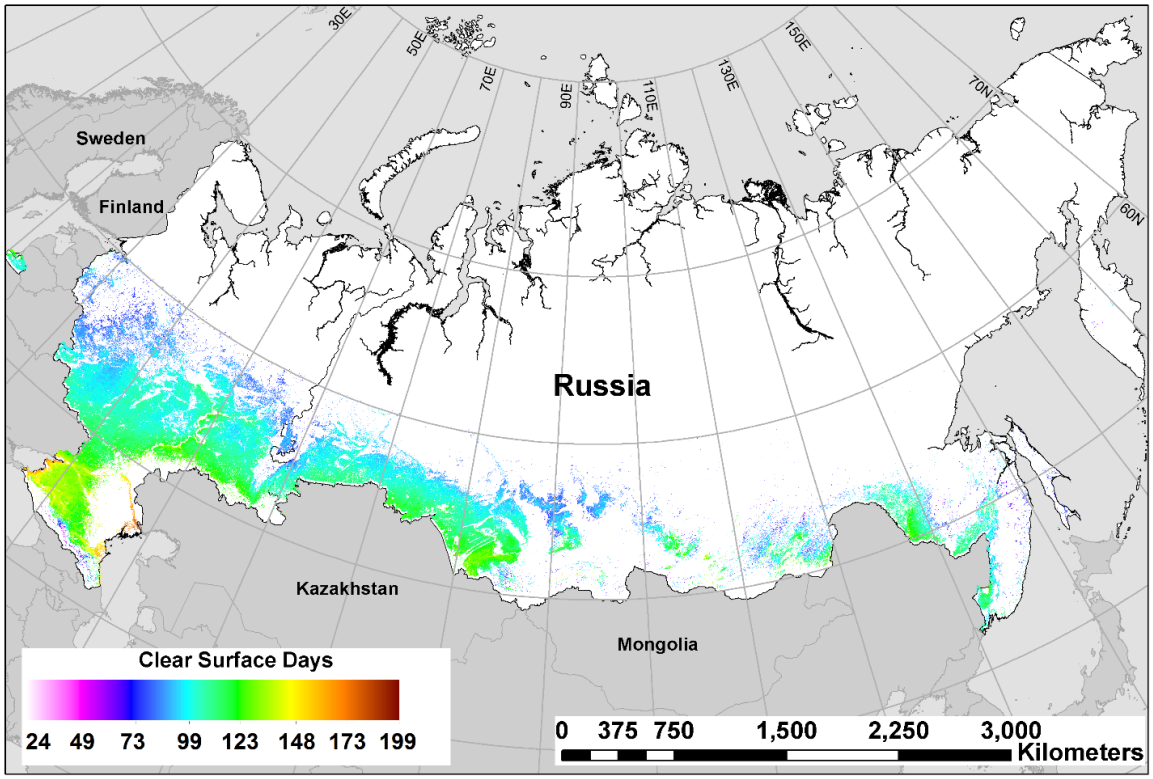

Figure 2.14: Mean number of cropland clear surface days per year between 1 March and 30 September (2003 and 2012) as defined by the 1 km MODIS quality assessment bit thresholds as set out in Section 2.3.1. This image corresponds to the combined Aqua and Terra dataset for the Russian cropland region.

The best conditions were found in the eastern section of Rostovskaya Oblast, while the worst conditions were found along the southern tip of the Russian cropland near the Ingushetia Republic. Although there was an increase in the number of clear views using the combined Aqua and Terra clear surface view time series, the frontal systems that move across Russia lead to periods of several days to weeks with no clear view of the surface. This inability to view the surface for several consecutive days likely leads to underestimation in cropland burned area.

Although MODIS has a daily overpass, this high temporal frequency is countered by a coarse (≥ 500 m) spatial resolution. As previously shown (Figure 2.4, Table 2.1) the median size of observed burns is 40 ha (< 2 MODIS 500 m grid cells) with a substantial amount of partial burning within the observed samples, therefore when using the MODIS 500 m daily surface reflectance data, the burned pixel's spectral signature is reduced in comparison with the surrounding unburned pixels. This decrease in spectral signature separability between field state types (burn, residue, plow and bare) further amplifies the difficulty in distinguishing between burned and plowed fields. This is a particular problem in the Mollisol soil regions, where the soil is characterized by its mollic epipedon which gives it a distinctive dark, almost black, appearance (Grunwald, 2015). As compared to other soil orders in the 350 – 2500 nm spectral range, Mollisol soils have the lowest reflectance curves with reflectance values less than 0.1 due to the high organic matter content (Sahoo, 2013). The low spectral reflectance throughout the visible, Near Infrared (NIR) and Shortwave Infrared (SWIR) portions of the electromagnetic spectrum can lead to further challenges in distinguishing Mollisol soils from older burn scars thereby leading to an increase in commission error and overestimation of burned area.

Spectral analysis was carried out on the VHR samples located in the dark soil (Mollisol, Vertisol and Chernozem; 92% of total VHR samples) regions and the light soil (Alfisol; 8% of total VHR samples) regions of the Russian cropland area both separately and combined. The dark soil samples showed no spectral separability between the burn and unburned categories with almost complete overlap between all four categories in all bands and spectral indices set out in section 2.3.3, while the light soil samples showed some separability between the classes. Since the Russian cropland region contains

predominately dark soils, we based the algorithm on all the samples regardless of soil type.

In addition to the low spectral contrast, the coarse (≥ 500 m) spatial resolution of MODIS can lead to further challenges during the field-to-pixel matching process. Matching the irregularly shaped field outlines to a MODIS 500 m grid cell further reduces the purity of the burn signal. The irregular shape of the fields and burn samples resulted in many of the matched pixels incorporating spectral signatures from surrounding areas. Analysis on the samples found that on average approximately 40% of the masked MODIS grid cells (Figure 2.15, light grey squares) were outside of the field boundary (Figure 2.15, dark grey shapes) and on average approximately 25% of the field boundaries were outside of the masked MODIS grid cells.

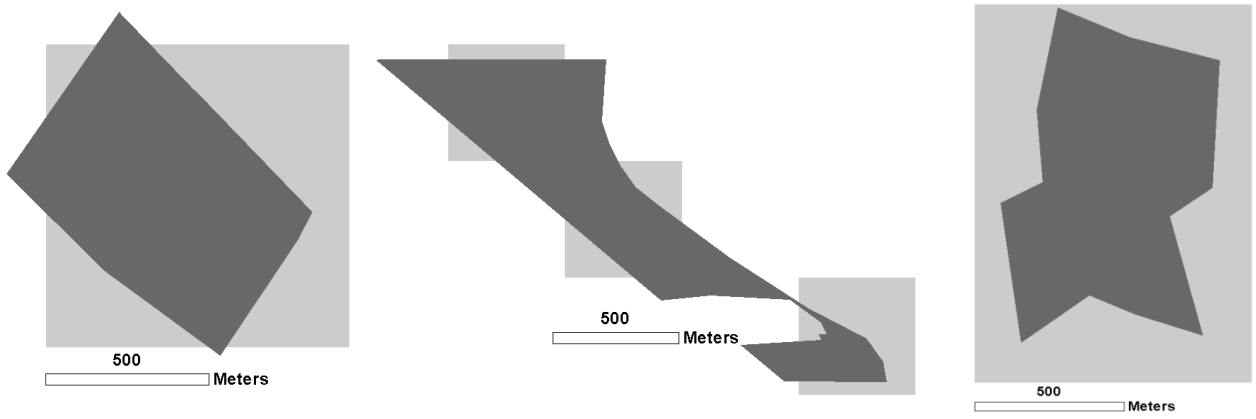

Figure 2.15: MODIS grid cell area masks (light grey squares) and field boundary area (dark grey shapes) overlay analysis.

Furthermore, at higher latitudes MODIS data are comprised of multi-angular observations compiled from the best available pixels acquired from as many as four overpasses to generate the daily image for Aqua and Terra (Schaaf et al., 2002; Loboda et al., 2011). Combining these multi-angular observations with the relative day-to-day variations in viewing and illumination geometries, in addition to the impacts of cloud cover and changing surface properties, leads to substantial BRDF effects. These effects produce radiometrically inconsistent views of the surface thereby further impacting the stability of the burn spectral signature.

2.6: Conclusion

Although agricultural burning is banned in Russia it is still a widespread practice (Pettus, 2009) and the challenges associated with mapping cropland burning have led to a wide range of burned area estimates. Accurate monitoring of cropland burning is an important task as countless studies have relied on these estimates for use in emission calculations for air quality and human health studies, in addition to studies on the impact of emissions on climate forcing (e.g. Jacobson, 2004, Lin et al., 2012; McCarty et al., 2012; Stohl et al., 2006; Witham and Manning, 2007).

In this study, we assessed three very different MODIS-based burned area algorithms which operate on the same input data and based on our analysis we concluded that coarse resolution (≥ 500 m) instruments, such as MODIS, are not optimal for mapping these small, short-lived fires. Our study demonstrates this through the analysis of the current MODIS-based products (MCD45A1 and MCD64A1) and our own custom MODIS-based burned area product. Clearly we did not complete an exhaustive analysis of all possible algorithms and although there are other algorithms we have no

recommendations about what these should look like. In addition, we were also able to identify major deficiencies in the MODIS data related to mapping cropland burning which we addressed in section 2.5.

Ultimately, the current coarse resolution (≥ 500 m) satellite capabilities are not adequate for measurement of burned area associated with agricultural fires. Coarse resolution (≥ 500 m) sensors like MODIS have the advantage of daily overpasses which are essential when mapping a transient process such as cropland residue burning; however, the small spatial scale of these burns requires moderate (10 – 50 m) spatial resolutions. The current moderate (10 – 50 m) resolution sensors like Landsat have the higher spatial resolutions; however, the 8 – 16 day repeat cycle (considering the possible constellation of two satellites as was achieved with Landsat 5 and 7 and is currently achieved with Landsat 7 and 8) is a limitation in mapping cropland burning. The preference to burn the remaining post-harvest residue as close to planting as possible leads to an increased likelihood of overlooking the burn signal without daily clear surface observations (Korontzi et al., 2006; Shroyer et al., 2013). Finally the very high resolution (< 5 m pixel) sensors like QuickBird have the high resolution needed to identify field state (plowed, burned, growing crop, or harvested); however there is no systematic data acquisition strategy which ultimately leads to opportunistic observations that do not support time series analyses. Future opportunities to accurately map cropland burned area may arise with the Sentinel-2 and Landsat constellation mission.

Chapter 3: Quantifying the potential for low-level transport of black carbon emissions from cropland burning in Russia to the snow-covered Arctic

3.1: Introduction

The recently published 2016 Arctic Report Card, utilized by the National Oceanic and Atmospheric Administration's (NOAA) Arctic Program to track the environmental changes in the Arctic relative to historical records, has reported persistent warming and loss of sea ice in the Arctic with historical low spring snow cover extents (NOAA, 2017). Over the past 30 years, the Arctic surface air temperature has risen at rates more than double of those anywhere else on Earth. This has resulted in significant regional and global impacts ranging from biophysical effects, like decreases in surface albedo with the loss of sea ice, to altering biogeochemical cycles through increased release of stored carbon and methane from the melting of permafrost, to impacts on migratory patterns of birds and animals (EPA, 2016; NOAA, 2017; NSDIC, 2017). Between October 2015 and September 2016, the average annual surface air temperature anomaly for land above 60°N was +2.0°C (relative to 1950 – 2010 baseline) as compared to the global anomaly of approximately +0.9°C; however, the seasonal variation in temperature anomaly is much more pronounced (NOAA, 2017). In winter 2016, several locations within the Arctic recorded January anomalies of +8°C. The impacts of these increased temperatures have already been reflected in land and sea ice extents. As previously mentioned in Chapter 1, according to the NSIDC, the Arctic sea ice area has decreased by approximately 13.3% per decade since 1979, while ice sheets on Iceland and Greenland

have lost approximately 281 billion metric tons of ice per year since 2002 (NSIDC, 2017).

The presence of short-lived climate pollutants, such as BC and methane, within the Arctic are further contributing to the amplification of warming in this already vulnerable region. One of the dominant sources of pollution above the Arctic Circle is open-source biomass burning (Hegg et al., 2009; Koch and Hansen, 2005; Pettus, 2009; Stohl et al., 2006; Yttri et al., 2014). As previously addressed in Chapter 1, BC is a product of incomplete combustion of carbonaceous fuels and its strong climate forcing has led to substantial short-term impacts in the Arctic. Unlike long-lived greenhouse gases, BC has a short atmospheric lifetime, on average approximately one week (Cape et al., 2012; Koch and Hansen, 2005), with temporal variations related to the type of deposition (wet or dry) and atmospheric processes, for instance, mixing with other aerosol compounds. Atmospheric removal of BC occurs within several days to weeks and the mixing of BC with other substances occurs within 1 – 5 days (Bond et al., 2013; Jacobson, 2001). Upon emission, BC is a hydrophobic particle, however, soon after the BC particle becomes mixed with other atmospheric aerosols, gradually becoming more hydrophilic (AMAP, 2015; Cooke et al., 1999). As these reactions with surrounding atmospheric chemical compounds continues, the likelihood of removal via precipitation or cloud scavenging increases. The precise influence of BC will depend on the underlying properties of the other chemical compounds; however in general BC has both direct and indirect climatic effects.

Although air pollution in the Arctic is comprised of several other components, including, ozone, sulfate aerosols, and methane this study emphasizes BC primarily due

to the effectiveness of its absorptive properties. Although studies have begun addressing the impacts of other pollutants, emphasis still lies with BC and the impact on the Arctic. Despite the ongoing scientific progress, major challenges lie in the inability to accurately simulate the temporal and spatial variations in Arctic air pollution and to accurately quantify the contribution of air pollution from the source regions (e.g. Monks et al., 2015). Although northern mid- and high latitudes have been identified as major source regions for Arctic pollution, there is still no consensus of their relative importance (Hirdman et al., 2010; Shindell et al., 2008). Shindell et al. (2008) examined the response of Arctic air pollution concentrations from various emission perturbations from Europe, East- and South Asia, and North America using simulations from 17 transport models from the Task Force on Hemispheric Transport of Air Pollutants (HTAP) project. Their modelled outputs showed large discrepancies between models. The largest contributing factor to these discrepancies was shown to be related to the uncertainty in modeling physical and chemical processes, the input emission inventories, and the dry transport differences between models (Shindell et al., 2008). Clearly, developing accurate crop residue burning emission inventories is a crucial as these estimates are fundamental inputs to these complex chemical-transport models. Unfortunately, crop residue emission estimates are notoriously difficult to quantify accurately as they are typically calculated following the equation originally developed by Seiler and Crutzen (1980):

$$\text{Emissions} = A * B * CE * e_i \quad (1)$$

Here, A represents the extent of burned area, B is the fuel load estimate, CE is the combustion efficiency, and e_i is the emission factor for the specific species of interest. Cropland burned area (A) is a key requirement in the calculation. As shown in Chapter 2,

current burned area (MCD5A1, MCD64A1 and CRAB) products were unable to map approximately 95% of the validation VHR burn samples within the Russian cropland. This inability to accurately map cropland burned area has large implications in both the magnitude and spatio-temporal patterns of calculated emissions. Fuel loads (*B*) are typically derived from yield statistics using a yield-to-residue coefficient factor. The accuracy of this data are dependent on both the data source and the spatial resolution. For Russia, the yield data are typically produced at the oblast level; however, variations between state official statistics and local expert data (compiled by USDA Foreign Agricultural Service, Mark Lindeman pers.comm.) has been identified in the yield tables. Finally, the values for the combustion efficiency (*CE*) and the emission factor for species i (e_i) are typically based on laboratory and experimental analyses with a number of emission based studies (e.g. McCarty et al., 2012; Wiedinmyer et al., 2011) utilizing the values quoted in a study by Andreae and Merlet (2001) which is defined by the authors as "best guess". Although numerous estimates of BC emissions from cropland burning in Russia have appeared in the scientific literature (e.g. Hao et al., 2016; McCarty et al., 2012), they are unlikely to present a realistic assessment as every component of the equation used to calculate BC emissions is either known to be highly inaccurate (e.g. burned area) or represents a "best guess".

At present, the majority of previous studies have utilized atmospheric chemical-transport models, such as GEOS-Chem, to quantify the contribution of BC emissions from northern mid-latitude source locations on the Arctic (e.g. Qi et al., 2017). Some have focused on modelled trajectories from atmospheric trajectory model outputs, such as NOAA's Hybrid Single Particle Lagrangian Integrated Trajectory (HYSPLIT) model, to

identify potential source regions (e.g. Larkin et al., 2012; Stohl et al., 2007). Atmospheric chemical-transport models (e.g. GEOS-Chem) typically utilize biomass burning emission estimates from sources such as the Global Fire Emissions Database (GFED; Giglio et al., 2013). The updated GFEDv4 has been released to include small fires (detailed in Randerson et al., 2012) and crop residue coefficient factors from Akagi et al., (2011); however, the underlying cropland burned area and emission coefficients are still plagued with the previously addressed uncertainties. Atmospheric trajectory models (e.g. HYSPLIT) are the other main type of model used in studies identifying potential BC emission transport to the Arctic through simulating atmospheric trajectories, primarily back trajectories, and dispersions (Stein et al., 2015). Emission estimates are also needed if users require air pollutant concentration information over the course of the trajectory.

This inability to accurately quantify crop residue emissions or determine their spatial and temporal variability is a key weakness in these complex atmospheric chemical-transport models. The added complexity produces a false sense of precision and accuracy which cannot be easily verified at any level. Given the combination of uncertainty surrounding the cropland burned area estimates, the yield values, and the coefficient factors, this study does not attempt to include any quantification of the magnitude of successfully transported cropland emission estimates to the Arctic. Instead, this study focuses on quantifying the fraction of cropland burning in Russia which potentially contributes to the deposition of BC on snow in the Arctic. This study does this through the development of a simple transport model based on wind direction, wind speed, and precipitation to identify potential BC source regions within the Russian cropland between 2003 and 2015. Since smoke injection heights for cropland fires are

lower than other biomass burns, due to the generally low intensity of fire events and limited fuel loads, the likelihood of successful transport decreases with shallower injection heights. Thus to address this impact on potential transport, the transport model will also allow for varying injection heights within the range of the literature (ranging between 500 m and 1500 m - Soja et al., 2012; Martin et al., 2010; Ichoku and Kaufman, 2005).

Quantifying the potential transport of BC emissions from Russian cropland is an important task as several studies have recently indicated that biomass burning sources as far south as 40°N are assumed to significantly impact the Arctic region (e.g. Cheng, 2014; Liu et al., 2015; Quinn et al., 2011; Sharma et al., 2013; Warneke et al., 2010). As previously addressed in Chapter 2, Russia is the world's fifth-largest wheat exporter with a cropland area of approximately 215×10^4 km^2, primarily located between 40°N and 55°N (Figure 3.1; FAOSTAT, 2015b; Hall et al., 2016). Although open-source burning is banned, based on visual analysis of VHR satellite imagery it is still a common practice often used to clear crop residue after harvest and before the next planting.

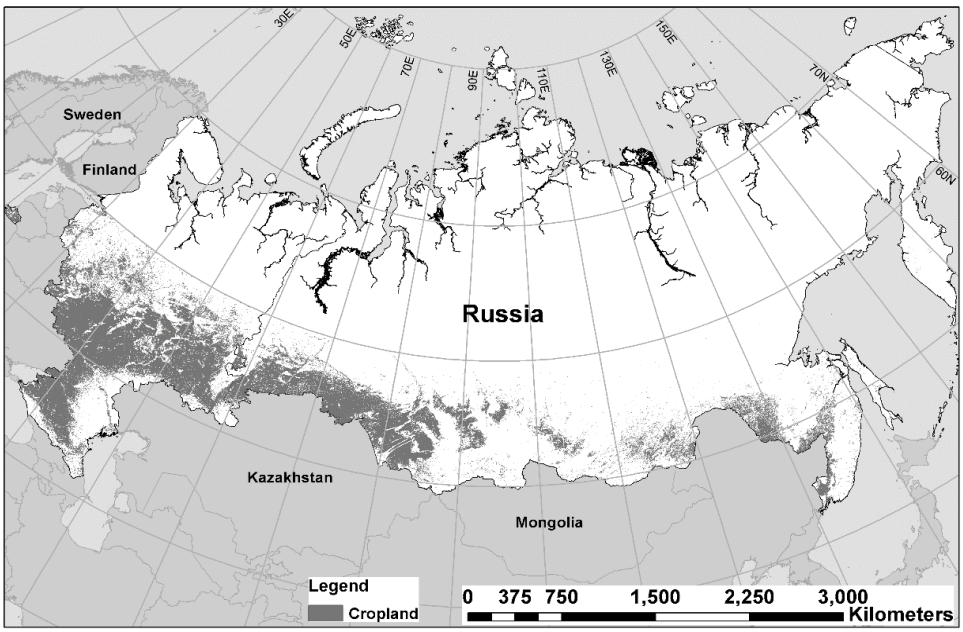

Figure 3.1: Russian cropland area as defined by the IGBP cropland/ natural vegetation mosaic.

Finally, in this research chapter I quantify the fraction of cropland burning in Russia that potentially contributes to the deposition of BC on the Arctic snow with a particular focus on the spatial and temporal variability of the transport patterns. This is undertaken by the development of a simple transport model which is described in section 3.3. The results of the transport model are highlighted in section 3.4 with the discussion (section 3.5) and conclusion (section 3.6) addressing important consequences of these transport results within the Arctic environment.

3.2: Data

Considerations of the impact of wind speed, wind direction, and precipitation on the analysis will use the European Centre for Medium-Range Weather Forecasts' daily, 0.75° resolution U- and V-Wind and Total Precipitation (mm) datasets from the ERA-Interim Reanalysis product (Berrisford et al., 2011). The wind datasets were analyzed at

the following five pressure levels; 1000mb (~110 m altitude), 975mb (~323 m altitude), 950mb (~540 m altitude), 925mb (~762 m altitude) and 900mb (~914 m altitude) to account for the reported variability of cropland burning emission injection heights. Total precipitation was evaluated at the surface. Daily averages of wind direction (*d*, units: rad) and speed (*s*, units: ms^{-1}) were computed using the *U*- and *V*-Wind vectors in the following equations:

$$d = \arctan\left(\frac{v}{u}\right) \tag{3.1}$$

$$s = \sqrt{(u^2 + v^2)} \tag{3.2}$$

The goal of this assessment is to quantify the potential deposition over snow and ice covered ground above 60°N. Therefore, daily Arctic snow masks were developed for the period between January 1, 2003 and December 31, 2015 using the standard daily, 0.05° collection 6 MODIS snow cover product at climate modeling grid (0.05°) resolution (MOD/MYD10C1; Hall and Riggs, 2016). Primarily the Terra-based product (MOD10C1) was used in the construction of the snow masks while the Aqua-based product (MYD10C1) was used to supplement any missing dates. This was due to the non-functional detectors in band 6 (short wave infrared band: 1628 – 1652 nm) on-board the MODIS instrument on Aqua (Riggs and Hall, 2015).

The active fire (MCD14ML; Giglio et al., 2003) Collection 6 product was used to identify ongoing burning within the Russian croplands between 2003 and 2015. Chapter 2 shows that no current available burned area product is able to capture the magnitude of crop residue burning in Russia. While active fire detections are not doing much better in terms of capturing the extent of burning, they very accurately estimate the timing of

burning. Therefore, this study will utilize the MODIS active fire dataset to represent the observed burning within the Russian croplands. To ensure analysis was performed over the Russian cropland region, a crop mask was created using a composite of the cropland and cropland/ natural vegetation mosaic layers from the 500 m Level 3 IGBP classification scheme within the MODIS land cover dataset (MCD12Q1; Friedl et al., 2010).

3.3: Methods

The transport is estimated using the daily precipitation, wind direction, wind speed, snow extent and hourly active fire locations between 2003 and 2015. All analysis was carried out at a 0.75° resolution between 0° – 180°E and 30° – 90°N. The spatial domain was chosen to encompass the Russian Federation and the majority of the Arctic (here defined as above 60°N).

3.3.1: Arctic snow cover extent

Creation of the snow cover extent required the snow cover percentage (Day_CMG_Snow_Cover), cloud cover percentage (Day_CMG_Cloud_Obscured) and the quality assessment (Snow_Spatial_QA) layers from the MOD/MYD10C1 datasets. The Arctic region remain snow-covered during a large portion of the year with a relatively short snow-free season, except for regions surrounding the pole. However, due to various reasons, the daily MODIS snow cover estimates are strongly impacted by gaps in observations, among the most substantial is the absence of solar irradiance during the polar nights (when surface observations through optical wavelengths is virtually impossible) and the substantial cloud cover in the Arctic regions during the sunlit period

(Schiffer and Rossow, 1983). In this analysis, snow cover is considered present until five consecutive clear (i.e. not impacted by cloud cover) land surface observations within a given grid cell remain snow-free. A five day window was chosen based on the observed persistent cloud cover patterns with the need to avoid late spring and early fall snow events which do not represent established seasonal snow cover. Similarly, snow cover is considered absent until five consecutive clear land surface observations within a given grid cell show the presence of snow. These two periods are subsequently referred to as "snow cover melt" and "snow cover establishment" with the details of the methodology developed to extract these values described below. The snow cover melt and snow cover establishment date layers were developed annually to cover the Arctic region above 60°N between 0° and 180°E.

The daily snow cover percentage layer was filtered using the quality assessment layer to retain only values of "best" and "good" quality (QA ≤ 2). All grid cells impacted by polar night conditions were considered snow covered. All grid cells not impacted by the lack or solar irradiance were subsequently classified as:

- Snow (1): filtered snow layer value ≥ 50% (majority snow cover)
- Cloud (2): filtered snow layer value < 50% and cloud percentage ≥ 50%.
- Water (3): values in any of the 3 original layers that were flagged as ocean, cloud obscured water, inland water, or lake ice.
- Fill (4): QA > 2 or any of the layers that were flagged as fill, no retrieval, or not mapped.
- No Snow/Clear (5): filtered snow layer value < 50% and cloud percentage < 50%.

1) A grid cell is considered permanent snow cover if it does not reach the snow melt criteria (see below) by October 1 (Julian Date 274 or 275 for leap year).
2) Snow establishment must follow snow melt.
3) If snow establishment does not occur by Julian Date 360, it is automatically assigned a snow establishment date of 365 (or 366 for leap year).

To extract the snow melt and snow establishment layers, a 5 day moving window is applied to each grid cell. Snow melt date is recorded within each 0.05° grid cell as the first date of a 5 consecutive clear (not cloud impacted) period of observations where land surface is reported as snow-free. A grid cell is considered permanently covered by snow if it does not reach the snow melt criteria by October 1 (Julian Date 274 or 275 for leap year). Snow establishment date must follow the snow melt date and is recorded as the first date of a 5 consecutive clear period of observations where land surface is reported snow covered. If the algorithm fails to determine the snow establishment date by Julian Date 360, it is automatically assigned a snow establishment date of 365 (or 366 for leap year). The output contains values for each grid cell that represent either a Julian Date or a reserved value indicating water or permanent snow cover. The 0.05° grids are aggregated to 0.75° to match the resolution of the meteorological variables from ERA-Interim Reanalysis product. During the aggregation, the median value (Julian Date) for the date of snow melt and establishment of the 15 x 15 0.05° grid cells was recorded into the corresponding 0.75° grid cell.

3.3.2: Cropland burning source locations

The MODIS orbital overlap provides the opportunity for much more frequent observations of the land surface than the nominal "daily" temporal scales. The date and time of fire detections were utilized to create hourly cropland burning layers between 30° – 90°N and 0° – 180°E. The specific time of detection was rounded to the nearest full hour following equation 3.3:

$$\begin{gathered} if\ (MM > 30)\ and\ (MM\ \leq 59)\ then \\ HHnew = HH + 1 \end{gathered}$$

$$\begin{gathered} if\ (MM \geq 0)\ and\ (MM\ \leq 30)\ then \\ HHnew = HH \end{gathered} \tag{3.3}$$

Here, *MM* represents the minute and *HH* represents the hour. All active fire detections associated with each hour were intersected with the 0.75° grid to create hourly cropland burning source regions within the Russian cropland. These source regions represent the starting burning location and times for the transport algorithm.

3.3.3: Transport algorithm development

The transport algorithm was designed to quantify the potential low-level, long distance transport of hypothetical parcels of BC emissions from cropland burning to snow-covered areas in the Arctic from Russian croplands between 2003 and 2015 within a specified time frame. Previous studies have used a wide range of transport cutoff times ranging from 96 hours up to 20 days (Larkin et al., 2012; Stohl et al ., 2007); however, due to the lower concentrations of BC emissions in crop residue fires as compared to other BC sources, this study has adopted a more conservative cut off time of 96 hours. This 96 hour cut off not only fits within the atmospheric lifetime of BC but has been also

used in a previous study (Larkin et al., 2012) focused on transport of BC from Russia to the Arctic.

The algorithm records the transport time (hours) from each cropland burning source grid cell to the first instance of reaching snow-covered ground in the Arctic. Furthermore, the algorithm records the trajectory of the parcel beyond the first instance of arriving on snow-covered ground above 60°N. The trajectory continues until either 96 hours has elapsed or if the parcel encounters precipitation. For all analysis, it is assumed total washout of BC from the atmospheric column if precipitation is encountered. Although the algorithm assumes that any precipitation will result in the complete wash out of BC from the atmosphere, if this occurs over snow-covered ground above 60°N then the transport will be terminated; however, the mapped output will indicate a successful event (assumed wet deposition on snow) and the time to that snow-covered grid cell will be recorded in the source cell.

The time of travel is calculated using the wind speed (ms^{-1}) and the great circle distance (m) between the center longitude and latitude values of the starting grid cell and the next grid cell. The longitude and latitude values of the next grid cell were determined through the wind direction using the following directional criteria (Figure 3.2).

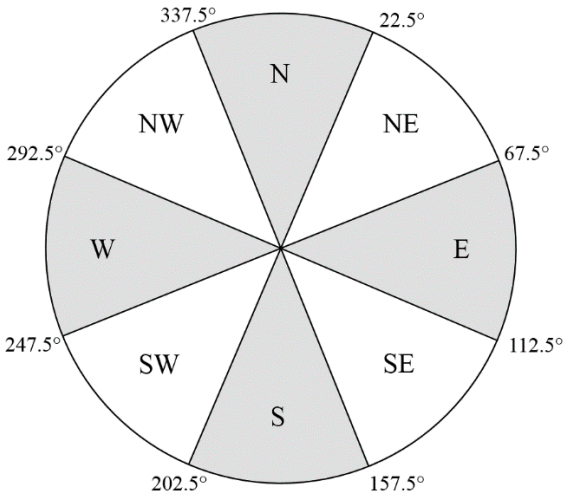

Figure 3.2: Directional criteria for the calculation of the following grid cell based on wind direction.

The time (distance / speed) is then added to the starting UTC time. This continues until the cumulative time has crossed the following day's threshold and then the next day's precipitation, wind direction, wind speed, and snow date are used in the next iteration. The next day's threshold is determined by the following set of criteria, where af_time is the hourly UTC starting time for the crop burning location: day1 = 24 hours – af_time; day2 = 48 hours – af_time; day3 = 72 hours – af_time; day4 = 96 hours – af_time; day 5 = 96 hours. This process continues until the parcel reached snow-covered ground beyond 60°N (within the allowed 96 hours period). The time at this point would be recorded in the starting source grid cell in the mapped output. If no precipitation was encountered or if the time had not exceeded 96 hours, then the trajectory output would continue recording the latitude and longitude values until 96 hour threshold is reached. During the iterations, if precipitation was encountered or if the parcel did not reach snow above 60°N within 96 hours then it is assigned a fill value and considered a "failed"

transporting event. This analysis was carried out at the hourly time step between 2003 and 2015 for five pressure levels (1000mb, 975mb, 950mb, 925mb, and 900mb) to gain an understanding of how the transport potentials are impacted by injection height.

3.4: Results

Quantifying the fraction of cropland burning in Russia that potentially contributes to the deposition of BC on snow in the Arctic requires an understanding of the spatial and temporal patterns of the successfully transported hypothetical emission parcels. Successful transport events are defined as those that represent grid cells producing hypothetical emissions parcels from on-going fires within cropped areas which are projected to reach the snow-covered Arctic within the 96 hour threshold through the transport algorithm described above.

3.4.1: Successful transport flow patterns

The number of successful transport events decreases gradually with a decrease in projected injection heights between 900mb (~914 m) and 1000mb (~110 m) atmospheric pressure levels (Figure 3.3). This decrease is likely the result of increased surface friction at 1000mb as compared to 900mb, causing lower wind speeds, and therefore increased likelihood of trajectories failing to reach the snow in the Arctic within 96 hours.

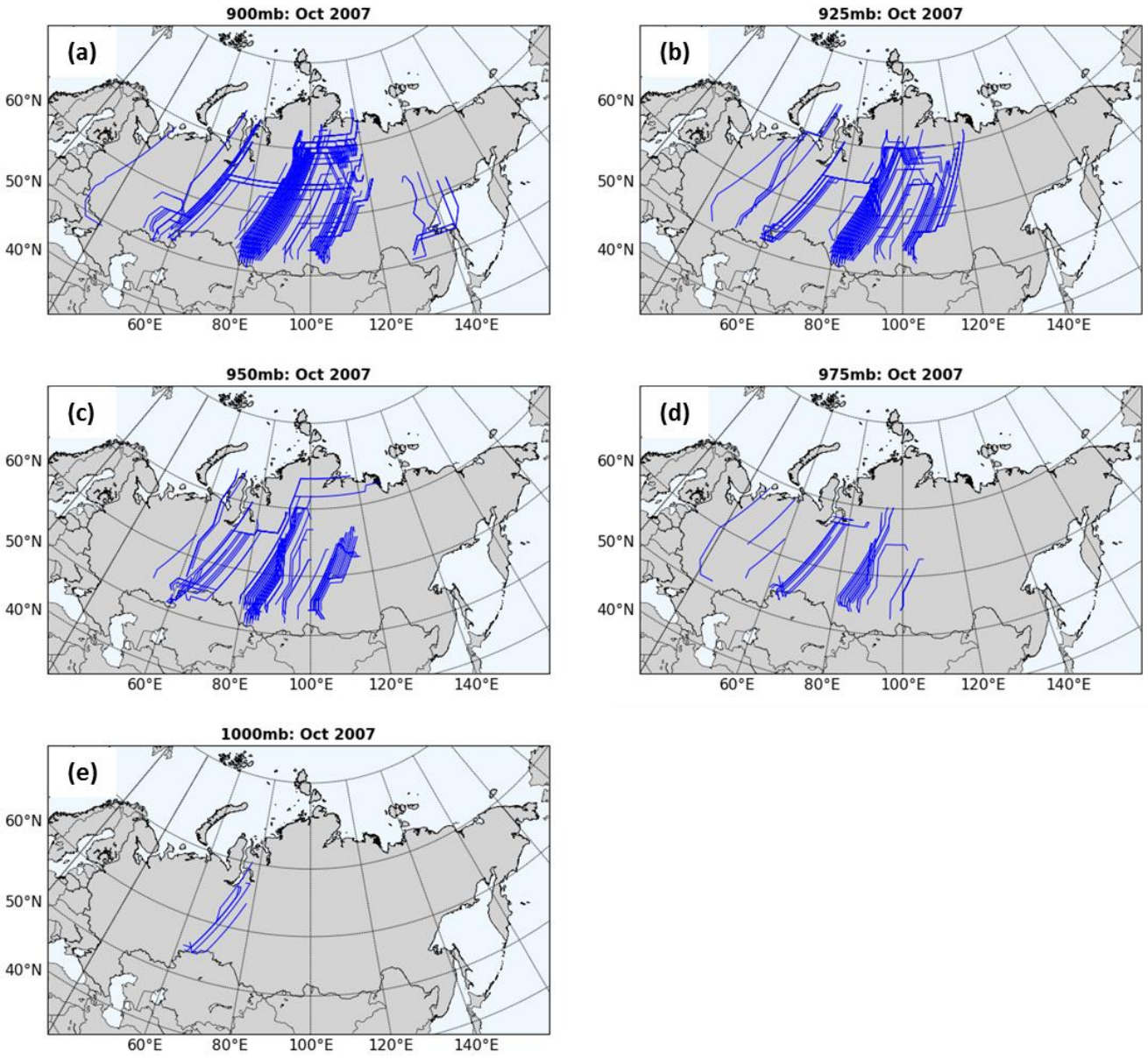

Figure 3.3: Transport trajectory line maps for successful events for October 2007 at five different pressure levels: 900mb (a); 925mb (b); 950mb (c); 975mb (d); 1000mb (e). For illustration purposes only October 2007 is shown, but the pattern is representative of the generally observed decrease in the number of successful events with shallower injection heights across all months and years.

Although not evident in every month, typically trajectories at 900mb show more curved patterns associated with cyclonic/anticyclonic air movement than at lower altitudes (Figure 3.4a); however, straight, northerly trajectories were the most prevalent (Figure 3.4b). These predominantly straight, northerly trajectories were fairly surprising as their pattern does not seem to fit any particular circulation pattern; however, review of the literature found these near straight, northerly flows are consistent with another transport study (Larkin et al., 2012). A possible explanation for the straight-line trajectories is related to either the northerly surge produced when a migratory cyclone approaches a blocked anticyclone (Iversen and Joranger, 1985; Raatz and Shaw, 1984; Raatz, 1989) or at the interaction zone between an anticyclone to the east and a cyclone to the west.

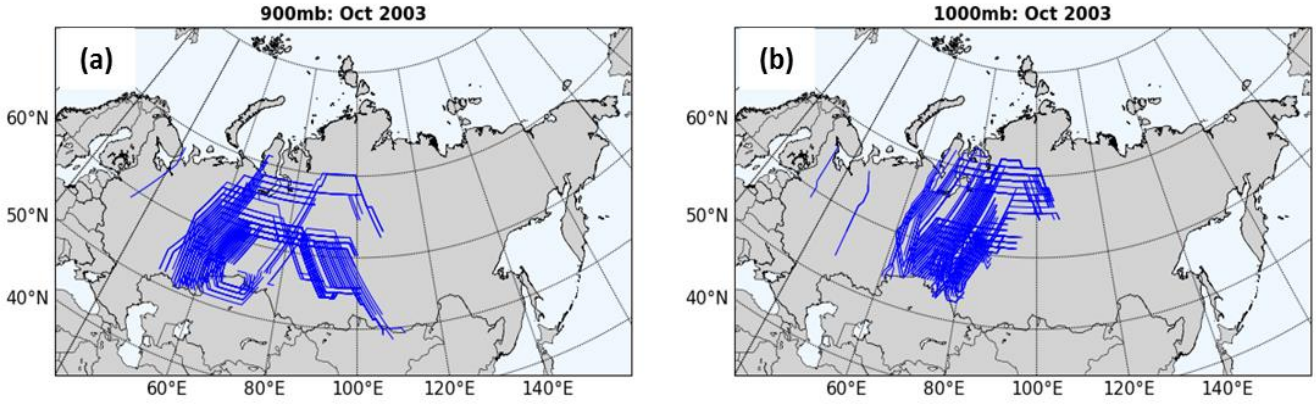

Figure 3.4: 900mb (a) and 1000mb (b) October 2003 successful trajectories highlighting the curved pattern evident in 900mb maps.

Trajectory count maps were generated to quantify the variability between years and pressure levels (Figure 3.5). Monthly snow extent maps are also produced to help interpret these successful transport patterns (Figure 3.6). Although there is a substantial amount of variability, a number of fairly consistent monthly patterns is also clear.

Generally in December, January and February the few successful events predominantly originated in the south-western regions of Russia near the Northern Caucasus (in the vicinity of 45°N, 40°E). The few fires located in the winter months are unlikely to represent crop residue burning in preparation for planting; however, they may be associated with other types of burning, such as bonfires or pile burning of agricultural waste. March, April and May saw the largest number of successful events, often several orders of magnitude higher than other months. Although other months, such as August contain a larger number of cropland fires, snow extent in the Arctic is at its minimum (Figure 3.6), hence, substantially limiting the potential for cropland burning-resultant BC deposition on snow. The main difference between these three springtime months is the location of the highest concentration of trajectories. In March, the hotspot in the density of overlapping trajectories is typically located along the western edge of Russia. This hotspot migrates east with time and reaches 80°E by May. By June, the density of successful transport trajectories is substantially reduced with the majority located around 90°E. July and August have little to no successful transport events, depending on the pressure level and year and a gradual increase is seen in September. October registers another increase in the number of successful transport events, mostly associated with a rapid establishment of snow cover in the Arctic, followed by a decrease in November driven by the overall decrease in crop residue burning. The 925mb 2003 – 2015 trajectory count maps are used to illustrate these general patterns (Figure 3.5).

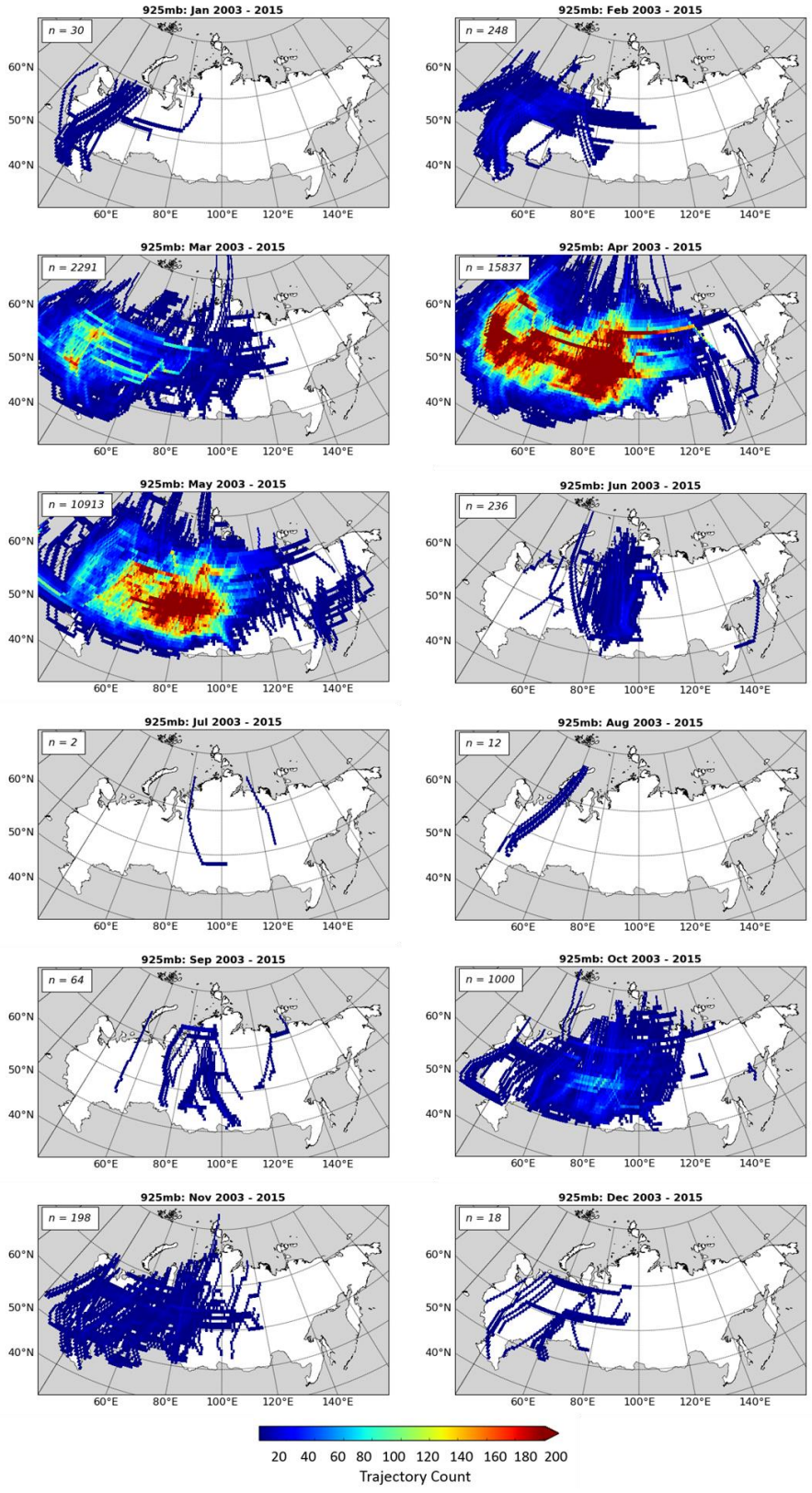

Figure 3.5: 925mb monthly successful trajectory counts (2003 – 2015).

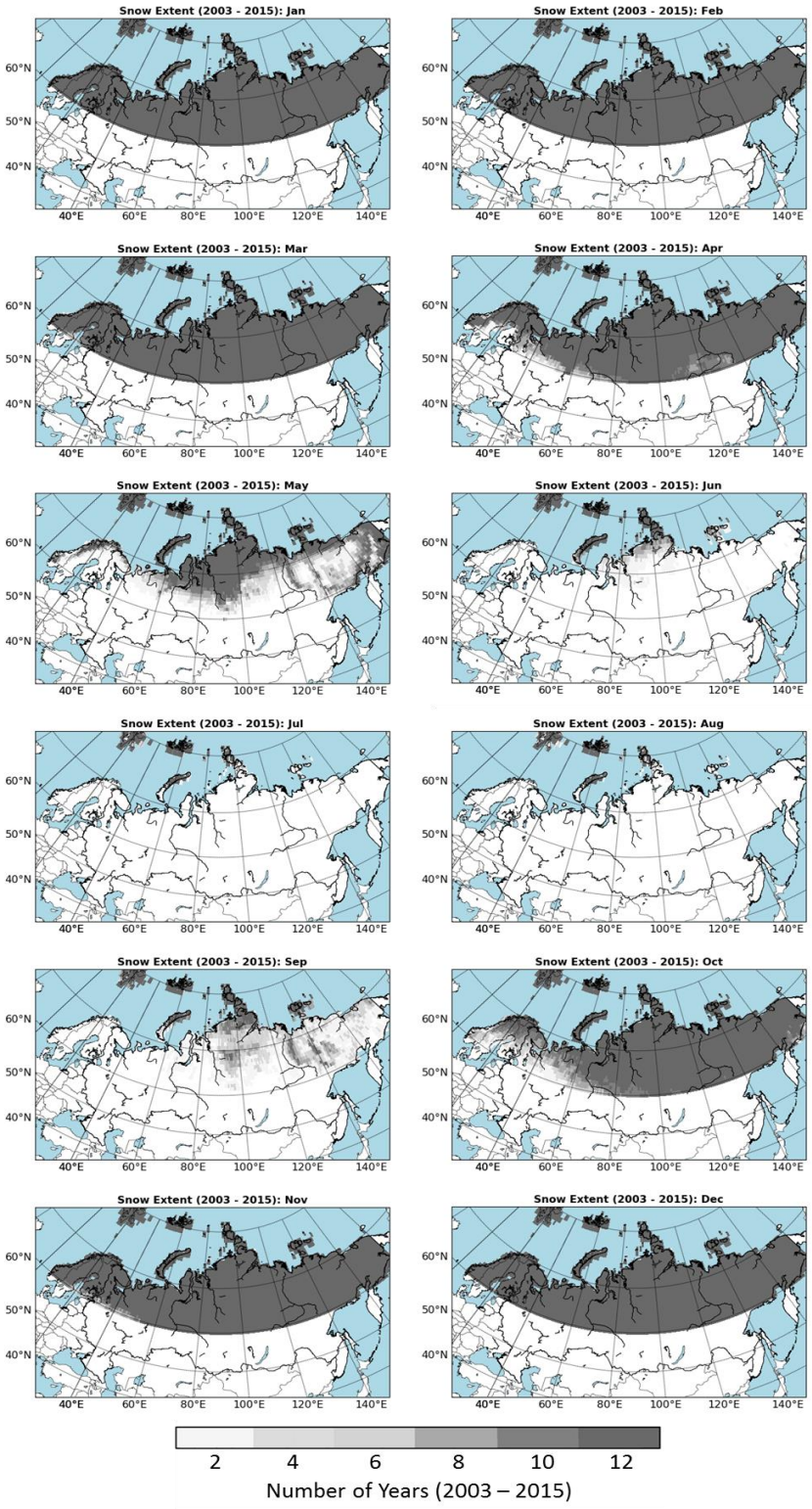

Figure 3.6: Monthly snow extent maps. The values represent the number of years each 0.75° grid cell contained snow between 2003 and 2015.

3.4.2: *Northern reaches of Russian cropland burning emission transport*

Further analysis shows that BC emissions from cropland burning in Russia can potentially be transported beyond 80°N. This potential for reaching far into the Arctic indicates that cropland burning not only has an impact on snow-covered land but also on sea ice. To determine how far north these successful trajectories can reach, the northern most latitude for each trajectory was recorded and summed over several latitude bands; 60° – 65°N, 65° – 70°N, 70° – 75°N, 75° – 80°N, and 80° – 90°N. This was carried out for every month between 2003 and 2015. The starting latitude was also recorded to help identify how far south within Russia a potential cropland burning emission source could be located to potentially deposit BC within each of these latitude bands. These results are visually summarized in Figures 3.7a – 3.7e. Each figure contains an inset table representing where the fires were located in the lower latitude bands (40° – 45°N, 45° – 50°N, 50° – 55°N, 55° – 60°N). Only contributions from March, April and May are included in the tables, because they represent the largest portion of successful transport to the Arctic snow. These springtime months are also the most critical in regards to the impact of BC deposition on the Arctic snow/ice albedo, thus it is crucial to quantify how far south the successfully transported emissions sources are located within Russian croplands.

(a)

Northern Extent: 2003 - 2015 Total
60 - 65 degrees latitude

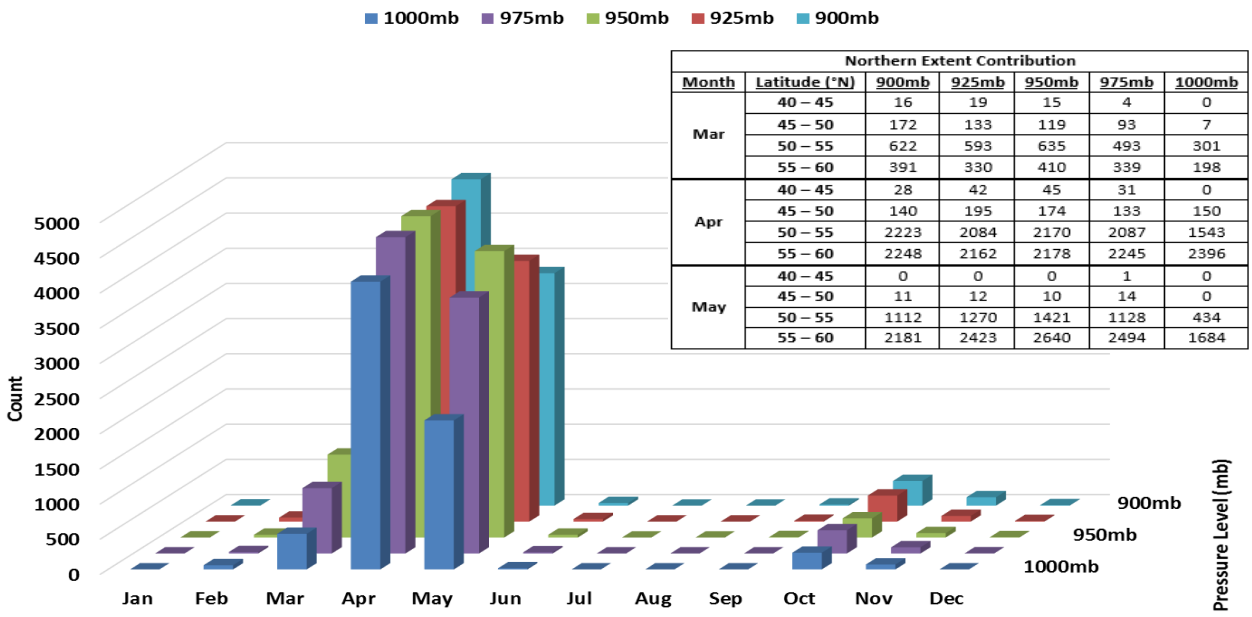

Northern Extent Contribution						
Month	Latitude (°N)	900mb	925mb	950mb	975mb	1000mb
Mar	40 – 45	16	19	15	4	0
	45 – 50	172	133	119	93	7
	50 – 55	622	593	635	493	301
	55 – 60	391	330	410	339	198
Apr	40 – 45	28	42	45	31	0
	45 – 50	140	195	174	133	150
	50 – 55	2223	2084	2170	2087	1543
	55 – 60	2248	2162	2178	2245	2396
May	40 – 45	0	0	0	1	0
	45 – 50	11	12	10	14	0
	50 – 55	1112	1270	1421	1128	434
	55 – 60	2181	2423	2640	2494	1684

(b)

Northern Extent: 2003 - 2015 Total
65 - 70 degrees latitude

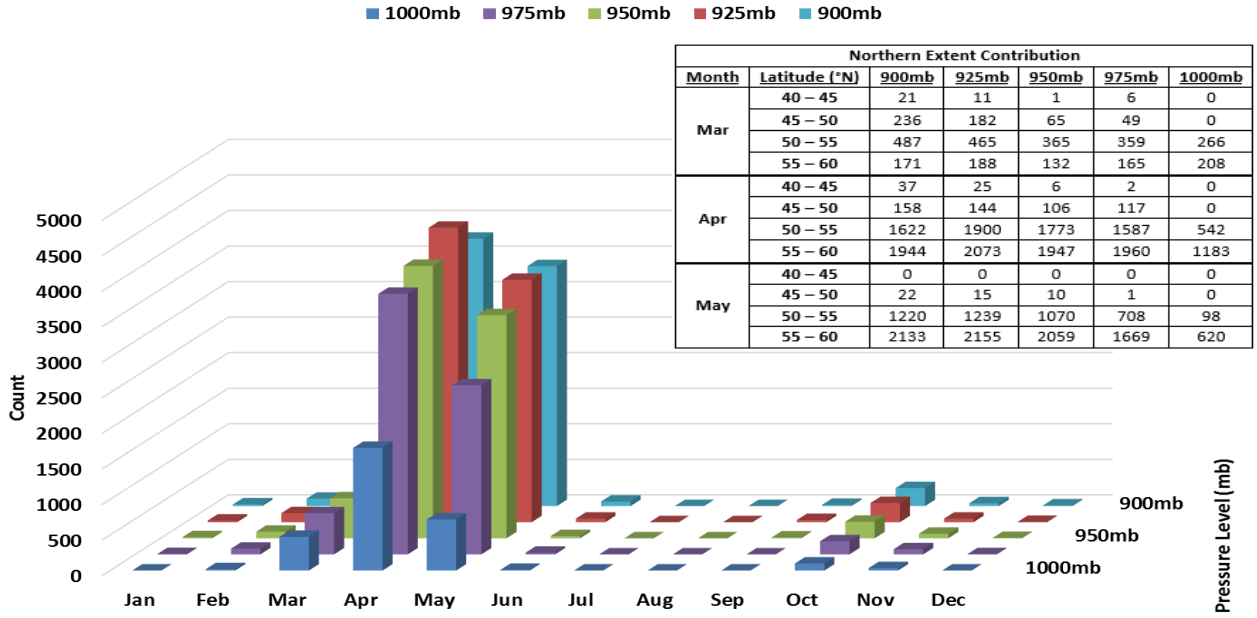

Northern Extent Contribution						
Month	Latitude (°N)	900mb	925mb	950mb	975mb	1000mb
Mar	40 – 45	21	11	1	6	0
	45 – 50	236	182	65	49	0
	50 – 55	487	465	365	359	266
	55 – 60	171	188	132	165	208
Apr	40 – 45	37	25	6	2	0
	45 – 50	158	144	106	117	0
	50 – 55	1622	1900	1773	1587	542
	55 – 60	1944	2073	1947	1960	1183
May	40 – 45	0	0	0	0	0
	45 – 50	22	15	10	1	0
	50 – 55	1220	1239	1070	708	98
	55 – 60	2133	2155	2059	1669	620

(c)

Northern Extent: 2003 - 2015 Total
70 - 75 degrees latitude

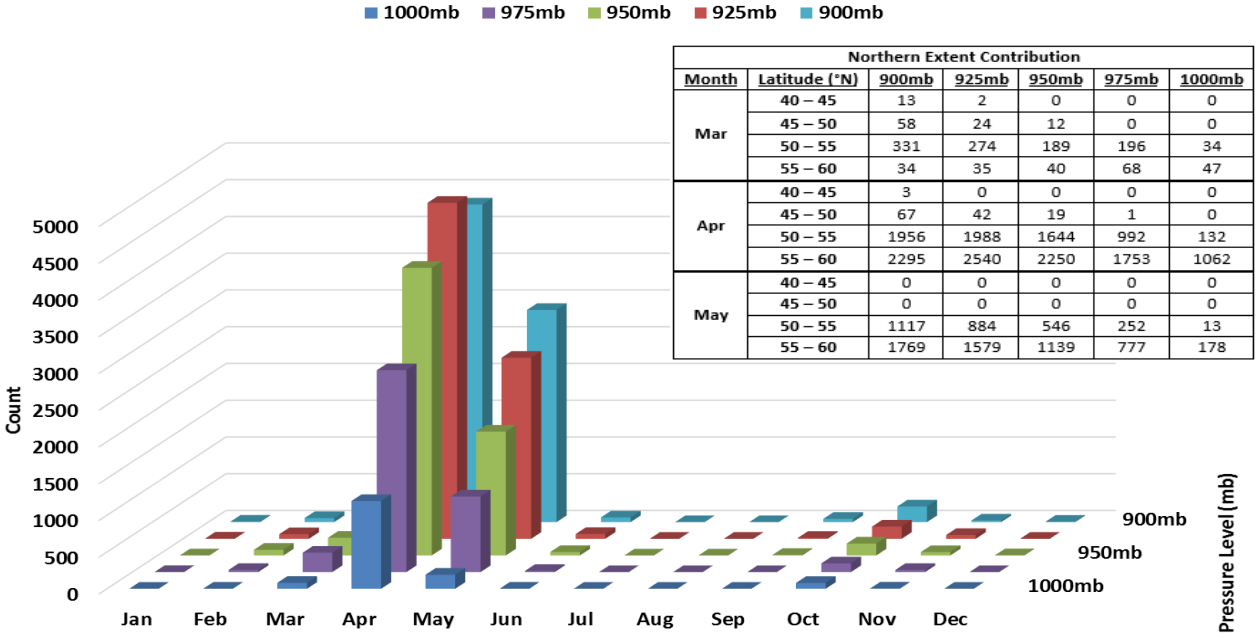

Northern Extent Contribution						
Month	Latitude (°N)	900mb	925mb	950mb	975mb	1000mb
Mar	40 – 45	13	2	0	0	0
	45 – 50	58	24	12	0	0
	50 – 55	331	274	189	196	34
	55 – 60	34	35	40	68	47
Apr	40 – 45	3	0	0	0	0
	45 – 50	67	42	19	1	0
	50 – 55	1956	1988	1644	992	132
	55 – 60	2295	2540	2250	1753	1062
May	40 – 45	0	0	0	0	0
	45 – 50	0	0	0	0	0
	50 – 55	1117	884	546	252	13
	55 – 60	1769	1579	1139	777	178

(d)

Northern Extent: 2003 - 2015 Total
75 - 80 degrees latitude

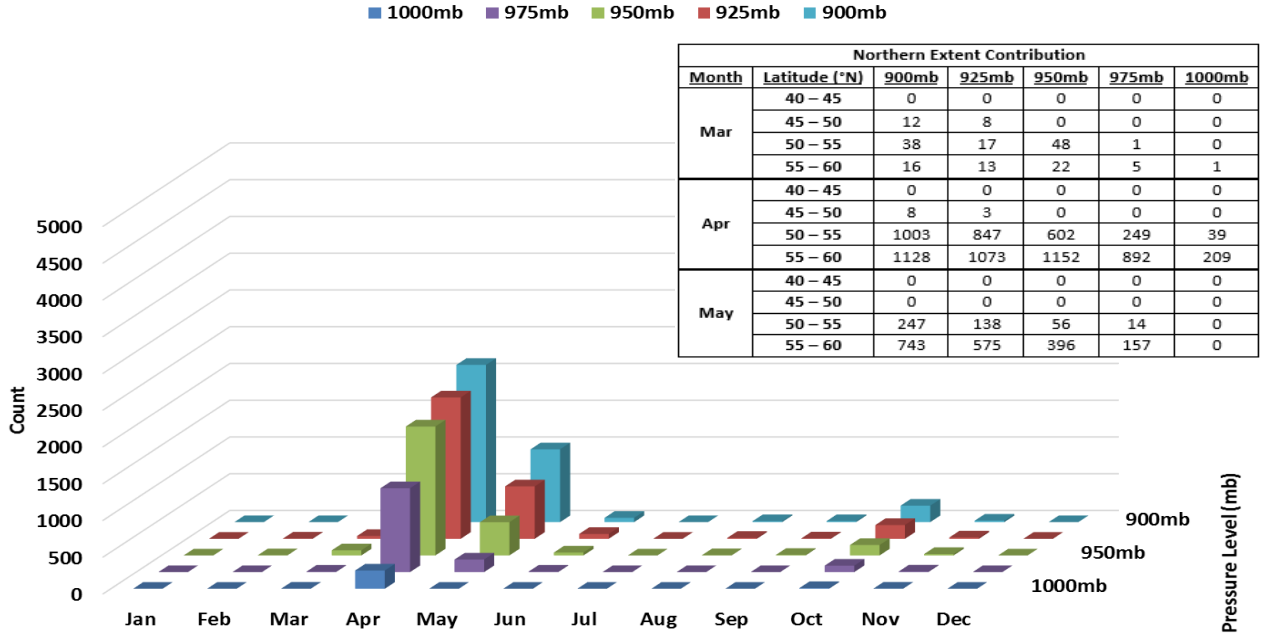

Northern Extent Contribution						
Month	Latitude (°N)	900mb	925mb	950mb	975mb	1000mb
Mar	40 – 45	0	0	0	0	0
	45 – 50	12	8	0	0	0
	50 – 55	38	17	48	1	0
	55 – 60	16	13	22	5	1
Apr	40 – 45	0	0	0	0	0
	45 – 50	8	3	0	0	0
	50 – 55	1003	847	602	249	39
	55 – 60	1128	1073	1152	892	209
May	40 – 45	0	0	0	0	0
	45 – 50	0	0	0	0	0
	50 – 55	247	138	56	14	0
	55 – 60	743	575	396	157	0

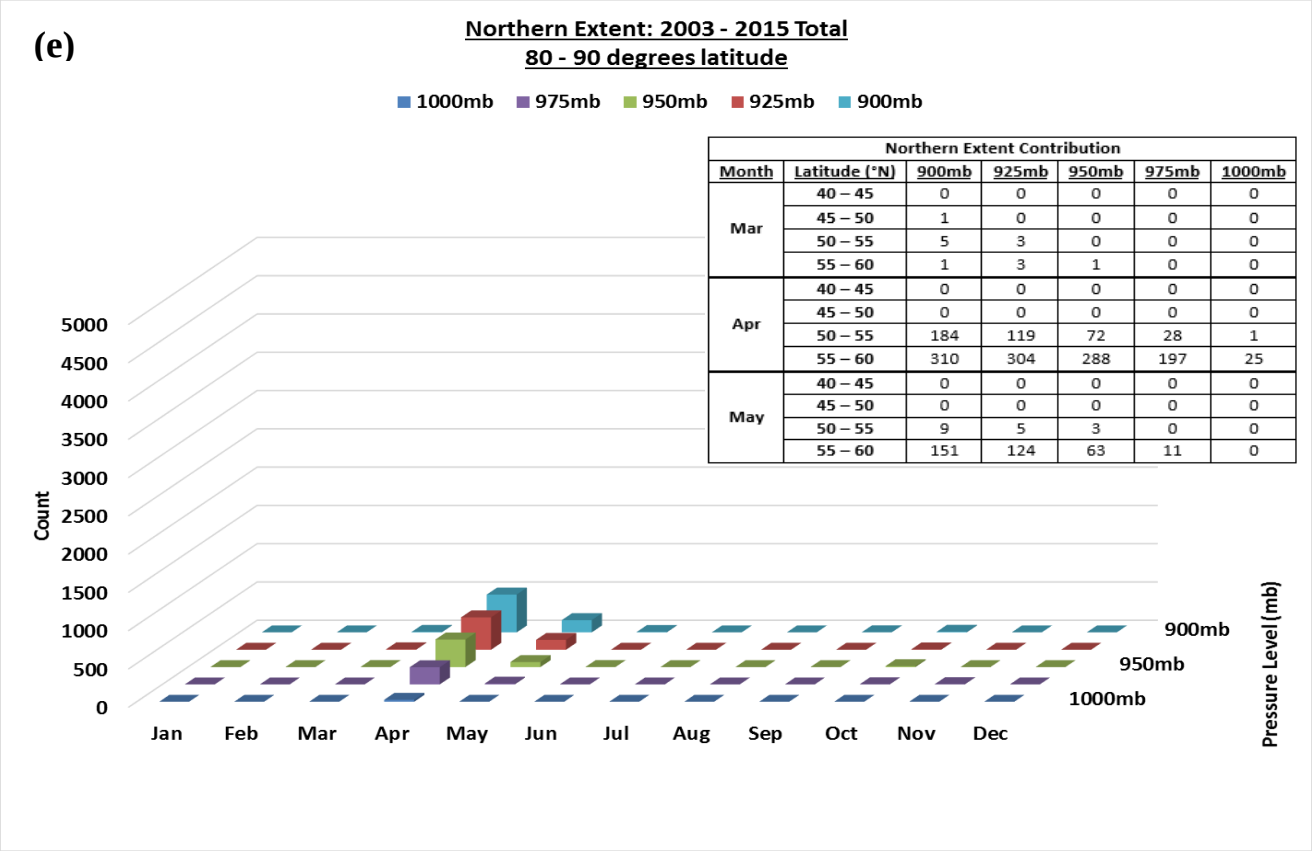

Northern Extent Contribution

Month	Latitude (°N)	900mb	925mb	950mb	975mb	1000mb
Mar	40 – 45	0	0	0	0	0
	45 – 50	1	0	0	0	0
	50 – 55	5	3	0	0	0
	55 – 60	1	3	1	0	0
Apr	40 – 45	0	0	0	0	0
	45 – 50	0	0	0	0	0
	50 – 55	184	119	72	28	1
	55 – 60	310	304	288	197	25
May	40 – 45	0	0	0	0	0
	45 – 50	0	0	0	0	0
	50 – 55	9	5	3	0	0
	55 – 60	151	124	63	11	0

Figure 3.7: Total number of successful events (monthly) between 2003 and 2015 that reach snow cover between 60° – 65°N (a), 65° – 70°N (b), 70° – 75°N (c), 75° – 80°N (d), 80° – 90°N (e) as their northern-most extent per pressure level. The inset table represents the contribution from the lower latitude bands (40° – 45°N, 45° – 50°N, 50° – 55°N, 55° – 60°N) for March, April and May.

The results of the northern extent analysis found that during the spring, BC emissions from as far south as 45°N (in March at the highest injection height) and 50°N (April and May at almost all injection heights) are able to be potentially transported as far north as 80° – 90°N. Deposition of BC this far north has important implications for the permanent sea ice cover in the Arctic. Furthermore, this analysis identified cropland

burning between 40° – 45°N was able to potentially deposit on the Arctic snow (in some cases up to 70° – 75°N) during March, April and May and under almost all injection heights.

3.4.3: Spatial patterns of BC transport to the Arctic snow

Quantifying the transport time is an important element in identifying the relative importance of the burning source regions to their potential contribution to the BC deposition on snow in the Arctic. As soon as BC particles are released into the atmosphere they undergo various reactions with other constituents of the atmospheric column. As the residence time increases, BC becomes increasingly mixed with other atmospheric constituents leading to changes in the optical properties and atmospheric lifetime of BC (Bond et al., 2013). The exact impact of deposited BC on Arctic snow relies on the chemical and microphysical processes within the atmosphere; however, as a general rule, the longer a molecule remains in the atmosphere the more mixing and alterations it will undergo before it is ultimately removed via wet or dry deposition.

Analysis of the average transport time (hours), the success (%) of each starting location, and the number of active fires within each grid cell of origin for a successful transport event was carried out to quantify the fraction of the potential contributions of BC deposition and to characterize the cropland burning source regions. A three map plot has been created for each month for both individual years and 2003 – 2015 inclusive (Figures 3.8 – 3.10). These maps highlight the spatial and temporal variability within all three metrics. Here only results from March, April and May (2003 – 2015) at 900mb and 1000mb will be shown as the majority of the successful fires occur during these months.

The 900mb and 1000mb results are shown to illustrate the two extremes of the injection height range used in this study.

On average, fire occurrence in January and February is very low with only 1 active fire per grid cell per year on average between 2003 and 2015 predominantly located in the south-western region of European Russia (45°N, 50°E). The few locations with successful transport were able to reach the snow-covered Arctic on average within approximately 50 hours (January) and 40 hours (February), depending on the injection height. By March, the total number of cropland fires increased to approximately 5 to 15 active fires per successful grid cell, while also increasing in spatial extent (Figure 3.8). As expected the success rate of potential crop residue emission transport decreases while transport time increases with lower injection heights; however, an interesting anomalous pattern occurs in March in the north-west region (centered on 55°N, 45°E) of the transport map. Instead of the transport time increasing with lower injection heights, the transport time actually decreases from approximately 40 – 50 hours to approximately 10 – 30 hours on average to the Arctic. Analysis of the transport pathways found that this anomalous pattern resulted from longer trajectories at higher injection heights associated with the more circular pattern (most likely due to the presence of an anticyclone) as compared to more straight trajectories at lower injection heights.

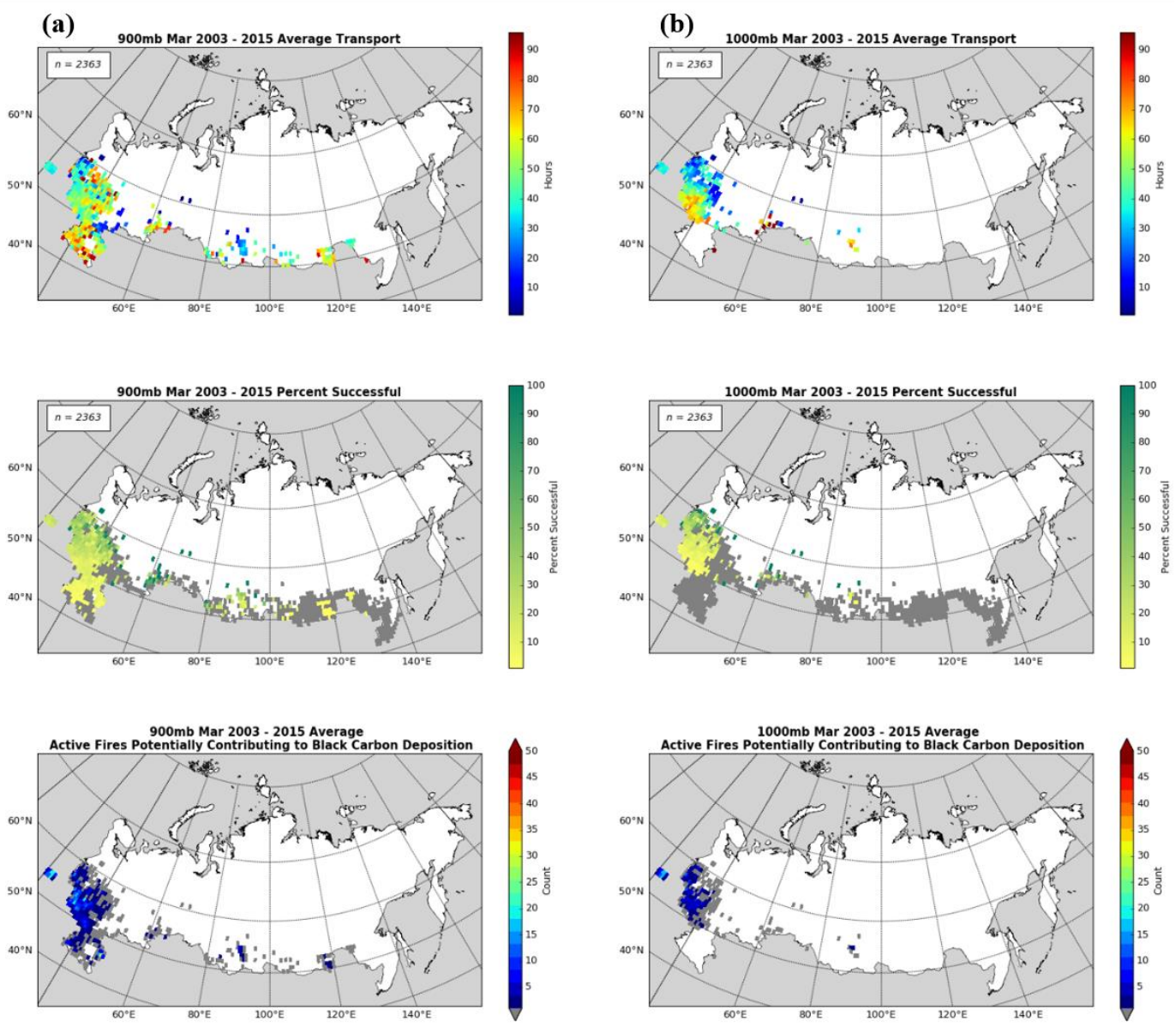

Figure 3.8: 900mb (a) and 1000mb (b) March 2003 – 2015 average transport (hours), percent successful and active fires potentially contributing to BC deposition on snow in the Arctic. The grey color in the percent successful maps (middle) represents the starting fire locations which were unsuccessful at reaching the snow in the Arctic within 96 hours.

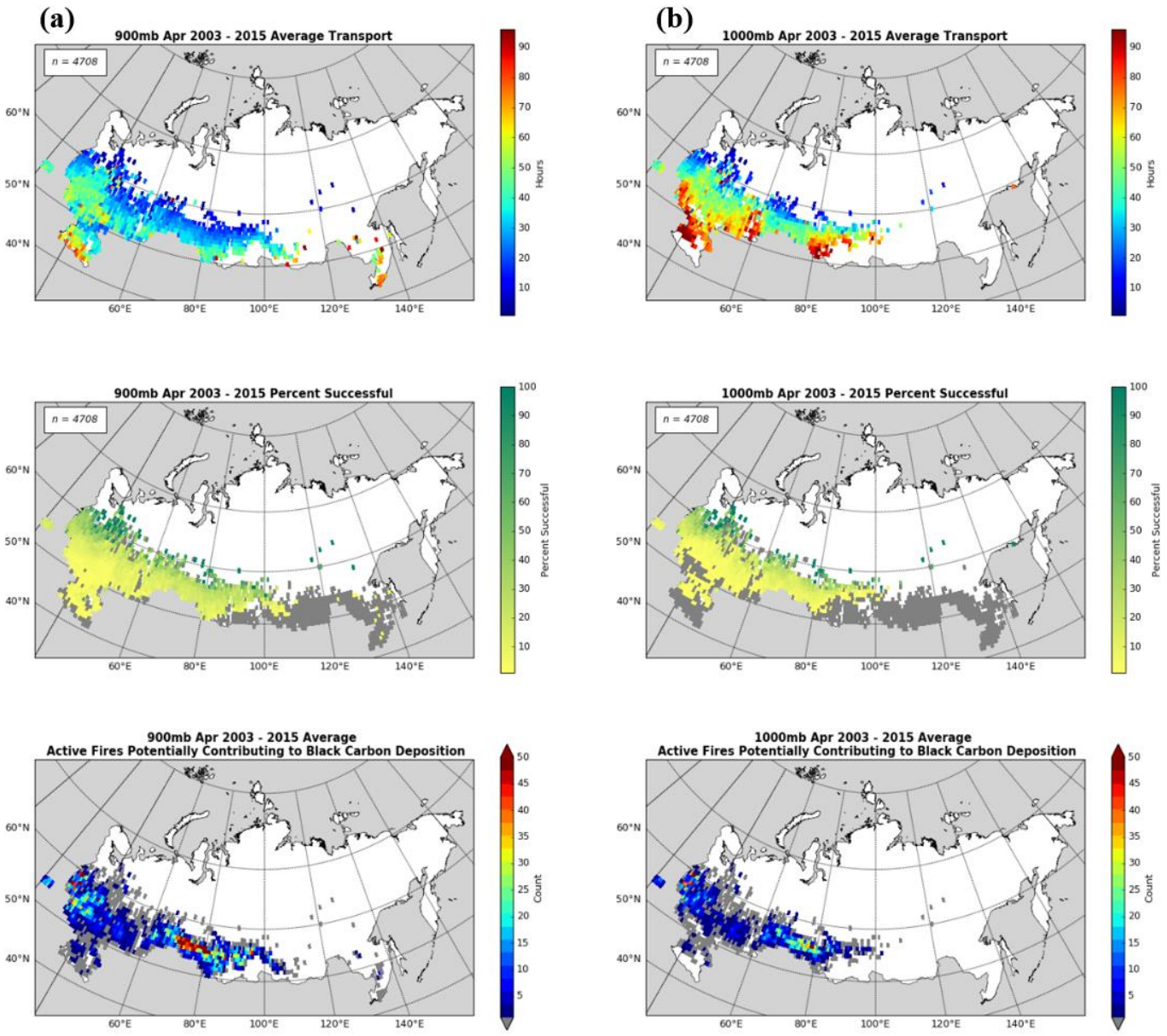

Figure 3.9: 900mb (a) and 1000mb (b) April 2003 – 2015 average transport (hours), percent successful and active fires potentially contributing to BC deposition on snow in the Arctic. The grey color in the percent successful maps (middle) represents the starting fire locations which were unsuccessful at reaching the snow in the Arctic within 96 hours.

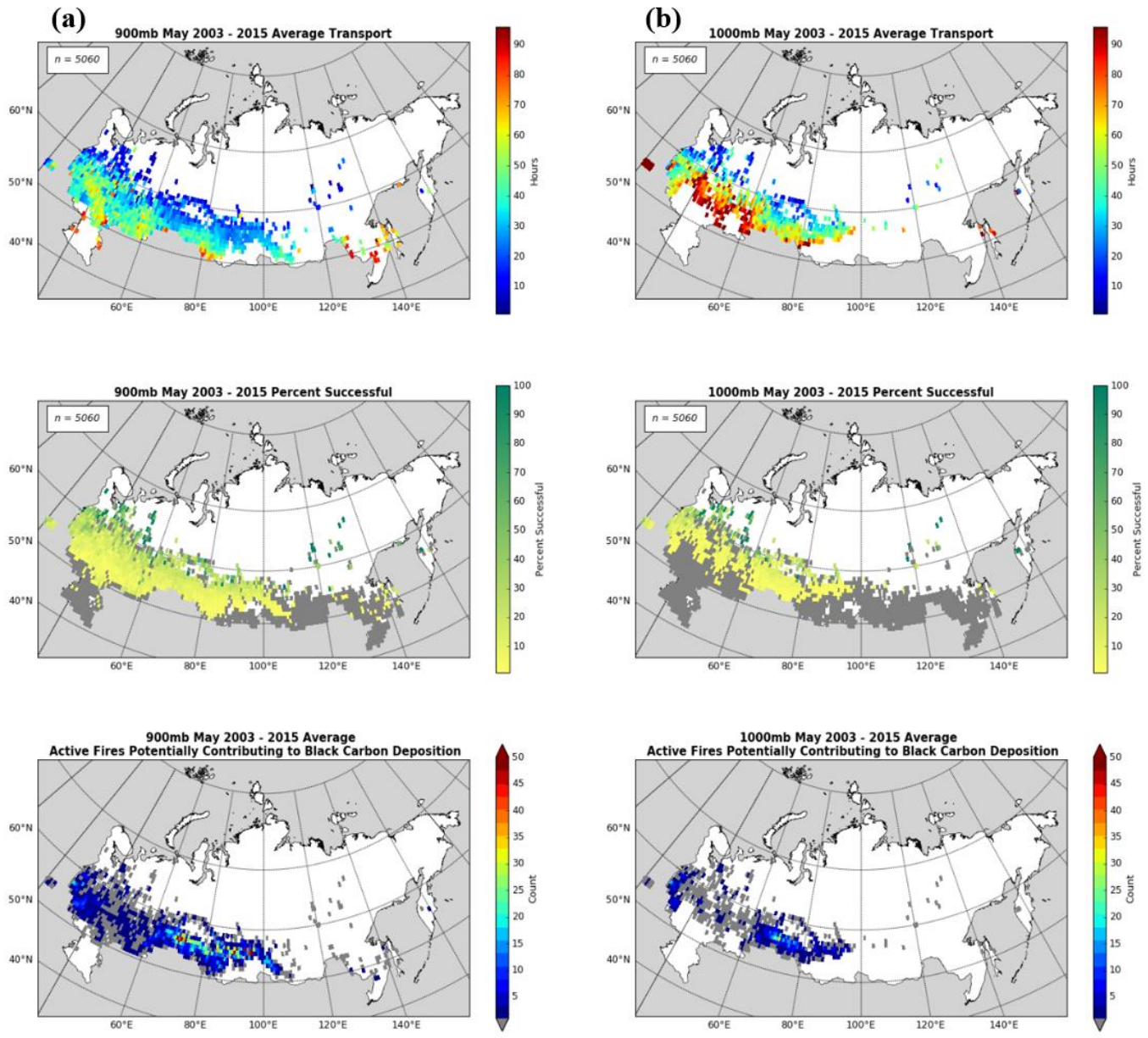

Figure 3.10: 900mb (a) and 1000mb (b) May 2003 – 2015 average transport (hours), percent successful and active fires potentially contributing to BC deposition on snow in the Arctic. The grey color in the percent successful maps (middle) represents the starting fire locations which were unsuccessful at reaching the snow in the Arctic within 96 hours.

In April, the successfully transported fire load reached a peak (100 – 130 active fires per grid cell – Figure 3.9) between 70°E and 80°E. Although this area has low success rates, the transport time to the Arctic remains relatively low in comparison to the surrounding regions, even at low injection heights. A slightly smaller peak in fire occurrence is located in the north-west corner (approximately 55°N, 35°E) with a coincidental increase in success rate. Transport times for both clusters vary between <10 – 50 hours, therefore the emissions from these higher fire loads will likely encounter less mixing and fall out than emissions with longer atmospheric residence times. Furthermore, at higher injection heights, successful transport of potential emissions can originate at least as far south as approximately 40°N, which is the limit of the Russian croplands.

In May, the success rate along the southern edge of the Russian cropland, particularly at lower injection heights, drops significantly except for the region located between 70°E and 80°E (Figure 3.10). As with April, this same area has slightly lower transport times to the Arctic as compared to the surrounding regions. Analysis of the transport pathways does not explain the decrease in transport time in that region. A possible explanation lies in the higher number of successful burning locations (see bottom map in Figures 3.9 and 3.10) in that area as compared to other areas in the Russian cropland. These maps show the average transport times which are more likely to be influenced by outliers within the regions with fewer successful fires as compared to the region located between 70°E and 80°E.

Furthermore, the highest density of cropland fires occur in the spring in the southern portion of the cropland in the Far East (approximately between 40° – 55°N and 110° – 130°E); however, there are very few fires with successfully transported emissions

within this region. Specifically, the success rate of fires east of 95°E are severely reduced with lower injection heights in comparison to the cropland fires within European Russia at similar latitudes. Analysis of the trajectories starting in the Far East croplands reveal short pathways often flowing towards the east over the Sea of Oshotsk (away from the snow extent), whereas the European Russian trajectories are much longer and tend to flow north. These differences are likely due to the varying atmospheric circulation patterns experienced throughout Russia.

Analysis on quantifying the fraction of the successful fires against all observed Russian cropland fires further illustrates the importance of the spring months. Table 3.1 summarizes the total cropland active fires and the successful active fire counts per atmospheric pressure level averaged between 2003 and 2015. Annual tables are available in the supplementary material (Table S4).

Table 3.1: Monthly average (2003 – 2015) successfully transported and total active fire counts within the Russian cropland.

	All Active Fires	**Successful Active Fire Counts**				
	Total	**900mb**	**925mb**	**950mb**	**975mb**	**1000mb**
Jan	109	5	4	3	1	0
Feb	763	79	85	74	52	32
Mar	11840	962	843	774	668	389
Apr	66335	7840	7966	7395	6285	3677
May	44994	4076	3953	3493	2735	1154
Jun	5545	49	48	28	11	5
Jul	10621	0	0	0	0	0
Aug	16564	3	3	1	0	0
Sep	13623	28	14	9	0	0
Oct	16027	296	300	238	209	119
Nov	2385	30	29	25	28	17
Dec	189	4	2	2	1	1

These values are based on the active fire (MCD14ML C6) dataset. The previous version of this product was shown to under represent burning in the Russian cropland region (Hall et al., 2016). However, based on these values on average between 2003 and 2015 approximately 4 – 10% of the March, April, and May observed fire occurrences (depending on injection height) are within regions with successful transport to the Arctic. These results represent a unique quantification of the fraction of observed burning within Russian cropland which are potentially able to contribute to the deposition of BC on the Arctic snow.

3.5: Discussion

3.5.1: Sources of uncertainty

Successfully quantifying the fraction of cropland burning in Russia that can potentially contribute to the deposition of BC on snow in the Arctic is a difficult task due to the inherent challenges associated with the underlying input datasets. As previously addressed in Chapter 2, current satellite capabilities are not adequate for mapping burned area associated with agricultural fires. This inability to accurately map cropland burned area has repercussions on the accuracy of cropland burning emissions inventories. Due to the lack of accurate emission estimates, this study explores the potential for BC transport from known areas of cropland burning to the Arctic based on known wind and precipitation patterns. While it has not been established quantitatively (because there are currently no accurate estimates of cropland area burned), active fire observations are assumed to be generally representative of the total biomass burning within the Russian cropland.

The spatial scale of the meteorological data used in this transport model determines the spatial granularity of resultant trajectories which were restricted to tracking the centers of the individual grid cells rather than the actual locations of the active fires. While very coarse compared to the 1km MODIS active fire pixels, ERA-Interim meteorological data (at 0.75°) records parameters at a finer scale than the more commonly used, in previous studies, 2.5° resolution NCEP/NCAR (National Centers for Environmental Prediction – National Center for Atmospheric Research Global Reanalysis; Kalnay et al., 1996) dataset. For example, the coarser NCEP/NCAR meteorological data is frequently used to drive HYSPLIT trajectory models (e.g. Huang et al., 2010; Larkin et al., 2012; Treffeisen et al., 2007). Additionally, 6-hour ERA-Interim wind and precipitation data fields were aggregated to daily values. While ideally, hourly wind and precipitation data would more accurately represent the actual meteorological conditions throughout the transport pathway, it is difficult to quantify how much actual precision is lost in using daily versus hourly data within a 0.75° grid cell. The general weather patterns across Russia's mid-latitudes are primarily influenced by cyclonic and anticyclonic activity which most frequently last more than one day (Lebedeva et al., 2016). It is likely that the aggregation of meteorological parameters to a daily temporal scale has impacted trajectories for fire events that occurred during the stages when the weather patterns were shifting between cyclones and anticyclones. However, it is expected that most of the burning occurs during anticyclonic weather patterns when the meteorological conditions produce drier fuels (a particularly limiting parameter for fire spread during post snow-melt conditions in the spring) that can support fire spread more readily.

Finally, an additional source of uncertainty is related to the satellite-based estimates of snow cover extent used in this study. The high northern latitudes are plagued with persistent cloud cover during the sunlit period and an absence of solar irradiance during the polar nights. Therefore, several assumptions had to be defined in order to create snow melt and snow establishment layers. The inability to observe surface conditions due to cloud presence introduces a considerable amount of uncertainty in identifying the exact date of snow melt and snow establishment. The 0.75° resolution further amplifies the uncertainty when a single value is assigned to represent conditions for the entire grid cell.

3.5.2: Comparison with previous studies

Transport trajectories and the resultant outputs generated by this methodology are consistent (although not directly comparable) with those produced within previously published studies. Several previous studies have indicated that biomass burning sources from northern mid-latitudes significantly impact the Arctic region (e.g. Cheng, 2014; Larkin et al., 2012; Liu et al., 2015; Quinn et al., 2011; Sharma et al., 2013; Warneke et al., 2010). One of the main findings of this doctoral study research chapter confirmed that cropland burning as far south as at least 40°N has the potential to contribute to the BC deposition on the Arctic snow. Furthermore, the spatial and temporal patterns of the successful transport success percentage in March, April, and May are consistent with the results from the United States Forest Service (USFS) AirFire Arctic Transport Potential Forecast and Climatology project (see Figure 3.11; Larkin et al., 2012). Unlike other studies, the output data for the AirFire project is available for download and the interface allows users to generate maps for particular timeframes

(https://www.airfire.org/data/arctic-transport-clim/). The AirFire study utilized NOAA's HYSPLIT model to run 7 day (climatological runs: 1980 - 2009) and 4 day (daily forecast: 2012 - present) forward trajectories. Starting locations were defined by the centroid of every 2.5° NCEP/NCAR land grid cell within Russia at starting heights ranging from 500 m – 5000 m altitude. The AirFire project outputs maps of percent days with transport to the Arctic between 1980 and 2009. A direct comparison between the results from this study's transport algorithm and the results from the AirFire project is not possible due to the differing temporal and spatial resolutions, the longer transport time threshold, and the inclusion of any other potential sources of emission beyond crop residue burning; however, comparisons of the overall patterns of transport success during March, April and May can be undertaken.

Focusing specifically on the south-western tip of Russia below 50°N, the AirFire results show a fairly low percentage (less than 50%) of successful transport days in May (1980 – 2009) which is consistent with the findings at all injection heights in this doctoral study as the first instance of widespread successful transport in May starts at 50°N (Figure 3.10). Furthermore, the general pattern of increased likelihood of successful transport from European Russia as compared to the Far East is consistent between the USFS AirFire study and the results of this doctoral study.

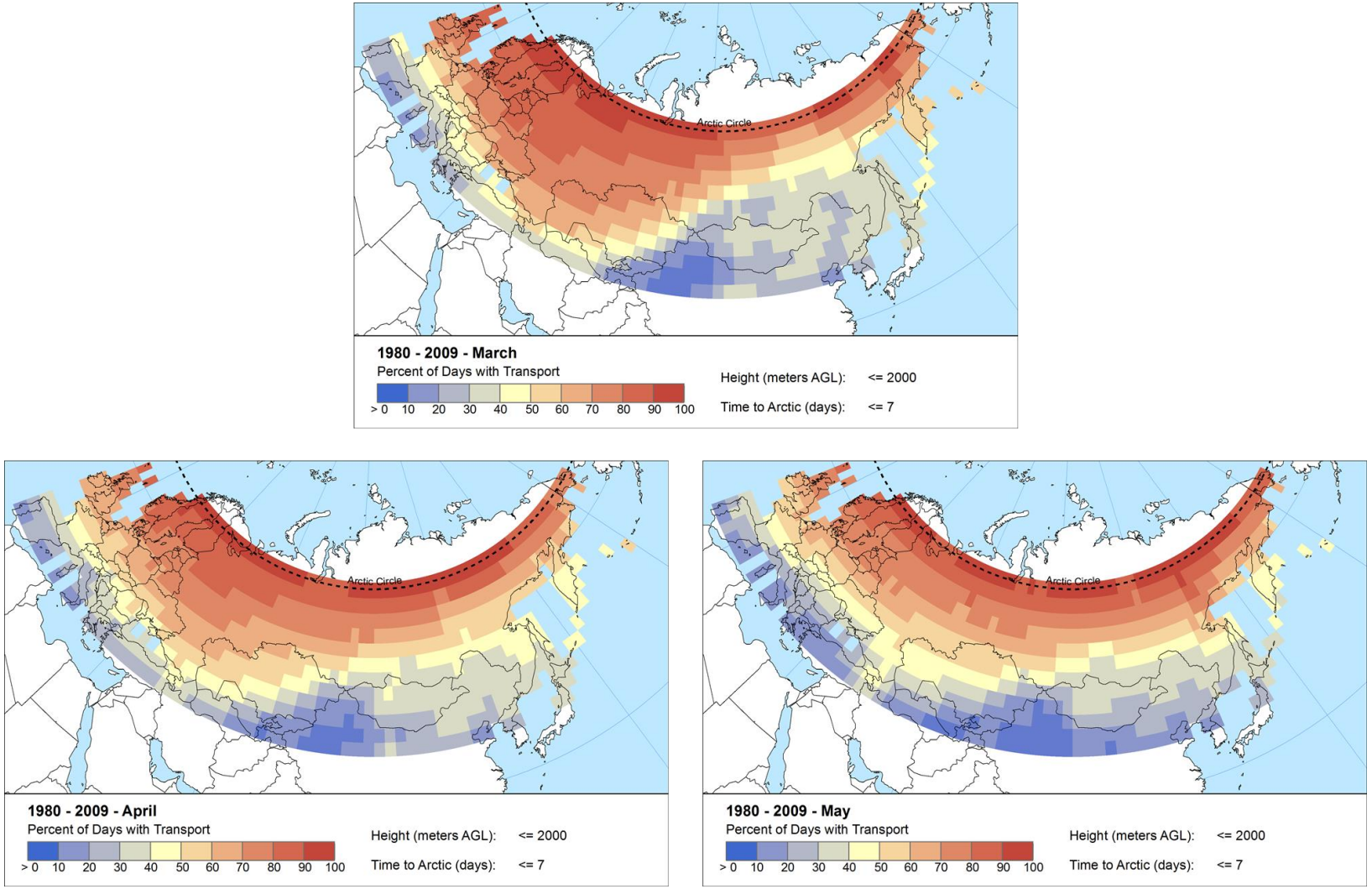

Figure 3.11: USFS AirFire Arctic Potential Transport Climatology maps (data source: https://www.airfire.org/data/arctic-transport-clim/). The figure was generated by the author using the USFS AirFire online data analysis system.

A study by Cheng (2014) focused on locating burning sources within Russia that potentially contributed to BC deposition in two Arctic sampling sites between 2000 and 2006. Their study found several BC emission source regions that likely contributed to the BC deposition in the two Arctic sampling sites. These included, a region surrounding Moscow (55°N, 37°E); a region stretching along the Ural Mountains; and a number of areas scattered from western Siberia to the Russian Far East (Cheng, 2014). Most of the regions were correlated with source types, including forest fires/biomass burning and power plants; however, a region located south of Moscow, which was identified as a significant source of BC emissions, could not be linked to either forest fires, oil combustion, or coal-fired power plants. Comparing their mapped outputs to the Russian cropland region, this area might be connected to cropland burning; however, the spatial resolution of their study was very coarse making it difficult to accurately determine the exact location of this significant source region via visual analysis of their maps.

Several additional studies have also indicated that biomass burning sources as far south as 40°N are assumed to significantly impact the Arctic region (e.g. Liu et al., 2015; Quinn et al., 2011; Sharma et al., 2013; Warneke et al., 2010). Based on the overall findings from Cheng (2014) and Larkin et al., (2012), burning in Russia as far south as at least 40°N has the potential to contribute to BC deposition in the Arctic, which is consistent with the results from this study. The comparison of this doctoral study's results with previous studies (focused on air pollution transport from northern mid-latitudes to the Arctic) has demonstrated that the simplistic form of the transport model has represented the key meteorological drivers appropriately and that the interpretation of the results are meaningful.

3.5.3: Significance of BC deposition from cropland burning on the Arctic snow

A key attribute of this study is focused on BC deposition on the snow in the Arctic. This nuance has important implications for the timing of burning. Although forest fires produce substantially more emissions than cropland fires due to higher biomass loading (e.g. Hao et al., 2016), the timing of the burning plays a key role in determining the relative importance of these source emissions to BC deposition on Arctic snow. Forest fires typically occur in the summer, when high temperatures, low humidity, and little precipitation drive the increase in forest flammability. On the other hand, crop residue burning in Russia usually follows the crop harvest cycles. A variety of crops are grown in Russia, however, wheat is the predominant grain (USDA FAS, 2016). Winter wheat is typically sown in fall, while spring wheat is sown in April. Burning of crop residue stubble usually occurs before planting to remove excess waste and pests from the field (McCarty et al., 2012). Analysis of the active fire dataset between 2003 and 2015 found two peaks in cropland fires – one in April/May and another smaller peak in August/September (see Chapter 2, Figure 2.2). Despite the peak in summer cropland fires, the contribution to BC deposition on the Arctic snow is negligible. Based on this analysis, it seems the coincidental timing of burning and snow cover extent is a linking factor in determining the importance of crop residue-related BC emissions and their impact on Arctic albedo.

This study confirmed the importance of springtime cropland burning in relation to the deposition on the Arctic snow. Based on the analysis of the transport time and the success percentage, it is clear that despite the low injection heights, potential BC emissions from cropland burning can be transported and deposited onto Arctic snow in

the spring from at least 40°N. This study also identified that the cropland regions within European Russia contained the highest percentage of successful transport to the Arctic snow. Although this study makes no attempt to quantify emissions, these regions contain the highest wheat yields within Russia, therefore they are likely to also contain the highest volumes of crop residues and larger BC emissions. Furthermore, there has been a focus on potentially expanding arable land through reclaiming Post-Soviet abandoned cropland (e.g. Meyfroidt et al., 2016; Schierhorn et al., 2014). In particular, a large concentration of cropland in European Russia is located along the fertile Chernozem soil belt which stretches from the southern tip of Russia towards Moscow - a region with higher wheat yields. Although an expansion of cropped area does not necessarily lead to an increase in fire activity, it does give rise to an increased opportunity for burning crop residue in the regions of higher transport potential. Moreover, if this increase in cropland area expands further north toward 50°N and leads to additional fire activity then based on the results of the northern extent analysis, there could also be an increase in BC deposition from cropland burning emissions on the permanent sea ice. Currently, scientists predict the Arctic might become nearly ice free in summers within a few decades (e.g. Laliberté et al., 2016; Wang and Overland, 2012) which will result in a diverse range of consequences including, impacts on wildlife and local populations; marine ecosystems (Ardyna et al., 2014); and changes in the atmospheric and oceanic circulation patterns (Liu et al., 2012). Increased BC deposition on the permanent sea ice during the spring, could potentially enhance the melting and lead to an earlier ice-free Arctic.

Finally, quantifying the transport time is important for understanding the potential impact of BC on the Arctic snow as the longer the aerosol remains in the atmosphere, the less potent it will be once it deposits. Due to the previously mentioned inaccuracies related to the various components for emission calculations, quantification of the potential potency of BC deposition on the Arctic cannot be undertaken; however, analysis on the temporal variability and the magnitude of cropland burning in Russia that potentially contributes to the deposition of BC on snow in the Arctic is possible. Identification of these critical time periods (when burning within the Russian cropland has a higher potential of contributing to the BC deposition on the Arctic snow) can help provide a foundation on which to base policy decisions and develop future adaptive and mitigation strategies.

3.6: Conclusion

This study was able to devise a new approach to assess potential BC deposition in the Arctic based on reanalysis data of observed meteorological conditions and confirmed cropland burning. The methodological framework allowed for quantifying the fraction and assessing the spatio-temporal dynamics of cropland burning that has the potential to impact Arctic snow cover. Approximately 10% of the observed cropland burning in March, April and May (7% annual) has the potential to contribute to the BC deposition on the Arctic snow. Despite the low injection heights, this study has shown that potential BC emissions from at least 40°N can be deposited on the Arctic snow. Furthermore, during the spring, which is the most vulnerable period for sea ice melt, potential cropland burning emissions can reach areas beyond 80°N.

It is clear based on the results of this study that cropland burning has the potential to significantly impact the Arctic via BC deposition. The magnitude of this impact, however, cannot be quantified well due to current inaccuracies surrounding cropland emission inventory calculations. Complex chemical-transport model outputs should be applied with caution, particularly when considering impacts from cropland burning. Additional improvements are needed to accurately represent the spatial and temporal cropland emission fluxes. Unfortunately, this also requires improved satellite capabilities for accurately mapping cropland burned area (Hall et al., 2016). Future work should be focused on improving the deficiencies associated with current cropland burning emission inventories.

Finally, this research study confirmed the ability for potential BC emissions from cropland burning in Russia to be transported via low-level transport to the snow in the Arctic. Analysis of the successful transport pathways identified areas containing concentrated trajectories particularly over European and Central Russia. These clusters of trajectories may be influenced by persistent wind patterns over these areas. Future studies should investigate the causes behind these concentrated pollution pathways to the Arctic with a focus on large-scale atmospheric patterns that can act to enhance atmospheric transport from lower mid-latitudes towards the Arctic.

Chapter 4: Quantifying the variability of potential black carbon transport from cropland burning in Russia driven by atmospheric blocking events

4.1: Introduction

The deposition of BC above the Arctic Circle from northern mid-latitude open-source biomass burning has been well documented in scientific literature (e.g. Cheng, 2014; Liu et al., 2015; Quinn et al., 2011; Sharma et al., 2013; Warneke et al., 2010). Based on the results of the transport algorithm developed in Chapter 3, it is evident that emissions from crop residue burning in Russia are potentially able to be transported by low-level winds and deposited on the snow in the Arctic within 96 hours. Using the results of the previous chapter, the purpose of this study is to examine another transport mechanism that could act to enhance potential transport of crop residue BC emissions to the snow in the Arctic. At present, there are a number of proposed mechanisms for long-range transport of emissions from northern mid-latitudes to beyond the Arctic Circle. The most well-known mechanism acts during northern hemisphere winter and early spring and is related to the formation of isentropic surfaces known as the Polar Dome (Klonecki et al., 2003). These surfaces of constant potential temperature form in the lower troposphere when the cold, stable Arctic air extends to lower latitudes during the winter and has been recorded as far south as 40°N in January (Barrie, 1986; Iversen and Joranger, 1985; Stohl, 2006). Isentropic surfaces slope upward toward the poles thus the Polar Dome causes northward moving air parcels to ascend adiabatically to conserve their potential temperature as they move towards the poles (Law and Stohl, 2007). Once in the stable Arctic troposphere, where there is little to no mixing, radiative cooling causes the slow descent of air parcels towards the surface with eventual dry deposition due to the

lack of precipitation (Klonecki et al., 2003). With the weakening of the polar vortex and disruption of the stable Arctic air mass in the spring, the likelihood of deposition on the Arctic surface increases (Koch and Hansen, 2005). In the summer, the transport mechanism changes with the majority of air parcels undergoing diabatic transport with increased mixing and dilution from increased atmospheric moisture.

Atmospheric blocking events – large scale patterns in the atmospheric pressure field that are nearly stationary and act to block migratory cyclones – present another potential transport mechanism. There are five major types of blocks: Omega Block, Rex Block, Ring of Fire, Split Flow and Cut-off Low, which are predominantly associated with high pressure systems; however, there are instances of stagnant low pressure systems creating blocks. They are often associated with prolonged periods of dry weather which can lead to extreme droughts in the summer or extreme temperature fluctuations in the winter; however, their impacts are dependent on both the location, magnitude, and seasonality of the blocking event. The temporal persistence and large spatial scale of these systems lead to a range of impacts on both natural and managed ecosystems, including, impacts on crop yield (USDA FAS, 2012), sow and harvest timings (USDA FAS, 2013b) and wildfire occurrence (Bondur, 2011).

The extreme weather events associated with these mid-latitude, synoptic scale weather patterns have led to an increase in scientific attention in recent years. Blocking events occur in the southern and northern hemisphere (NH) mid-latitude regions and their development in the NH is related to the presence of a strong mid-latitude cyclone upstream of the block (Lupo and Smith, 1995; Tsou and Smith, 1988). These mid-latitude cyclones typically develop via cyclogenesis from a perturbation along the Polar Front.

Seasonally, NH blocking events have higher frequencies in winter and spring compared to summer, while winter blocking events are also typically larger, more intense, and have longer durations than in the summer. The increased duration and intensity of winter blocks as compared to summer blocks is linked to the strength of the mid-latitude cyclone (Lupo and Smith, 1995).

Focusing specifically on the NH, these blocking events are distributed globally with the highest blocking frequencies occurring in the Atlantic/European region (approximately 0° – 45°E) and the Central Pacific regions (approximately 180° – 200°E) (Barriopedro et al., 2006; Pelly and Hoskins, 2003). The longitude ranges for the highest frequency of blocking events vary slightly depending on the specific blocking index and the seasonality of the blocking event (Scherrer et al., 2006). Several studies have focused on the ability of these blocking events to transport pollutants to regions outside of the emission source (Raatz and Shaw, 1984; Witte et al., 2011). Primarily focusing on blocking highs (an atmospheric block associated with a stagnant high pressure system) the persistent anticyclonic wind field leads to either the accumulation of air pollutants within the circulating wind field or leads to the accelerated transport of pollutants along the periphery where the pressure gradients are relatively strong. The transport of pollutants to regions outside of the emission source can be seen during the July – August 2010 extreme blocking event in European Russia. A study on Russian wildfires found that emissions from fires on the southern boundary of a blocked anticyclone are transported westward or northward due to the position of the wind fields in a high pressure system; whereas emissions from fires within the blocked anticyclone become pooled within the circulating wind field (Witte et al., 2011). The stagnant nature and

geographic position of the July 2010 blocking event relative to the fire activity (Figure 4.1a) led to the transport and eventual accumulation of atmospheric pollutants over densely populated regions, such as Moscow (Figure 4.1b). During this event, roughly 55,000 people lost their lives in Russia due in part from the heat wave and the extreme concentration of atmospheric pollutants (Guha-Sapir, 2010).

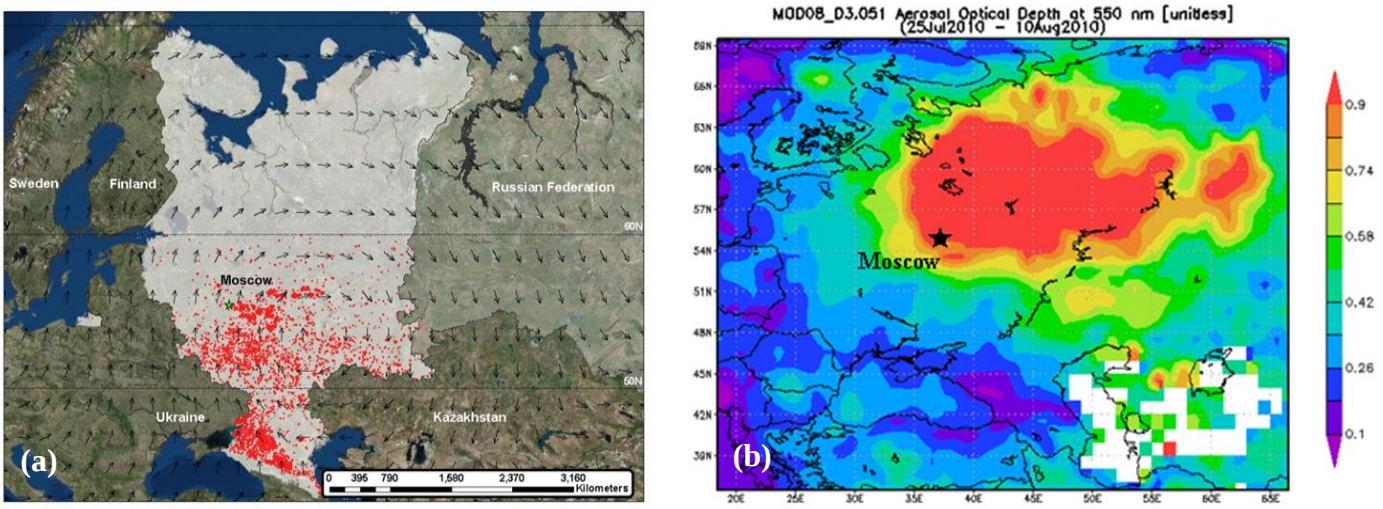

Figure 4.1: (a) Average wind direction (arrows) and MODIS active fire (MCD14ML; red points) cropland fires and (b) Aerosol Optical Depth (MOD08; Hubanks et al., 2008) between 25th July and 10th August 2010. The persistent anticyclonic wind pattern transported the emissions from the southern regions of European Russia and pooled them over Moscow and surrounding regions. (Aerosol Optical Depth data source: Giovanni, 2013).

Studies linking the long-range transport to the Arctic associated with atmospheric blocks first appeared in the scientific literature in the early 1980's; however, these studies are focused on specific instances of atmospheric blocking events (Iversen and Joranger, 1985; Raatz and Shaw, 1984; Raatz, 1989). In particular, these studies tend to start with a blocked anticyclone that pools air pollutants, similar to the July 2010 blocking event in

European Russia, followed by the approach of a migratory low pressure system. This generates an increase in the pressure gradient between the two systems leading to a surge of pollutants that travel north within 7 – 10 days. Unlike these previous studies, this doctoral study specifically focuses on the persistent wind patterns associated with these quasi-stationary meteorological conditions. Furthermore, this study assesses whether atmospheric blocking events can enhance the likelihood of transport or accelerate the transport of pollutants to the snow-covered Arctic from Russian cropland burning based on the persistent wind patterns in comparison to conditions without blocking events. Atmospheric blocking conditions under the presence of a blocking event will be referred to as a "blocked" condition throughout the rest of the dissertation. Conversely, conditions that are not influenced by a blocking event will be referred to as a "nonblocked" condition.

In the previous chapter, the potential for transport of crop residue burning emissions from Russia to the Arctic snow has been established. The identification of a potential transport mechanism that can accelerate the transport of BC emissions has important implications for the potency of deposited BC on the Arctic snow. As the residence time increases, BC becomes increasingly mixed with other atmospheric constituents leading to changes in the optical properties and atmospheric lifetime of BC (Bond et al., 2013). The exact impact of deposited BC on Arctic snow relies on information of the chemical and microphysical processes within the atmosphere; however, as a general rule, the longer a molecule remains in the atmosphere the more mixing and alterations it will undergo before it is ultimately removed via wet or dry deposition.

This study's primary focus is on quantifying the variability in transport of potential crop residue emissions from the Russian cropland to the snow-covered Arctic based on the persistent wind patterns of atmospheric blocking events between 2003 and 2015. The overall aim is to establish if atmospheric blocking events; 1) impact the number of agricultural fires and thus the subsequent BC emissions that could be potentially transported to the Arctic; 2) improve the success rate of transport to the Arctic, which ultimately determines what fraction of the cropland burning contributes to the BC deposition in the Arctic; and 3) accelerate the transport time which is crucial for understanding the potential increase in potency of BC depositions on Arctic snow.

4.2: Data and Methods

4.2.1: Low-level transport model data

The successful transport trajectories and corresponding transport time (hours) data layers created via the low-level transport algorithm developed in Chapter 3 (described in detail in Section 3.3) form the basis of this analysis. The transport algorithm is developed from the ERA-Interim (0.75° grid cell) U- and V- wind components and precipitation data. Hourly starting cropland burning locations were determined by the MODIS active fire (MCD14ML C6) dataset and the IGBP cropland mask (see Section 3.2). The transport trajectories were tracked at five pressure levels to account for the reported differences in crop burning injection heights: 1000mb (~110 m altitude), 975mb (~323 m altitude), 950mb (~540 m altitude), 925mb (~762 m altitude), and 900mb (~914 m altitude). The algorithm was designed to only record successful transport and deposition of potential BC emissions from cropland burning locations to the Arctic (defined as above 60°N) if the hypothetical emission parcel reached the snow-covered ground within

96 hours. The 96 hour threshold was chosen based on the combination of a literature search of other transport models and the atmospheric lifetime of BC (Larkin et al., 2012). A transport trajectory was determined to be unsuccessful if the emission parcel encountered precipitation, as the algorithm assumed total washout of BC from the atmosphere. The only exception to this was if the precipitation was encountered while over snow-covered ground in the Arctic – i.e. wet deposition. The transport trajectories and corresponding transport time were used to develop the following metrics: time to successful deposition (hours) and percent success which is defined as the percentage of successful transport events.

4.2.2: Atmospheric Blocking Index

To analyze the impacts of atmospheric blocking events on the transport time and success rate to the Arctic, the Center of Blocking Studies in the Atmospheric Science Research Program at the University of Missouri-Columbia atmospheric blocking index dataset was used in this study (Lupo et al., 2008). The dataset is available for the southern and northern hemispheres between 1968 and present and is based on the 2.5° NCEP/NCAR (Kalnay et al., 1996) 500mb geopotential height (GPH). The Lupo et al., (2008) atmospheric blocking index criteria are taken from a study by Lupo and Smith, (1995) which are based on a modified version of the Lejenäs and Økland, (1983) index and the Rex (1950) blocking criteria. These are both widely accepted methods for calculating and defining atmospheric blocking events (e.g. Barriopedro et al., 2006; NOAA, 2005). To summarize, the Lupo et al., (2008) blocking index criteria, included, defining a blocking event as having a minimum duration of 5 days, a horizontal extent of

over 30 degrees longitude, and an amplitude of at least 5 degrees latitude. The NH atmospheric block must also begin poleward of 35°N.

The dataset contains several variables, including; time and dates of blocking onset and decay, longitude of block onset, blocking size (based on the definition found in Lupo et al., 1995) and blocking intensity (based on the definition found in Wiedenmann et al., 2002). Blocking intensity is based on the magnitude of the GPH gradient and represents increasing wind speeds. To ensure consistency, this study used the same definitions for blocking intensity (BI) categorization as Weidenmann et al., (2002): weak (BI < 2.0); moderate (2.0 < BI < 4.3); strong (BI > 4.3). The blocking size is defined as the distance between the upstream and downstream inflection points along the 500hPa GPH contour. Assessment of the NH blocking index dataset was carried out to remove any blocks that did not originate between 0°E and 175°E. Although the analysis focuses on Russian cropland, the larger spatial area was chosen to extend the western edge of the analysis field to account for atmospheric blocks that may occur over Central and Eastern Europe. The blocking index was further refined to only include blocks between 2003 and 2015 to account for full years of both MODIS Aqua and Terra active fires.

4.2.3: Development of daily atmospheric blocking layers

To quantify the impact of atmospheric blocking events on the potential transport to the snow on the Arctic, daily atmospheric blocking layers were created based on the blocking dates, starting longitude, and block size. The block size was supplied in units of kilometers, while the starting longitude was defined in degrees. To create spatial blocking layers, the ending longitudes (degrees) had to be estimated using Vincenty's formula which calculates the distance between two points on the surface of a spheroid. Since the

starting latitude is unknown, which is one of the drawbacks of current blocking indices, a starting latitude of 60°N was used for the calculations. The use of 60°N as a central latitude in atmospheric blocking research is a common assumption since these phenomena are primarily mid-latitude weather patterns (Pelly and Hoskins, 2003; Tyrlis and Hoskins, 2008). The daily blocked masks were created between the two longitudes and all latitudes between 35°N and 85°N. The final longitude was rounded to the nearest 0.75° grid cell. The purpose of these blocking layers is to visually identify the easterly movement of the blocks and to identify any blocks which were separated in the original data table but were in fact part of the same blocking structure. For example, in July – August 2010, the long lasting blocking event was separated into two separate blocks based on the definition of blocking events used in the Lupo et al., (2008) blocking index. However, when the daily blocking layers were created between July and August 2010 there was overlap between the eastern edge of the first block and the western edge of the second block. These blocking layers were further grouped into weak, moderate, and strong events based on the reported blocking intensity. Overall five separate time series of blocking layers were created between 2003 and 2015: weak blocks, moderate blocks, strong blocks, all intensity blocks and nonblocks. Nonblocked layers were areas outside the blocking boundary (regardless of intensity) or on days with no blocks at all.

These daily atmospheric blocking layers are used to extract the cropland burning grid cells (with corresponding transport time to the Arctic) which are temporally completely within the atmospheric blocking event and whose location is spatially completely within the blocking boundary. In addition, the same criteria is applied to cropland burning grid cells which do not occur within a blocking boundary and whose

transport time is not interrupted by a block. To further clarify, Figure 4.2 illustrates the criteria required in selecting "pure" blocked and nonblocked cropland burning grid cells. Assuming each of the 4 grid cells (A – D) have transport values of 72 hours to the Arctic, the selection of the purest grid cells (A and B) requires the fire to be located spatially within (A) or outside (B) the blocking extent (grey) for the entire length of transport time. The two remaining scenarios (C and D) are "mixed". In these two mixed scenarios, the cropland burning grid cells start either within (C) or outside (D) of a block, but before 72 hours has passed either the block has terminated (C) or has developed (D). Undertaking the analysis in this manner allows only the purest scenarios to be included to ensure the persistent wind patterns associated with blocking events are isolated as much as possible.

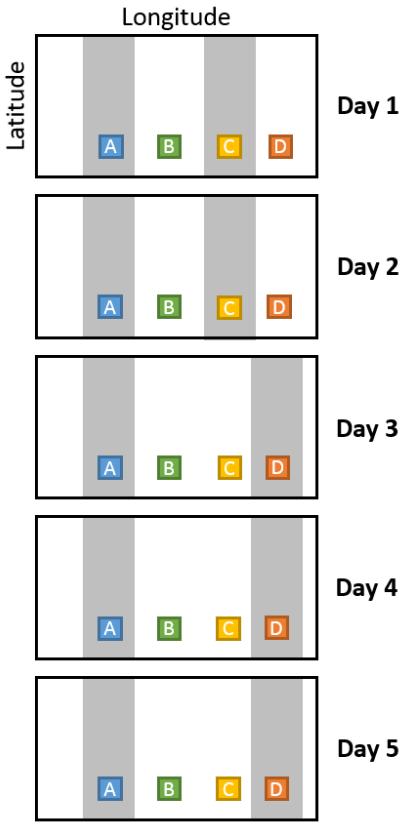

Figure 4.2: Illustration representing the selection of a pure blocked grid cell (A) and a pure nonblocked grid cell (B). The two mixed scenarios (C and D) are also represented. Hypothetical blocking events (grey) are shown over a five day period.

4.3: Results

4.3.1: Atmospheric Blocking Index

Despite the severe impacts on fire activity and subsequent human health impacts caused by the transport and pooling of the emissions, the July – August 2010 atmospheric block that occurred over European Russia is only considered to be a moderate intensity block – as defined by the blocking intensity outlined in Weidenmann et al., (2002). Analysis of weak, moderate and strong atmospheric blocks between 2003 and 2015 found that the strongest blocks occur in winter and early spring (Figure 4.3). This is consistent with studies utilizing other blocking indices (e.g. Barriopedro et al., 2006; Pelly and Hoskins, 2003)

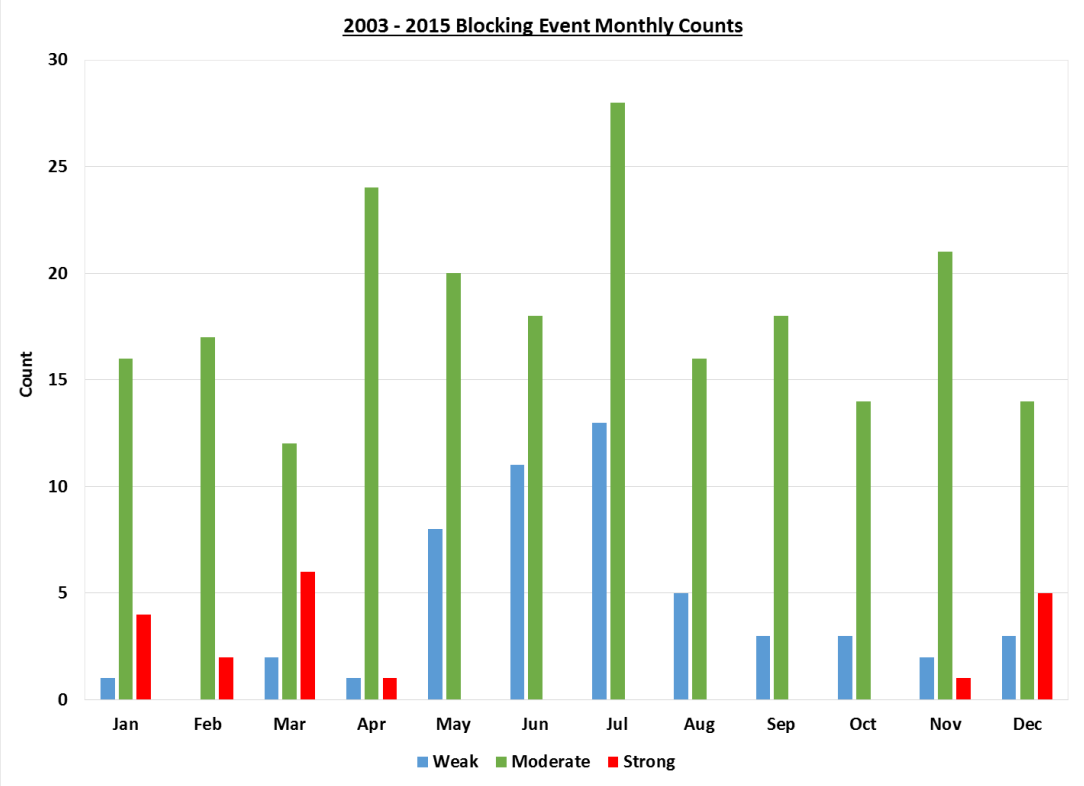

Figure 4.3: Monthly counts of weak, moderate and strong blocking events between 2003 and 2015.

So why was the 2010 blocking event so extreme and yet not recorded as a strong intensity block in the blocking index dataset? As previously mentioned, the blocking intensity values are proportional to the GPH gradient; however, these values do not consider duration as a factor for intensity. Typically, summertime Eurasian blocking events last on average 10 days; however, the 2010 block lasted almost 30 days (Dole et al., 2011). During the 2010 block, this increase in duration combined with the already increased summertime temperatures in the region led to severe drought and ultimately a surge in fire activity. Specifically, focusing on the July 2010 Russian fire activity, the majority of fires occurred south of Moscow, but the persistent anticyclonic winds transported and began pooling the emissions over the Moscow region, ultimately leading to thousands of deaths related to severe air pollution (Shaposhnikov et al., 2014).

Therefore simply utilizing blocking intensity as a measure for enhanced transport (due to high wind speeds) could potentially miss these significant events. The other possible transport mechanism is created by the establishment of persistent wind patterns which can ensure poleward transport of pollutants from southern agricultural regions to the Arctic over a prolonged period of time, associated with the block duration. However, relating block duration to transport is difficult to assess as the block can subtly move eastward throughout its life time causing the recorded duration to vary at different locations along its path. Therefore the recorded durations in blocking indices could potentially underestimate the duration of the longer blocking events depending on the specified blocking criteria. However, based on the durations recorded in the Lupo et al., (2008) blocking index, monthly counts between 2003 and 2015 found March and April to contain blocks with durations up to 15 days, whilst May has a number of blocks with

durations between 15 – 30 days (Figure 4.4). The persistent wind associated with these longer duration blocking events, especially in May, could have a large influence on the long-range transport of BC emissions to the Arctic during the most vulnerable period for sea ice melt.

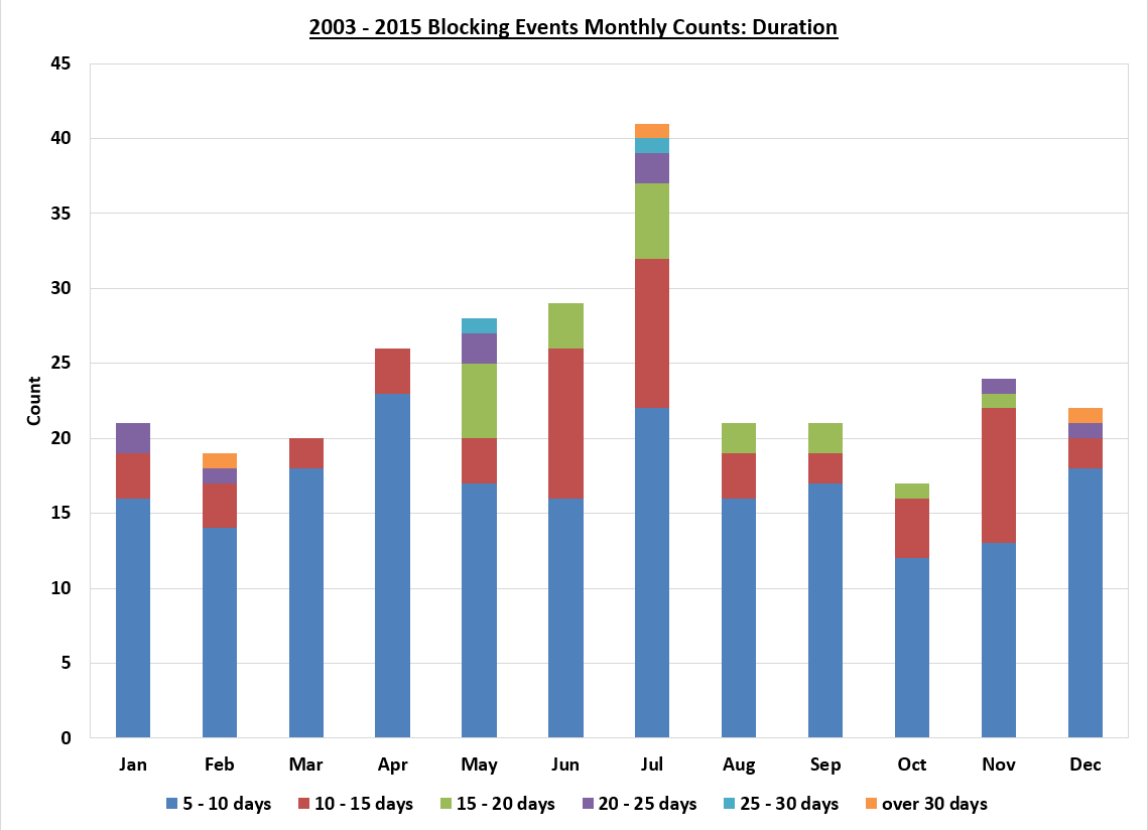

Figure 4.4: Monthly counts of blocking events duration between 2003 and 2015.

Another key factor of how blocking events can have an impact on emission transport lies in the geographic location of the blocking event. The 2010 blocking event was situated in such a location that the anticyclonic wind pattern coincided with the fire activity allowing the transport and subsequent pooling of emissions (Witte et al., 2011). Analyzing the spatial extent of the blocking events reveals the highest concentration

occur between 30°E and 90°E (Figure 4.5), corresponding to an area containing approximately 80% the of Russian cropland area (see Figure 3.1).

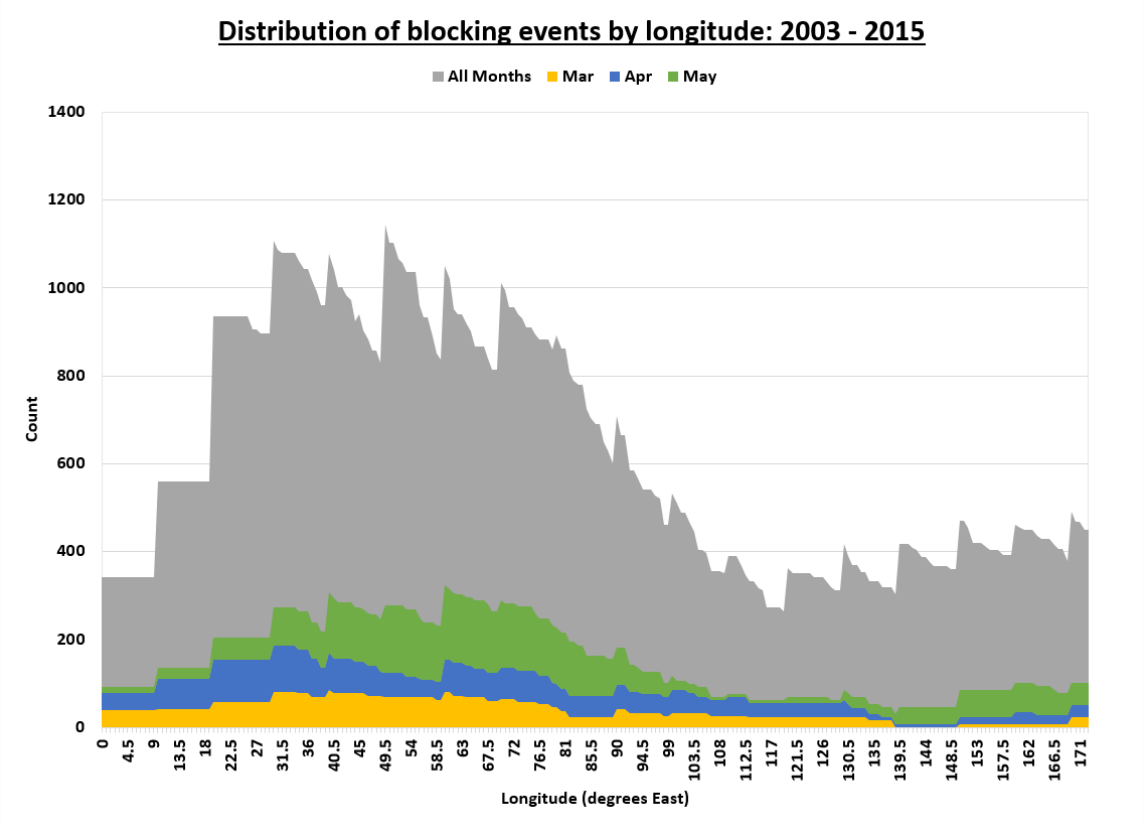

Figure 4.5: Total monthly count (grey) and March, April and May (yellow, blue, and green respectively) between 2003 and 2015 for all blocking events. Blocking events are defined sharply at different longitudes causing the observed exaggerated effect on this graph.

The frequency of block occurrence over such a vast section of the Russian cropland and the proclivity for strong blocks in March and long duration blocks in May, have important consequences for the BC deposition on the Arctic snow.

4.3.2: Cropland Burning and Atmospheric Blocking Events

The relationship between atmospheric blocking events and forest fires has been well-documented (e.g. Hayasaka et al., 2016; Johnson and Wowchuk, 1992; Skinner et al., 1998). The persistent hot and dry conditions in the summer often lead to intense droughts and therefore increased wildfire activity; however, the relationship between blocking events and managed fires has not been well established. Analysis of monthly active fire detections normalized by cropland area and number of days under blocked and nonblocked conditions between 2003 and 2015 found no clear relationship between cropland burning and blocking event occurrence (Figure 4.6). Interannual variations between fire occurrence and blocked/nonblocked days are evident; however, no statistically definable consistent pattern emerged in this analysis.

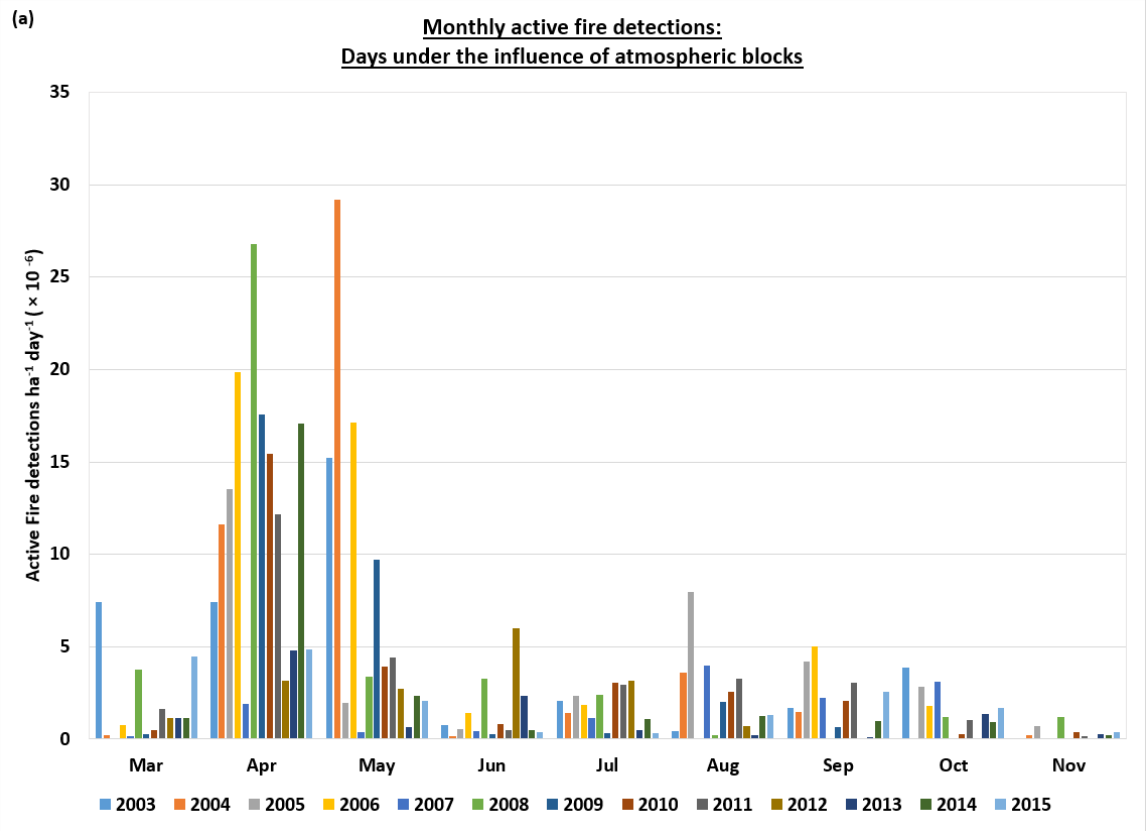

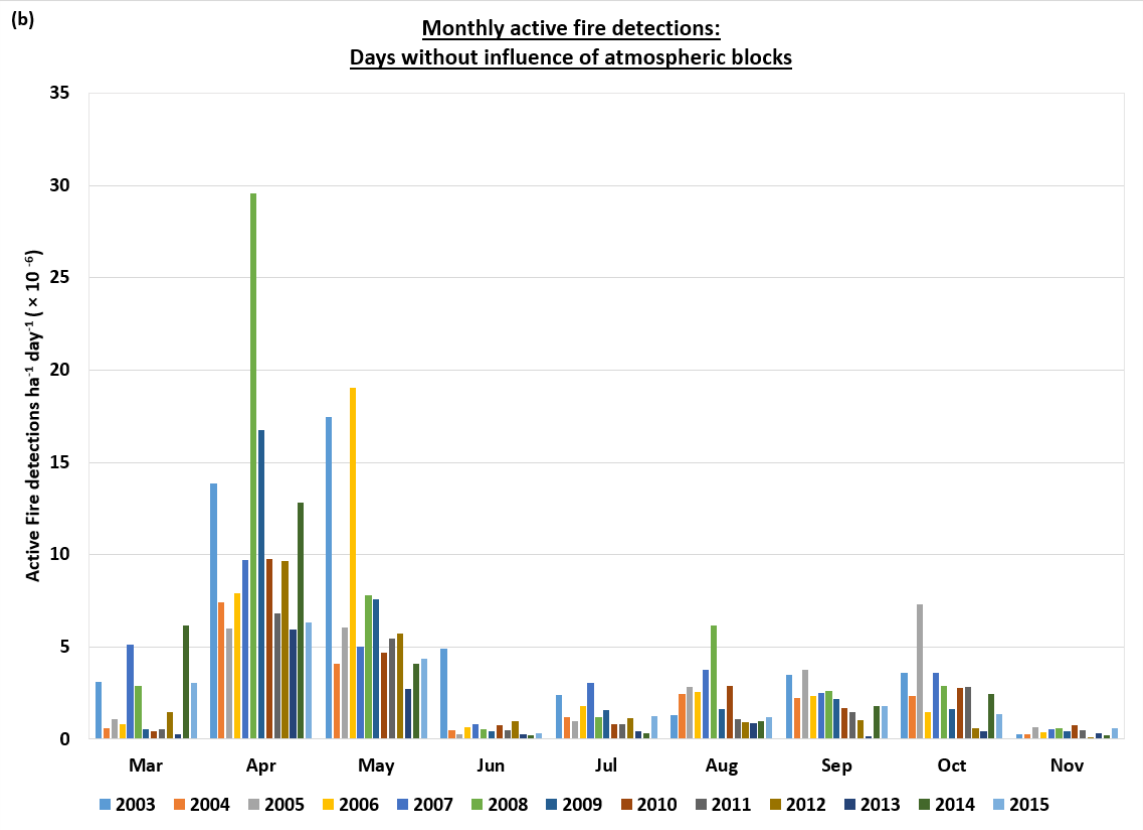

Figure 4.6: Monthly active fire detections normalized by cropland area and number of days under blocked (a) and nonblocked (b) conditions between March and November (2003 – 2015). The data was normalized to account for the larger number days without influence of atmospheric blocks.

Although there seems to be no relationship between blocking events and cropland burning occurrence based on the above analysis, there is a potential for a lagged relationship. A delayed response in burning may occur based on the potential impact of a blocking event during the crop growth cycle and sow/harvest timings, however, this aspect of blocking influence is outside the scope of this study.

4.3.3: Transport patterns under blocked and nonblocked conditions

Analysis of the transport time (hours) and the success (%) of reaching the snow-covered Arctic found that on average (over the entire Russian cropland) transport under both nonblocked and blocked conditions was fairly comparable in certain months (e.g. April, and May); however, there were vast differences in other months (Table 4.1). For example, late fall and winter, transport under blocking conditions was slower to reach the Arctic snow, whilst in March transport under blocking conditions was faster. In addition, analysis of the percent success found on average under blocking conditions the hypothetical emission parcels were more likely to reach the Arctic than under nonblocked conditions. The main exceptions were noted in January and October (Table 4.2). Although quantifying the overall averaged transport time and success rate under both blocked and nonblocked conditions is useful to summarize the general impact over the whole Russian cropland region, it oversimplifies a fairly complex spatial output.

Table 4.1: Monthly average transport time (μ, hours) and associated n value (n) between 2003 and 2015 under blocked (B and nonblocked (NB) conditions for all injection heights.

	900mb				925mb				950mb				975mb				1000mb			
	B (μ,n)		NB (μ,n)		B (μ,n)		NB (μ,n)		B (μ,n)		NB (μ,n)		B (μ,n)		NB (μ,n)		B (μ,n)		NB (μ,n)	
Jan	-	0	52	35	-	0	54	30	-	0	62	20	-	0	67	7	-	0	36	1
Feb	46	29	38	216	44	27	38	224	43	25	37	187	47	19	39	113	73	2	50	78
Mar	40	645	50	1990	34	474	47	1839	30	307	44	1758	28	264	44	1529	34	246	42	827
Apr	36	4593	32	11104	35	4509	32	11373	35	4246	33	10530	37	3779	36	8836	43	2193	47	5398
May	34	4150	32	7081	33	3983	33	6962	34	3950	35	5948	38	3244	38	4447	51	1559	48	1839
Jun	42	73	36	176	46	74	35	164	51	55	39	121	58	24	51	47	68	4	66	25
Jul	-	0		0	78	1	37	1	-	0	-	0	-	0	-	0	-	0	-	0
Aug	84	9	92	5	77	7	94	5	65	1	94	2	76	1	69	1	-	0	-	0
Sep	71	32	52	65	84	12	55	53	84	10	66	29	-	0	44	2	88	1	52	1
Oct	71	34	40	1027	73	31	40	975	75	40	41	791	56	26	44	707	63	8	53	427
Nov	61	91	43	117	52	83	40	124	48	89	34	106	51	113	37	98	63	59	60	56
Dec	37	8	33	17	33	5	34	14	55	6	20	12	53	5	10	9	15	1	5	6

Table 4.2: Monthly average success rate (μ, %) and associated n value (n) between 2003 and 2015 under blocked (B and nonblocked (NB) conditions for all injection heights.

	900mb				925mb				950mb				975mb				1000mb			
	B (μ,n)		NB (μ,n)		B (μ,n)		NB (μ,n)		B (μ,n)		NB (μ,n)		B (μ,n)		NB (μ,n)		B (μ,n)		NB (μ,n)	
Jan	1	95	6	565	1	95	5	565	1	95	4	565	1	95	1	565	1	95	0	565
Feb	8	367	8	2573	7	367	9	2573	7	367	7	2573	5	367	4	2573	1	367	3	2573
Mar	17	3886	7	29039	12	3826	6	29099	8	3714	6	29211	7	3699	5	29226	7	3738	3	29187
Apr	18	26078	8	130937	17	26143	9	130872	16	26132	8	130885	14	26220	7	130797	8	26166	4	130851
May	14	30413	7	95352	13	30460	7	95305	13	30587	6	95170	11	30657	5	95108	5	30682	2	95083
Jun	1	5609	1	23548	1	5614	1	23543	1	5603	1	23554	0	5590	0	23567	0	5583	0	23574
Jul	0	18087	0	33734	0	18087	0	33734	0	18087	0	33734	0	18087	0	33734	0	18087	0	33734
Aug	0	17213	0	58518	0	17212	0	58519	0	17212	0	58519	0	17212	0	58519	0	17212	0	58519
Sep	0	9492	0	54092	0	9492	0	54092	0	9492	0	54092	0	9492	0	54092	0	9492	0	54092
Oct	0	7498	2	46377	0	7497	2	46378	1	7493	2	46382	0	7498	2	46377	0	7502	1	46373
Nov	3	2685	2	6971	3	2692	2	6964	3	2693	2	6963	4	2692	1	6964	2	2682	1	6974
Dec	5	165	2	866	3	166	2	864	4	168	1	863	3	168	1	865	1	166	1	867

Based on the importance of BC deposition on the Arctic snow during the spring, the following results will be focused on March, April and May for the two extremes in the range of analyzed injection heights (900mb will be illustrated and 1000mb included in the text). Analysis was undertaken on the impact of weak, moderate and strong blocks; however, the results are generally focused on all blocks (regardless of intensity) and nonblock scenarios. This is primarily because the majority of blocking events over Russia are moderate blocks and the already low number of blocked grid cells was reduced further upon splitting the analysis into the three different blocking intensities. To quantify the spatial variability under blocked and nonblocked conditions, mapped outputs of average transport time, the percent success for each starting grid cell, and the number of fire occurrences in each successful cropland burning grid cell was performed (Figures 4.7 – 4.9). Difference maps (nonblock minus block) were also included in the results to highlight the difference between nonblocked conditions and blocked conditions in the three metrics. Only grid cells which contained values in both blocked and nonblocked maps were subtracted. The difference map color bars have been created so that red grid cells indicate that transport under blocked conditions was either quicker, more successful or contained higher fire loads compared to the blue color indicating that transport was quicker, more successful or had higher fuel load under nonblocked conditions.

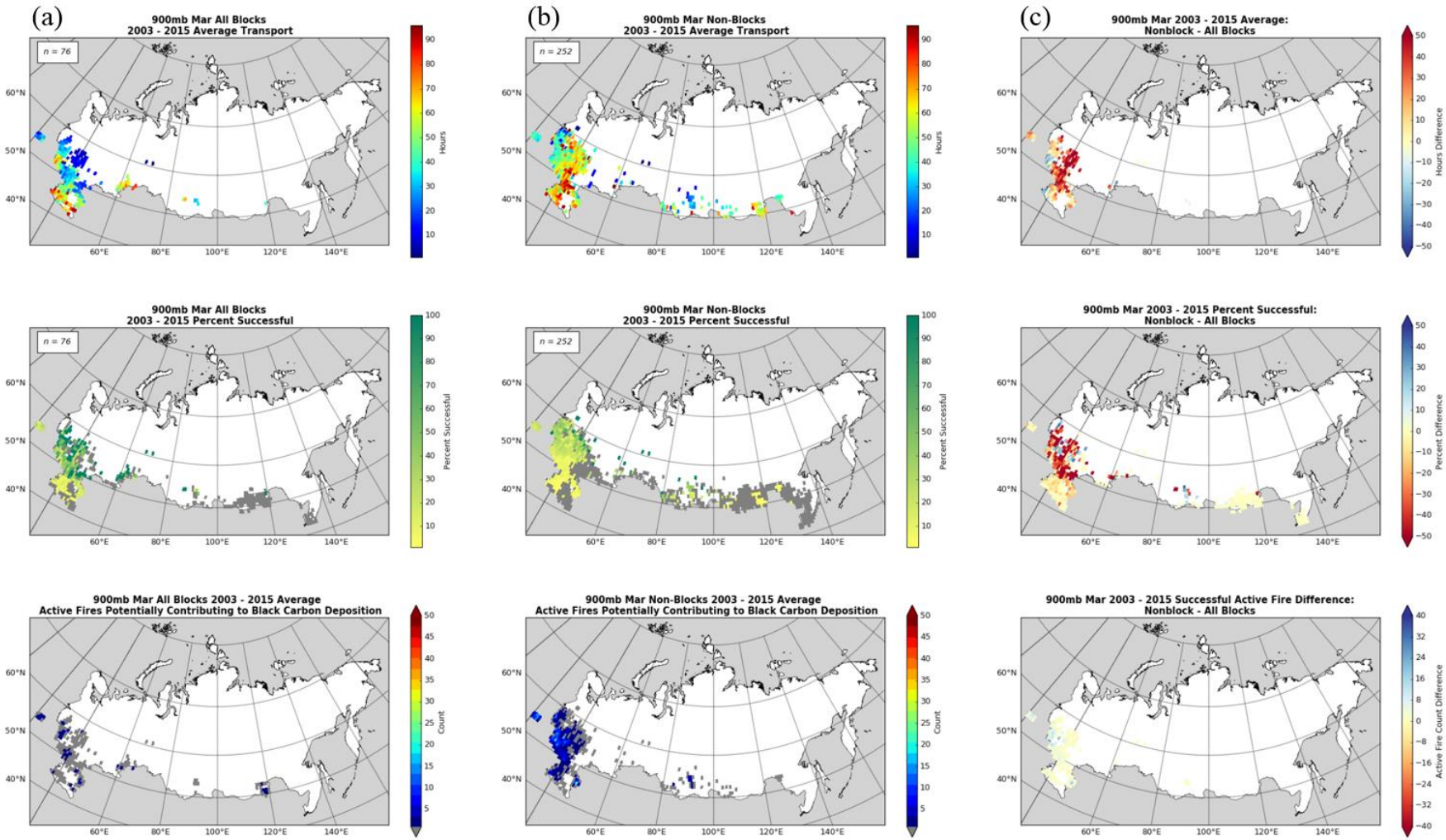

Figure 4.7: 900mb March 2003 – 2015: The average transport time (top), percent success (middle) and successful active fires (bottom) are highlighted for All Blocks (a), Nonblocks (b) and Difference (c) maps. Only grid cells which contained values in both block and nonblock maps were differenced. The difference map color bars have been created so that red grid cells indicate transport under blocked conditions was either quicker, more successful or contained higher fire loads compared to the blue color indicating that transport was quicker, more successful or had higher fuel load under nonblocked conditions.

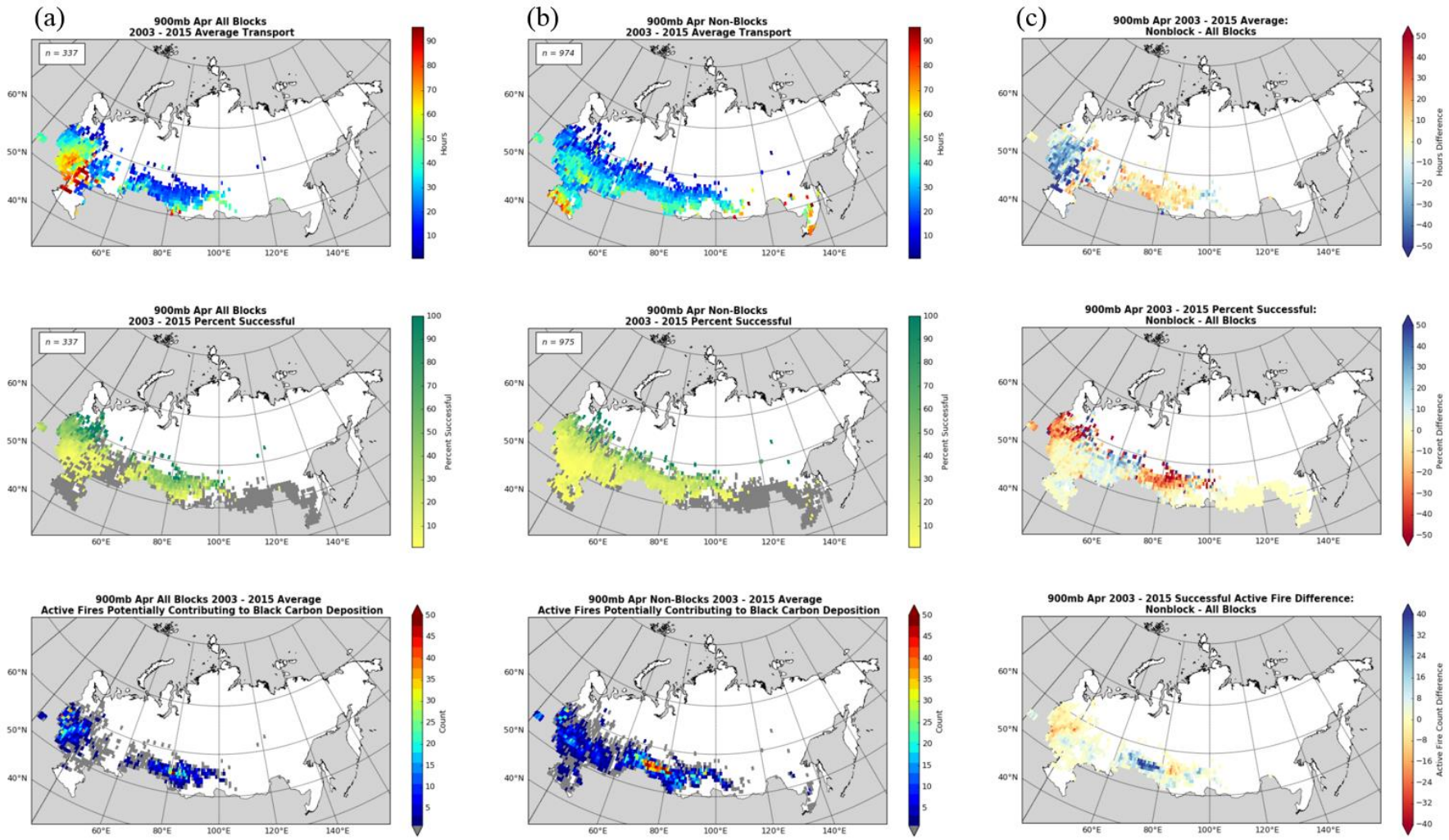

Figure 4.8: 900mb April 2003 – 2015: The average transport time (top), percent success (middle) and successful active fires (bottom) are highlighted for All Blocks (a), Nonblocks (b) and Difference (c) maps. Only grid cells which contained values in both block and nonblock maps were differenced. The difference map color bars have been created so that red grid cells indicate transport under blocked conditions was either quicker, more successful or contained higher fire loads compared to the blue color indicating that transport was quicker, more successful or had higher fuel load under nonblocked conditions.

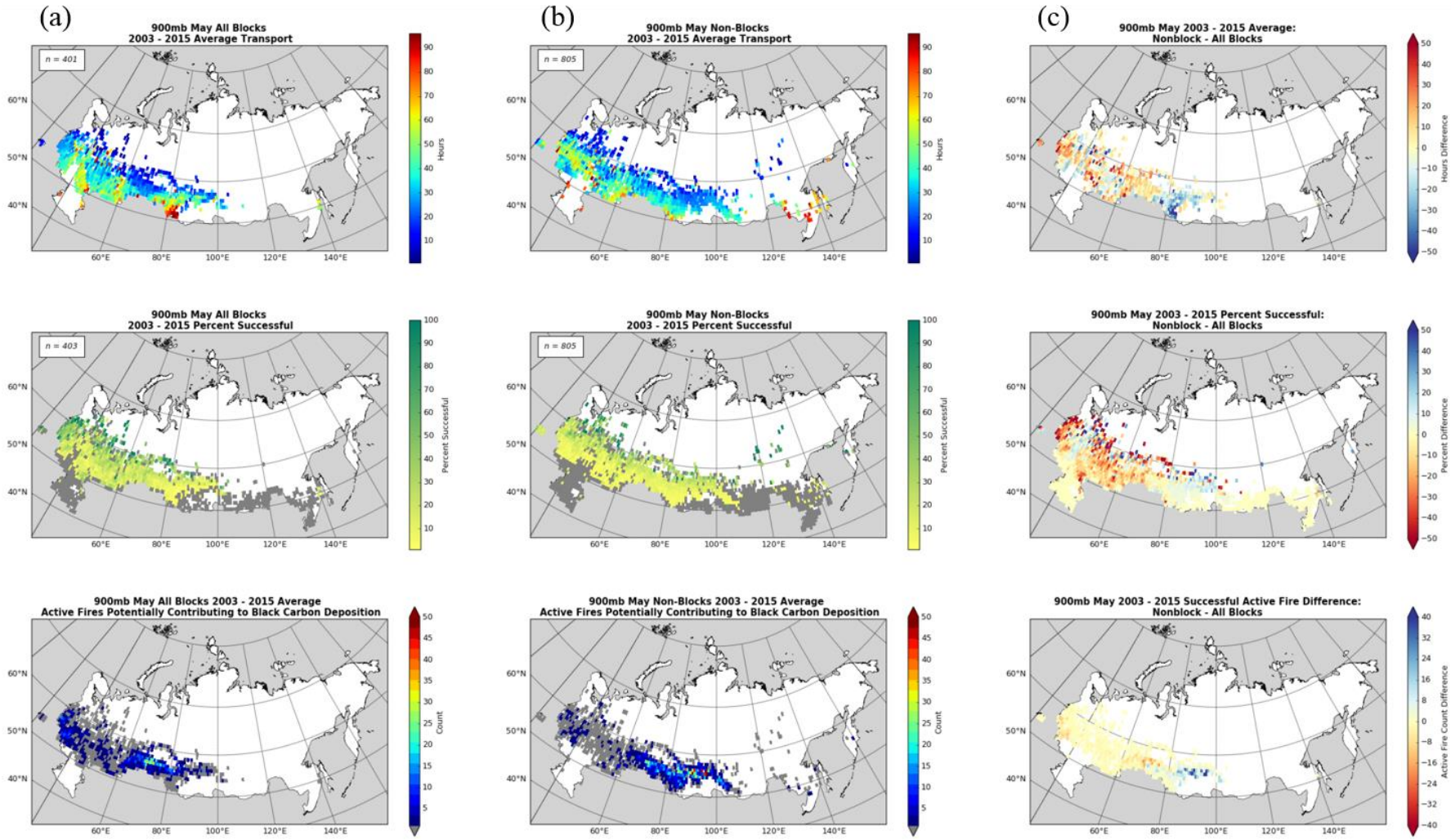

Figure 4.9: 900mb May 2003 – 2015: The average transport time (top), percent success (middle) and successful active fires (bottom) are highlighted for All Blocks (a), Nonblocks (b) and Difference (c) maps. Only grid cells which contained values in both block and nonblock maps were differenced. The difference map color bars have been created so that red grid cells indicate transport under blocked conditions was either quicker, more successful or contained higher fire loads compared to the blue color indicating that transport was quicker, more successful or had higher fuel load under nonblocked conditions.

The difference maps indicate that overall blocking events are more successful and are quicker at transporting potential BC emissions to the snow-covered Arctic during March and May, regardless of injection height. Although the lower injection heights are associated with longer transport times and decreased success rates as compared to the higher injection heights.

Overall, in March, the transport time to the Arctic is shorter (in some areas over 50 hours less at higher injection heights) and the success rate is also much higher during blocked conditions (Figure 4.7). Although the number of fire occurrences within these regions is fairly low (< 15 active fires on average between 2003 and 2015) they are associated with areas with the highest wheat yields in the Russian cropland. Therefore the fires could possible contain higher volumes of crop residue leading to a higher amount of BC emissions. At the lowest injection height, the success percentage was still much higher during blocked conditions and the transport was still quicker as compared to nonblocked conditions; however, the magnitude of the time difference was lower.

May also illustrates that transport under blocked conditions is generally more successful and are also quicker than nonblocked conditions; however, unlike March there is considerable spatial variability (Figure 4.9). The area in blue, centered on 90°E in both the transport and active fire difference maps shows that those areas contain not only more cropland fires during nonblocked conditions but the potential emissions are also transported to the Arctic faster during the nonblocks. This result has implications on the BC deposition in the Arctic as nonblocked conditions are more prevalent than blocked conditions. At the lowest injection height, the percent

success decreased overall with two exceptions. The region centered on 90°E is still present but not as pronounced; however, the north-west corner (approximately 55°N, 45°E) still showed differences of over 50% in successful transport under blocking conditions.

April is the notable exception with slower transport times in the western region of European Russia (centered on 55°N, 40°E) and less successful transport in the region centered on 80°E (Figure 4.8) under blocking conditions. These two sections are most distinct at higher injection heights but can still be identified at the lowest injection height. Further analysis revealed a large portion of the successfully transported fires in the western region of European Russia under blocking conditions were driven by a single blocking event in April 2006. This moderate blocking event lasted 10 days with a spatial extent between approximately 10°E and 45°E. There were two other blocking events during April 2006; however, they were located further east, starting at 60°E and 100°E respectively. The location of this blocking event in relation to the fire activity created an ideal example of the gradation of transport times caused by the circulating wind patterns associated with the blocked high pressure system (Figure 4.10). Under this atmospheric pattern, many fires that started around 55° – 58°N, first traveled south reaching 50°N following the anticyclonic winds before turning west and subsequently north thus substantially extending the atmospheric transport pathway before reaching the snow above 60°N.

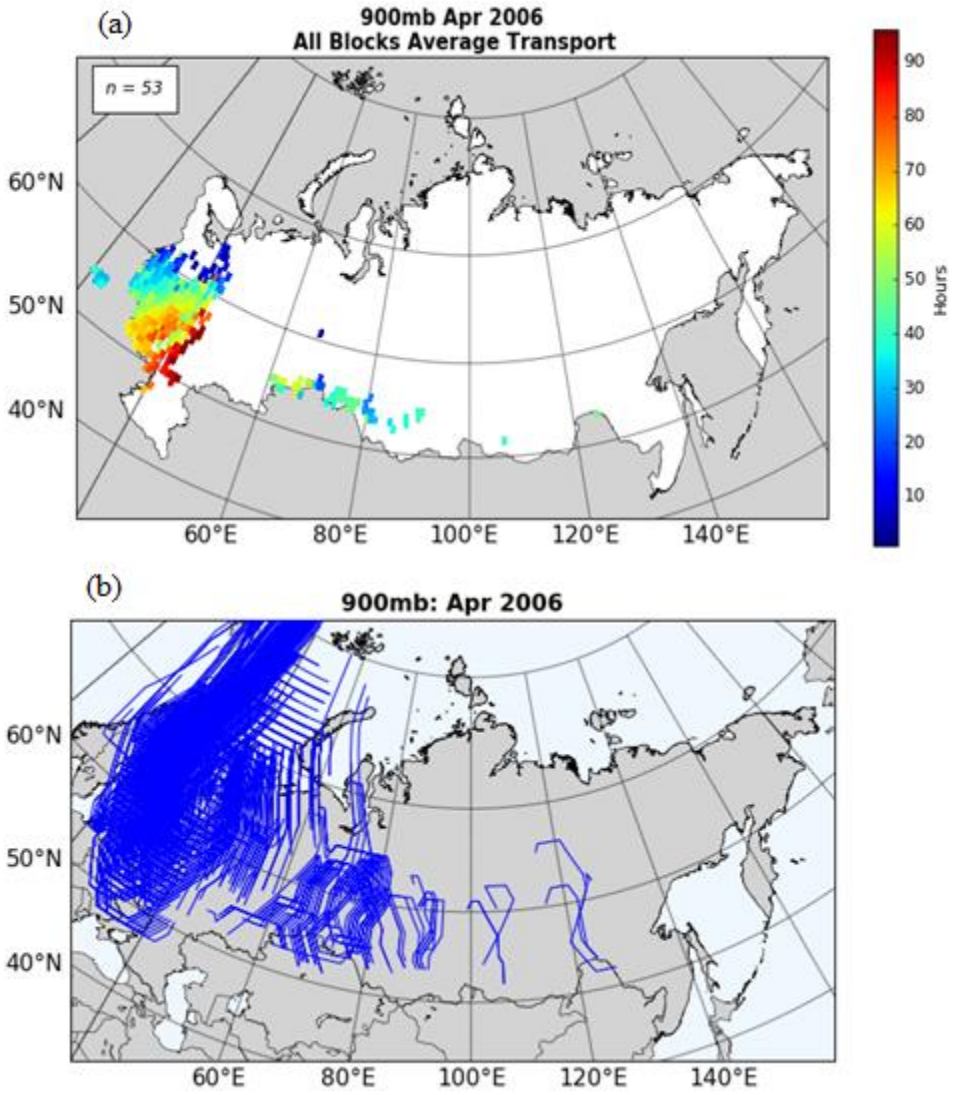

Figure 4.10: 900mb April 2006 blocking event transport time to the snow-covered Arctic within 96 hours of burning (a) and corresponding trajectories (b).

4.3.4: Latitudinal variability

Statistical tests were carried out on the transport time (hours) data to compare the average transport times to the snow-covered Arctic during blocked and nonblocked conditions at the following latitude bands: 40° – 45°N, 45° – 50°N, 50° – 55°N, 55° – 60°N, 60° – 65°N and > 65°N at each of the five injection heights (pressure levels). The average transport time and spread of the data between blocks and nonblocks varied depending on the month, injection height and latitude band. To help focus the analysis, significance testing using the Welch's two-sided t-test was undertaken on the mean transport time for all blocks and nonblocks at every latitude band and injection height (Table 4.3). The Welch's t-test assumes the populations do not have identical variances and have normal distributions. The null hypothesis states that the mean transport time under blocked conditions is equal to nonblocked conditions, whilst the alternative hypothesis states that the means are not equal. Using both a 90% and 95% confidence level, p- and t-values were evaluated. This test was used as an indicator for the general significance for each latitude band to help focus the latitudinal analysis on latitude bands with the highest likelihood of significant transport differences. The box plot graphs (Figures 4.11 – 4.13) indicate that most of the data populations are close to normal, thus the use of a parametric test can be justified in this instance.

Table 4.3: Welch's two-sided t-test results comparing the difference in the mean transport time (hours) under blocked and nonblocked conditions for all injection heights (pressure levels). P values: < 0.05 (blue); < 0.1 (green); > 0.1 (grey; null hypothesis accepted). The dashes (-) indicate there was either no data for either one or both scenarios.

		Latitude Bands (°N)					
		40	**45**	**50**	**55**	**60**	**65**
900mb	**March**						-
	April	-					-
	May	-					
925mb	**March**						-
	April	-					-
	May	-					
950mb	**March**	-					-
	April	-					-
	May	-					
975mb	**March**						-
	April	-					-
	May	-					
1000mb	**March**	-	-				-
	April	-	-				-
	May	-	-				

Based on these results, successful transport of hypothetical BC emission parcels from cropland fires which occurred above 60°N reached the snow-covered ground at similar times (on average) under both blocked and nonblocked conditions. Therefore these were not included in the following latitudinal analysis. In addition, analysis below 45°N was not included as there were very few or no successful transport grid cells under blocked conditions. April, for example, contained the highest number of successful transport grid cells below 45°N (0 – 67 grid cells over 13 years, depending on injection height); however, all of these were under nonblocked conditions.

The majority of successfully transported hypothetical emission parcels originated between 45°N and 60°N and based on the results of the significance testing, further analysis was restricted to latitude bands 45° – 50°N, 50° – 55°N, and 55° – 60°N. Box plots illustrating the transport time to the snow on the Arctic under blocked and nonblocked conditions for the lowest (900mb) and highest (1000mb) injection heights are highlighted for March, April and May (Figures 4.11 – 4.13). Table 4.4 highlights the difference in mean transport values for March, April and May (2003 – 2015) for all injection heights between the three main latitude bands.

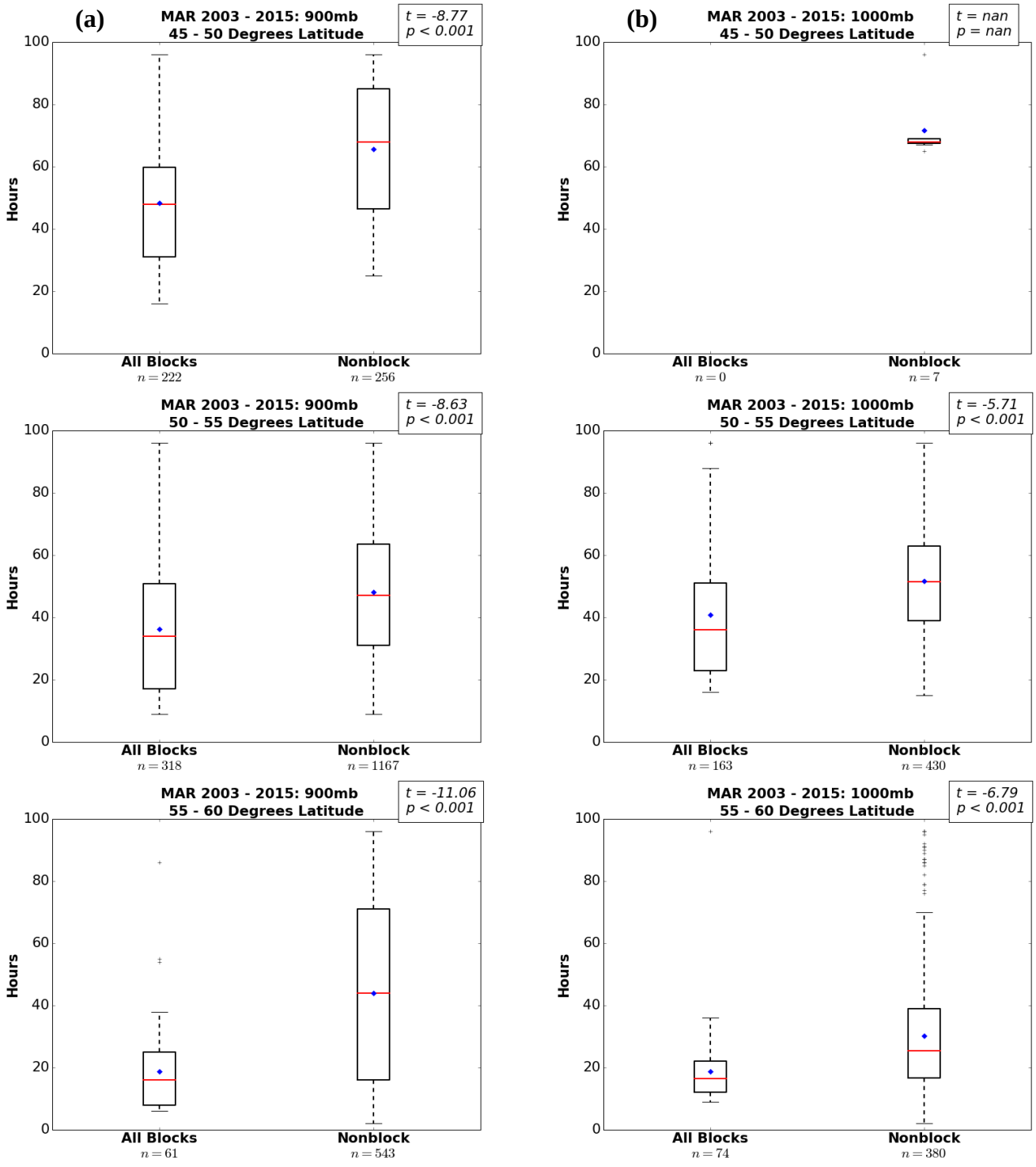

Figure 4.11: March average (2003 – 2015) transport time under blocked and nonblocked conditions at 900mb (a) and 1000mb (b) for latitude bands: 45° – 50°N, 50° – 55°N, and 55° – 60°N.

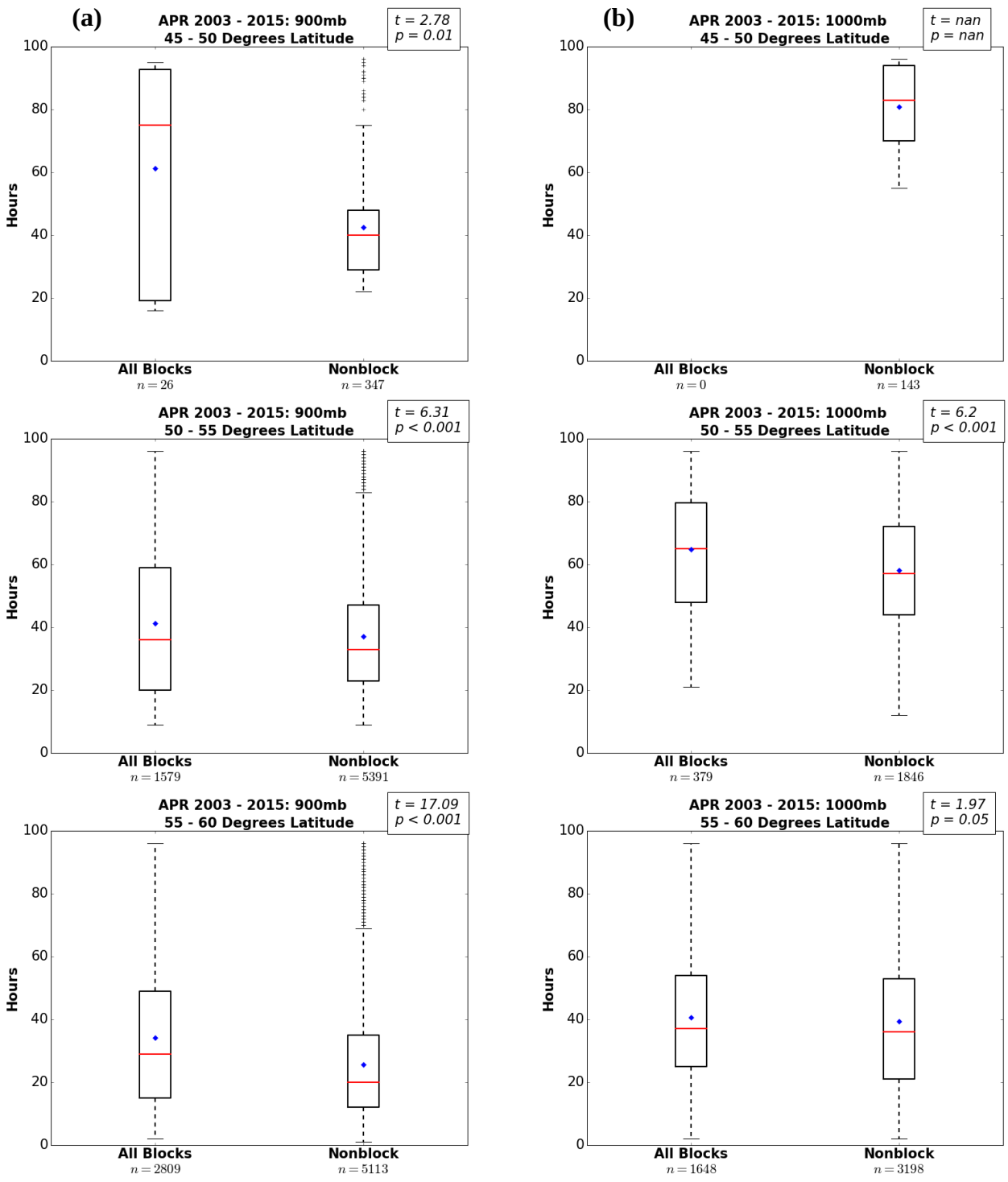

Figure 4.12: April average (2003 – 2015) transport time under blocked and nonblocked conditions at 900mb (a) and 1000mb (b) for latitude bands: 45° – 50°N, 50° – 55°N, and 55° – 60°N.

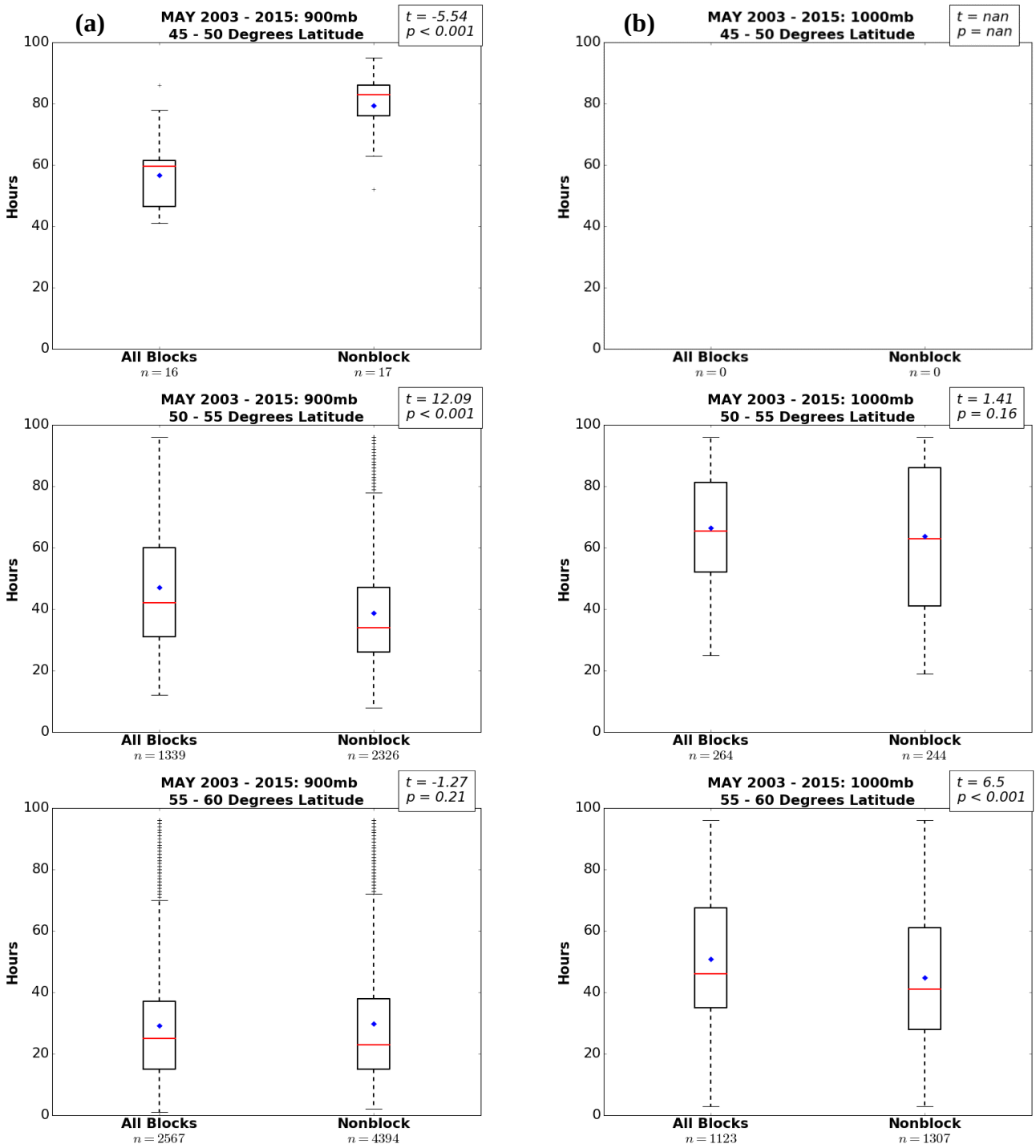

Figure 4.13: May average (2003 – 2015) transport time under blocked and nonblocked conditions at 900mb (a) and 1000mb (b) for latitude bands: 45° – 50°N, 50° – 55°N, and 55° – 60°N.

Table 4.4: Difference in mean transport time to the snow-covered Arctic. Negative values indicate transport to the snow-covered Arctic was on average quicker under blocking conditions, whereas the positive values indicate nonblocked conditions were quicker.

Month	Latitude	900mb	925mb	950mb	975mb	1000mb
March	**45°N – 50°N**	-17	-16	+9	+3	--
	50°N – 55°N	-12	-14	-15	-18	-11
	55°N – 60°N	-23	-23	-20	-20	-11
April	**45°N – 50°N**	+19	+6	+16	+24	--
	50°N – 55°N	+4	+4	+4	+3	+7
	55°N – 60°N	+8	+8	+7	+5	+1
May	**45°N – 50°N**	-23	-20	-13	-17	--
	50°N – 55°N	+8	+6	+2	+2	+2
	55°N – 60°N	-1	-2	-1	+1	+6

Quantifying the difference in the mean transport time between blocked and nonblocked conditions found that, in general, when successful transport occurs under blocked conditions it is not only faster but the magnitude of the difference is greater than when faster transport occur under nonblocked conditions (Table 4.4). The main exception occurs in April between 45°N and 50°N. This difference is likely the result of the April 2006 blocking event which skewed the transport time results - the transport followed the anticyclonic circulation pattern effectively lengthening the transport trajectory (see Figure 4.10 and the accompanying text above).

4.4: Discussion

4.4.1: Atmospheric Blocking Index uncertainty

The original Lejenäs and Økland (1983) index, henceforth known as L&O83, forms the basis for the derivations of the most commonly used blocking indices. For example, the National Weather Service Climate Prediction Center utilizes the index developed by Tibaldi and Molteni (1990), which is a modified version of the L&O83 index (NOAA, 2005). For this study, the Lupo et al., (2008) blocking index dataset is used and this too is based on a modified version of the L&O83 index. These blocking indices calculate the GPH gradient surrounding a static central latitude (60°N) for each longitude. A key drawback of this type of blocking index is the inability to determine the north-south extent of the blocking event (Diao et al., 2006). In recent years, development of new blocking indices have been underway to try capture the latitude of the blocking events (e.g. Scherrer et al., 2006). For example, Pelly and Hoskins (2003) constructed a blocking index based on the meridional potential temperature difference along a potential vorticity surface allowing the central blocking latitude to vary with longitude.

Although there is a lack of latitudinal information, the Lupo et al., (2008) index was utilized in this study as the fundamental blocking equations are widely accepted in the scientific literature. At present there are numerous blocking indices all with slight variations in the blocking criteria, equations and underlying datasets (e.g. Diao et al., 2006; Scherrer et al., 2006). Blocking events are important atmospheric phenomena which can have a wide range of impacts on both humans and the environment, thus there is an urgent need to create a consistent blocking index

methodological framework (Barnes et al., 2011). Furthermore, depending on the scientific question, the importance of identifying the north-south extent of the blocking is crucial. As seen in the results of this study, the geographic location of the blocking event in relation to the fire activity in April 2006, led to large variability in the transport time to the Arctic. The importance of location was also observed during the July 2010 blocking event in European Russia where the location of the block and the fire activity led to significant transport and pooling of the burning emissions. Therefore, identifying the latitudinal extent of the blocking event is an important task in relation to understanding the potential impacts on emission transport.

4.4.2: Atmospheric Blocking Events: implications for cropland emission transport to the Arctic snow

The focus of this study was to identify if blocking events could enhance the likelihood of transport or accelerate the transport of pollutants to the snow-covered Arctic from Russian cropland burning based on the persistent wind patterns in comparison to nonblocked conditions. Only the purest scenarios were chosen to isolate the wind patterns associated with blocked and nonblocked conditions. Due to the already infrequent nature of blocking events, in comparison to nonblocked conditions, the additional refinement of only including "pure" fire occurrences further reduced the initial lower numbers of days under blocking events. When undertaking the comparison between the blocking and nonblocking outputs, care has to be taken to account for the disproportionately higher number of cropland burning grid cells under nonblocked conditions. For example, when comparing the latitudinal variability of the transport times at the lowest latitude band (40° – 45°N), there was an absence of

successfully transported fire occurrences under blocking conditions. Although, based on this data, this does indicate that nonblocks were more successful at transporting potential emissions to the snow-covered Arctic; it also indicates that there is not enough data to determine if blocks don't have an impact on transport to the Arctic from between 40°N and 45°N.

Based on the above analysis, transport of BC emissions to the Arctic snow under blocking conditions is generally quicker and more successful than during nonblocking conditions under all injection heights; however, there is both spatial and temporal variability across the Russian croplands. The main exception is in April; however, previous analysis found that the cause of the higher transport times was driven by a single blocking event in April 2006. Furthermore, based on the mean differences and spread of the box plot transport data under blocks and nonblocks, it is clear that blocking events can substantially enhance the transport to the Arctic. This accelerated transport has large implications for the potency of deposited BC on the snow and potentially sea ice in the Arctic.

4.5: Conclusion

This study quantifies the contribution of large-scale, quasi-stationary meteorological blocking events to the transport of potential BC emissions from cropland burning in Russia to the snow in the Arctic. Although blocking events do not appear to influence managed burning patterns, this study determined that they do influence the success and, in many cases, the timing for these emissions to be transported and deposited on the Arctic snow. The majority of the BC emission source locations that experienced accelerated transport to the Arctic snow occurred in

European Russia which contains more than 80% of all Russian cropped area and where the wheat yield values are the highest. Therefore, the accelerated transport of hypothetical BC emissions is likely to occur from cropland burning on fields with higher volumes of crop residue, thus impacting the quantity and potency of BC emissions deposited on the Arctic snow and sea ice during spring.

Further work needs to be undertaken to not only improve blocking indices to include the latitudinal extent of the blocking event, but to also ensure these datasets are publicly available and are consistently used in scientific studies. In addition, as previously addressed in Chapter 3, improvements are needed to accurately represent the spatial and temporal cropland emission fluxes. The exact impact of deposited BC on Arctic snow relies on information of the chemical and microphysical processes within the atmosphere. Thus accurate emission estimates are required to determine how the accelerated transport under blocking conditions might impact the efficacy of the deposited BC emissions on the Arctic snow.

Chapter 5: Conclusion

5.1: Major research findings

The aim of this dissertation has been to advance the scientific understanding of the relationship between northern mid-latitude cropland burning and the climatic impacts within the Arctic region. Specifically, this dissertation focused on answering the overarching question: *How does crop residue burning in Russia contribute to the BC deposition on snow in the Arctic from low-level transport?* This was achieved through addressing three research questions which were outlined in Chapter 1, Section 1.2 and described in Chapters 2 – 4.

The development of the CRAB product was driven by the availability of VHR imagery which allowed for a detailed analysis of the Russian agricultural practices; particularly with respect to distinguishing between burned and plowed fields. With the widespread use and importance of emissions estimates based on these burned area products, it was essential to create a new more accurate Russia-specific burned area product. Unfortunately, through the challenges detailed in Chapter 2, Section 2.5, the current coarse resolution satellites are inadequate for mapping these small scale, short-lived fires. Although coarse resolution satellites, like MODIS, allow for multiple overpasses per day, the persistent cloud cover over Russian croplands can leave on average 106 clear views (with a range from 24 – 199 clear views) of the surface per growing period between 2003 and 2012. This inability to obtain reasonable estimates of burned area has implications far beyond the realm of burned area mapping. Countless studies have relied on these estimates to quantify cropland

burning emissions (e.g. Hao et al., 2016; McCarty et al., 2012), which are ultimately used in a wide range of studies from air quality and human health to impacts of emissions on climate forcing (e.g. Jacobson, 2004, Lin et al., 2012; Stohl et al., 2006; Witham and Manning, 2007). Furthermore, the emission calculation parameters which are widely used in the literature are based on "best guess" estimates. Thus, through the course of addressing the first research question, it was discovered that cropland burning emission estimates could not be utilized in answering my overall research question and any estimates predicted from those assumptions would only contribute to further proliferation of erroneous results.

Despite the inability to accurately estimate cropland emissions, I set out to develop a methodological approach that still allowed me to answer the overarching question. By focusing on active fire detections within the Russian cropland, I was able to determine the fraction of cropland burning that has the potential for a hypothetical BC emission parcel to be transported and deposited on the Arctic snow. Through using the active fire detections I was able to ascertain the actual timing of fire occurrences. The use of the active fire product also allowed me to test a different approach to many other transport studies, which typically use the cropland emission estimates as the input source to chemical-transport models. Through the development of a simplified, low-level transport model, I was able to determine that approximately 10% of the observed cropland burning in March, April and May (7% annual) have the potential to contribute to the BC deposition on the Arctic snow. Although the highest density of all cropland fires occur during the spring in the southern portion of the cropland in the Far East (approximately between 40° – 55°N and 110° – 130°E), the

majority of the cropland burning which successfully transported potential BC emissions was located in European Russia which contains more than 80% of all Russian cropped area and where the wheat yield values are the highest. Therefore, the successful burning is also likely to occur on fields with higher volumes of crop residue, thus impacting the quantity of BC emissions transport to the Arctic snow during spring. Further, results from the transport model identified possible BC emissions potentially transported beyond 80°N, and that burning as far south as at least 40°N was potentially able to contribute to the deposition of BC on the Arctic snow (above 60°N). These were key findings as the largest impact on the snow/ice albedo in the Arctic from BC deposition occurs during spring when the solar energy is increasing while still retaining the maximum snow cover extent (Quinn et al., 2011). With the current accelerated warming in the Arctic region and the considerable loss of snow cover and sea ice, quantifying the contribution of cropland burning in Russia to potential BC deposition on Arctic snow during this vulnerable time period is an important step towards creation of mitigation strategies.

Finally, I explored the potential mechanisms for accelerated transport of cropland BC emissions from Russia to the snow in the Arctic, specifically atmospheric blocking events. Longer residence times leads to increased mixing with other atmospheric constituents thereby altering the absorptive properties of BC. Specifically focusing on the snow/ice albedo effect in the Arctic, accelerated transport of BC during the spring may lead to greater absorption of incoming solar radiation thereby accelerating the snow and sea ice melt. With potential deposition of BC emissions from Russian cropland burning north of 80°N, a more concentrated BC

particle from accelerated transport has additional implications for permanent sea ice cover. Transport via the persistent winds associated with atmospheric blocking events formed the basis for the final research chapter. It was also hypothesized that blocking events might affect the cropland fire occurrences; however, future work focusing on a potential lagged relationship related to the impact of blocking events on crop conditions should be carried out to definitively characterize the relationship. Although current analysis suggests there is no relationship with cropland burning occurrence, blocking events do influence the success rate and transport time to the Arctic during the spring. In general, blocking events, particularly during March and May, accelerate the transport and increase success rates to the Arctic at almost all injection heights.

Through addressing the three research questions, I was able to answer my overall question. Despite the low injection heights, crop residue burning BC emissions in Russia can potentially deposit on the Arctic snow even reaching sea ice above 80°N and can be deposited on the snow from burning events that occur as far south as at least 40°N. Furthermore, the results of this study highlighted the importance of the timing of burning in relation to BC deposition on the Arctic snow. Although forest fires produce substantially more emissions than cropland fires due to higher biomass loading, cropland burning occurs during the crucial time period for impacts on the Arctic snow/ice albedo. Finally, the enhanced transport of BC has important implications for the efficacy of deposited black carbon. Therefore, understanding these relationships could lead to possible mitigation strategies for reducing the BC deposition impact in the Arctic from these managed fire events.

5.2: Contribution of this research to the broader Arctic science agenda and policy implications

5.2.1: Broader Arctic science agenda

The unique characteristics of the Arctic region has spurred a resurgence in Arctic science research as the amplified regional warming is leading to a range of biophysical and socio-economic impacts. The Arctic is not an isolated, desolate region but rather an integrated, dynamic ecosystem which supports both local and global climatic structures. At the local level, the Arctic landscape supports an abundance of wildlife and local human populations. The sea ice, coastal zones, wetlands, and estuaries are all crucial habitats for local and migratory animals and important hunting grounds for native populations. At the global level, the Arctic is responsible for helping moderate the global temperature through atmospheric and oceanic circulation transporting warmer air from the tropics to the colder polar regions. The presence of sea ice also helps limit the extreme weather activity through reducing the availability of moisture to the atmosphere (NSDIC, 2017b).

These crucial functions within the Arctic region are under attack from the amplified effects of climate change. At present, the loss of snow cover and sea ice has led to a number of devastating local effects; however, with the projected rise in temperatures from current climate models (Stocker et al., 2006) these could eventually be experienced on a global scale. Over the past few decades, scientists have debated whether the sea ice loss can lead to a climate tipping point (e.g. Amstrup et al., 2010; Lindsay and Zhang, 2005; Ridley et al., 2012; Winton, 2006). Although the presence of a tipping point leading to irreversible ice loss is under

debate, there is a consensus that there will be substantial sea ice loss over the next few decades (Overland and Wang, 2013). This reality of large scale snow cover and sea ice loss has led to a rise in the number of international interdisciplinary initiatives focused specifically on addressing various issues within the Arctic environment. For example, the NASA Arctic-Boreal Vulnerability Experiment (ABoVE) is established to study the environmental changes in the Alaskan and Western Canadian Arctic and Boreal regions and their implications for social-ecological systems (NASA, 2017). Specifically, the loss of sea ice and thawing permafrost has led to alterations in the Arctic and Boreal ecosystem structures and functions. The key objectives of ABoVE are aimed at providing a scientific foundation for policy-makers to make informed decisions on activities that will impact this vulnerable region.

The Arctic Council is the leading intergovernmental assembly established to ensure cooperation between all Arctic States with the goal of sustainable development and environmental protection of the Arctic (Arctic Council, 2017). The Arctic Council is comprised of six Working Groups which focus on activities ranging from conservation of Arctic flora and fauna to emergency prevention, preparedness and response; however, the Working Group dedicated to assessing the impacts of pollution and the adverse effects of climate change is of particular relevance to this doctoral research. The Arctic Monitoring and Assessment Programme (AMAP) recently released a new report on BC and ozone with a focus on the emissions, transport pathways, and modelling methods used in studies of these short-lived climate forcers (AMAP, 2015). Several of the key recommendations from this report included, a need for more accurate estimates of emission sources with a particular

focus on regional assessments to improve the latitudinal uncertainties; and a need for improved modelling capabilities to more accurately represent these short-lived pollutants. The development of CRAB, a Russia specific cropland burned area algorithm, was designed to improve the accuracy of cropland emissions; however, it instead has highlighted the current mapping challenges and subsequent inaccuracies within emissions estimates that need to be addressed. Furthermore, this study helped identify the latitudinal variations of the contribution of Russian cropland burning to the potential transport and deposition of BC emissions on Arctic snow.

Another recently established initiative is NOAA PACES which is designed to specifically focus on air pollution in the Arctic (Arnold et al., 2016). As previously mentioned, a key motivation in the PACES initiative is to improve the predictive capabilities of the current earth system and chemical-transport models with a focus on accurately simulating the temporal and spatial variations in emission sources and identifying the potential transport pathways from the various pollution sources. This dissertation research study focused on not only assessing the potential for the deposition of BC emissions from cropland burning in Russia through low-level transport, but also on identifying a possible transport mechanism that may enhance the transport of BC emissions to the Arctic.

At present, the chemical-transport model outputs form the basis for climate policy development (Arnold et al., 2016). The need for improved quantification of emission sources is essential for ensuring policy-makers are able to make informed decisions. Initiatives like the ones mentioned above are crucial for ensuring the Arctic science agenda stays on the correct track.

5.2.2: Policy implications

The results of this dissertation have confirmed the importance of Russian cropland burning as a contributor to the potential BC deposition on the Arctic snow during the most vulnerable period for sea ice melt. As previously mentioned, open-source burning in Russia is banned; however, from visual analysis of various earth-observing VHR satellites, it is clearly a widespread occurrence within the Russian croplands. Identifying spring as a key time period for increased successful transport to the Arctic snow is crucial as it serves as a scientific basis for creation of BC mitigation strategies. Reducing the emissions of BC and other short-lived climate aerosols presents an achievable near-immediate reduction in the risk of abrupt climate change from these strong but short-lived climate forcers. In addition, the reduction of deposited BC on Arctic snow and sea ice will also benefit the surrounding environment. Dissolved BC in the Arctic Ocean has likely increased due to the melting of Arctic snow and sea ice which has consequences on both the Arctic biogeochemical cycles and the global carbon cycle (Elmquist et al., 2008; Fang et al., 2016; Jurado et al., 2008; Mari et al., 2014). Once dissolved, BC can be converted to carbon dioxide through exposure to solar radiation in surface ocean waters (Stubbins et al., 2015); however, research is still underway to determine the proportion of this carbon dioxide that can reach the atmosphere. Furthermore, the reduction in BC emissions will also present an improvement in air quality with a subsequent reduction in negative human health impacts. BC is a large contributor to the fine particulates (PM2.5) released from burning (EPA, 2017). BC is a known carcinogen and the small size allows the BC particle to enter the lungs, leading to respiratory distress and heart

failure which was a major contributing factor in the death of thousands of vulnerable people during the July 2010 blocking event in Russia (Shaposhnikov et al., 2014).

Clearly based on the observed fire occurrences in the Russian cropland, the burning ban is not well enforced. Although this seems to be the easiest option of reducing BC emissions, it requires the participation of all Russian farmers. Therefore, I would recommend a broad public (with a special focus on farmers) educational campaign that draws attention to the impact of cropland burning not only on the Arctic but also on air quality and the harmful impacts of particulate matter on human health. An additional focus of this educational campaign would be related to the benefits of retaining crop residue within the fields instead of removal via burning. Studies have identified a change in soil characteristics and pH during burning (depending on intensity), which ultimately have impacts on soil erosion (depending on the fire intensity and timing in relation to planting), crop yield, and retention of nutrients (Hamman et al., 2007; Schillinger et al., 2010).

Mitigation campaigns aimed at reducing the ability for short-lived pollutants, such as BC, to reach the Arctic are essential as the effects from the amplified warming within this vulnerable region are already seen on a global scale. Although currently under debate, the potential for the snow and sea ice loss to amplify mid-latitude extreme weather events – i.e. blocking events – could potentially lead to further melting of the snow and sea ice. The results of this dissertation highlight the role of blocking events to accelerate transport of hypothetical BC emissions from Russian cropland burning to the Arctic snow. If the increased snow/ice loss results in more frequent blocking events (depending on the seasonality and geographic

location), there is a potential for more concentrated BC emissions to be transported to the Arctic snow from Russian croplands. Thus, the creation of an education campaign may help alleviate the BC burden on the Arctic from these managed fires.

5.3: Future research directions

An underlying theme within this dissertation has been the need for more accurate representation of cropland emissions, in both the magnitude and spatio-temporal patterns. Specifically, the complexity of chemical-transport models adds an unnecessary level of precision which will not improve the understanding of the transport of cropland emissions without substantial improvements of the underlying emission inputs. First and foremost, we need to develop burned area estimates that are able to capture the cropland residue burning. Based on the assessment carried out in Chapter 2, the burned area algorithm will have to be driven by moderate resolution (10 – 50 m) observations that are able to capture the burning within individual fields. Due to the persistent cloud cover in the northern high latitudes, multiple overpasses are required to enhance the likelihood of capturing these short-lived events, whose spectral signatures are also often lost to the subsequent plowing of the field. Utilizing all available Landsat and Sentinel-2 observations with infusion of VHR imagery could offer a potential new opportunity for improving the accuracy of cropland burned area estimates. A combination of Landsat 8 OLI and Sentinel 2A and 2B sensors will provide a 10 – 30 m multi-spectral global coverage every 3 days (Yan et al, 2016). However, this 3 day coverage will still lead to gaps in the observational time series due to the persistent cloud coverage in high northern latitudes. Due to the limitations associated with persistent cloud cover, an alternate approach could include

utilizing synthetic aperture radar (SAR) to estimate the change in surface roughness from harvest to burn scar. SAR has the ability to penetrate clouds and smoke, therefore presents a possible option to increase the likelihood of mapping cropland area (McNairn et al., 2009) and burned scars (Polychronaki et al , 2013); however, future work must also focus on the potential impact on surface roughness from plowing after harvest without burning.

The next major effort should be focused on the improvement of the other components needed to calculate cropland emissions as the magnitude and source locations are crucial inputs for chemical-transport models. The complexity within these models is important to identify the impact of deposition BC on the Arctic snow. These models simulate the chemical and physical changes of a BC particle throughout the transport pathway and can help determine the likely climatic impacts of the BC particle in both the atmosphere and upon deposition. Specifically focused on Russia, the majority of burning that was successfully transported to the Arctic occurred in European Russia which contains the highest wheat yields in the Russian cropland. Transport of BC emissions from this region to the Arctic is likely to have a much larger impact than other regions with lower yields. Since the transport algorithm only focuses on the potential for transport of BC to the Arctic further analysis can be carried out on validating the outputs through the incorporation of BC data from NASA's AERONET sites. The AERONET network provides data on aerosol optical depth at over 250 sites worldwide. Specifically, the spectral range of the observations allows for the extraction of inferred BC information (Sato et al., 2003). At present,

there are 7 AERONET sites within Russia, 5 sites in Norway, 6 sites in Finland, and 5 sites in Sweden (within the scope of BC transport from Russian croplands).

Another area for future study is the creation of a standardized blocking index which accounts for the latitudinal extent of the atmospheric blocking event. The accelerated transport and increase in successful transport was demonstrated in this dissertation; however, the influence of a single blocking event on these metrics was also presented. Standardizing the definition of these events and ensuring the north-south extent is also represented will help more accurately determine how the location of a blocking event can impact transport from Russian croplands to the Arctic. Although this study focused on Russian cropland burning, studies should be conducted to assess the impact of spring burning across Europe, Asia, and North America on the BC deposition on the Arctic snow. Analysis of the average number of active fires per month (2003 – 2015) within various land cover types (e.g. forest, cropland, and grassland) found burning peaks in spring within the United States of America (lower 48 states), Kazakhstan, Ukraine, and Mongolia; however, the relative contribution of burning from croplands compared to other land cover types differed for each of these countries. For instance, burning within Kazakhstan predominantly occurred within grasslands, whilst burning in Ukraine predominantly occurred within croplands (see supplementary material Figure S3). Furthermore, this study identified atmospheric blocks as a potential transport mechanism to enhance the transport to the Arctic snow. Atmospheric blocking events occur throughout the NH mid-latitudes thus future studies identifying their potential impact over other circumpolar cropland regions may identify a different influence on the transport of BC to the Arctic.

At present, prediction of atmospheric blocking events is not possible with current weather models; however, ongoing improvements could eventually lead to the accurate prediction of these long-lived mid-latitude weather extremes (NOAA, 2005). Also, ensuring blocking events are accurately represented in chemical-transport models is essential for identifying periods of enhanced transport from northern mid-latitude BC source locations to the Arctic. Finally, upon improvement of cropland emission inventories, an early warning system could be developed in the future to forecast conditions that are likely to transport BC emissions from various circumpolar sources and deposit them on the snow in the Arctic.

Appendices

Supplementary Material Figures

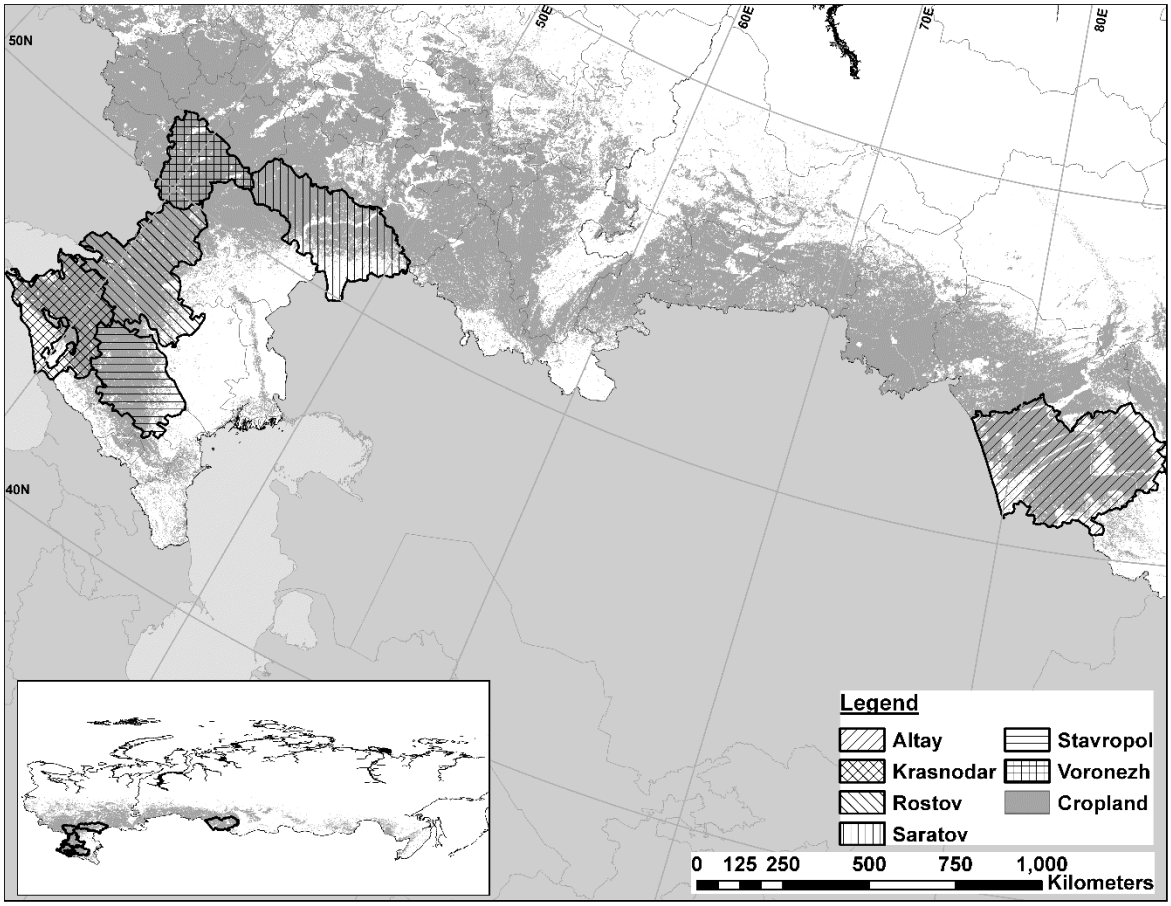

Figure S1: SovEcon (2013) survey results.

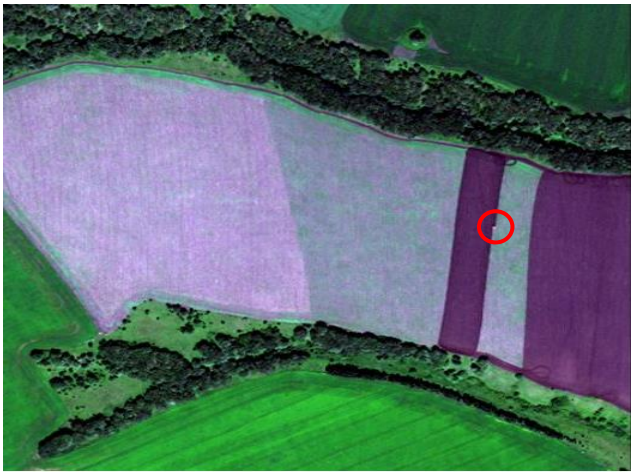

Figure S2: An example of a field that is plowed and likely not burned before plowing. A tractor (red circle) is visible in the imagery with the trail of darkened plowed soil behind it.

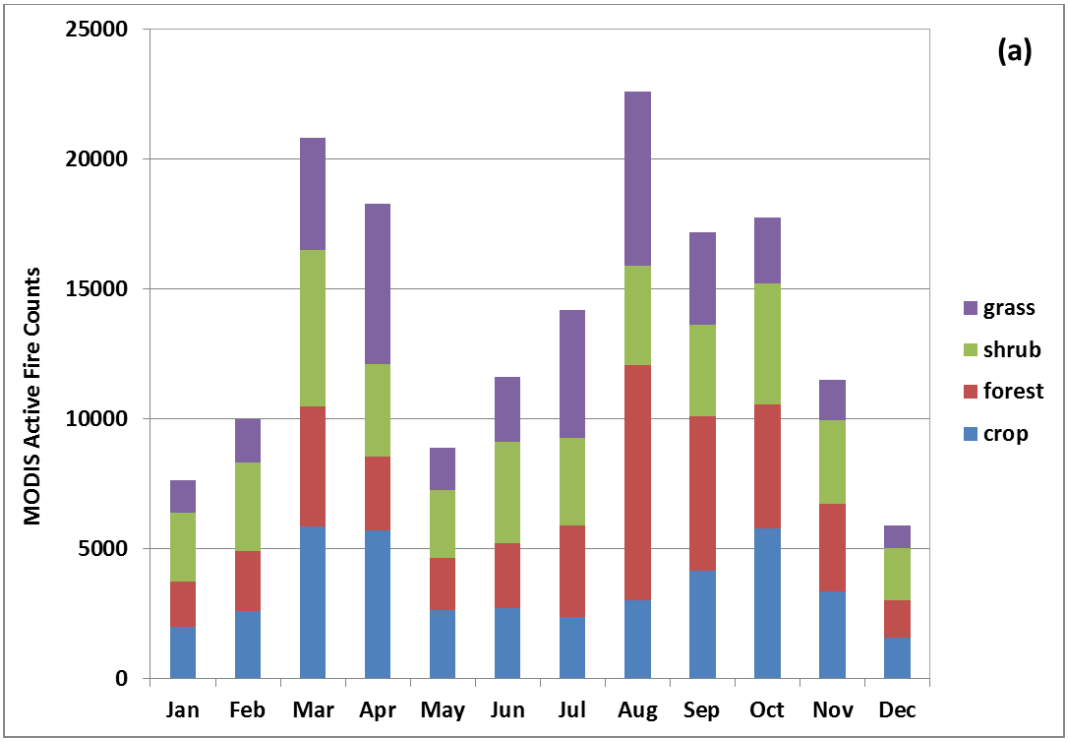

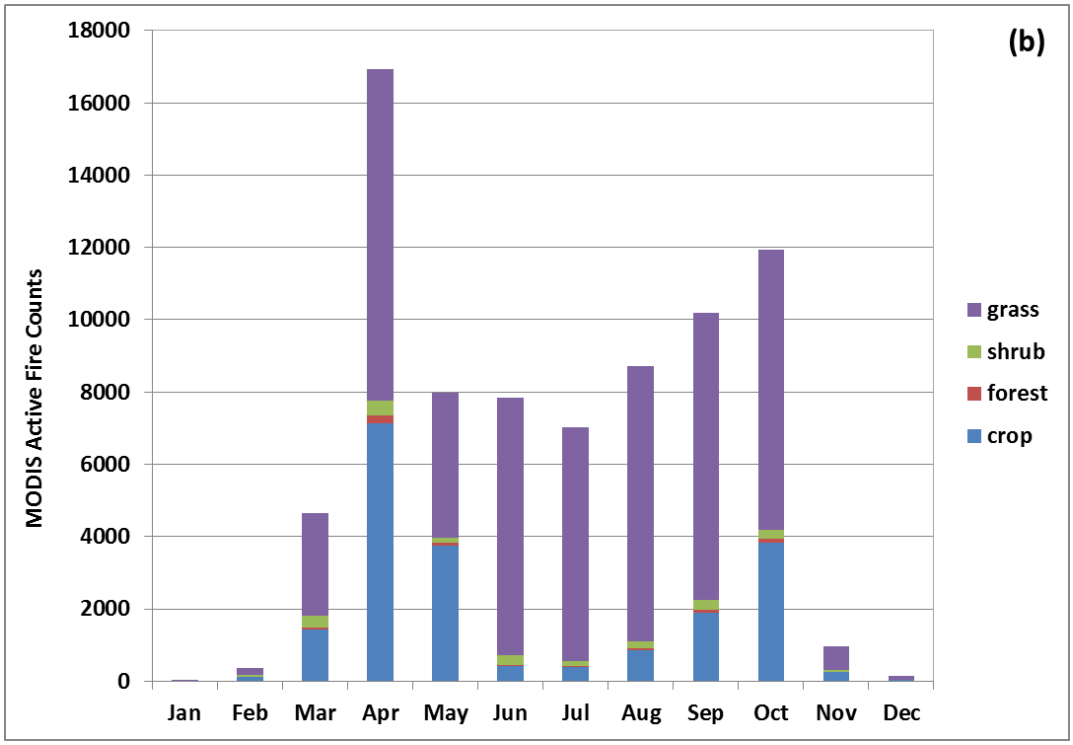
(b)
MODIS Active Fire Counts
18000
16000
14000
12000
10000
8000
6000
4000
2000
0
Jan
Feb
Mar
Apr
May
Jun
Jul
Aug
Sep
Oct
Nov
Dec
grass
shrub
forest
crop

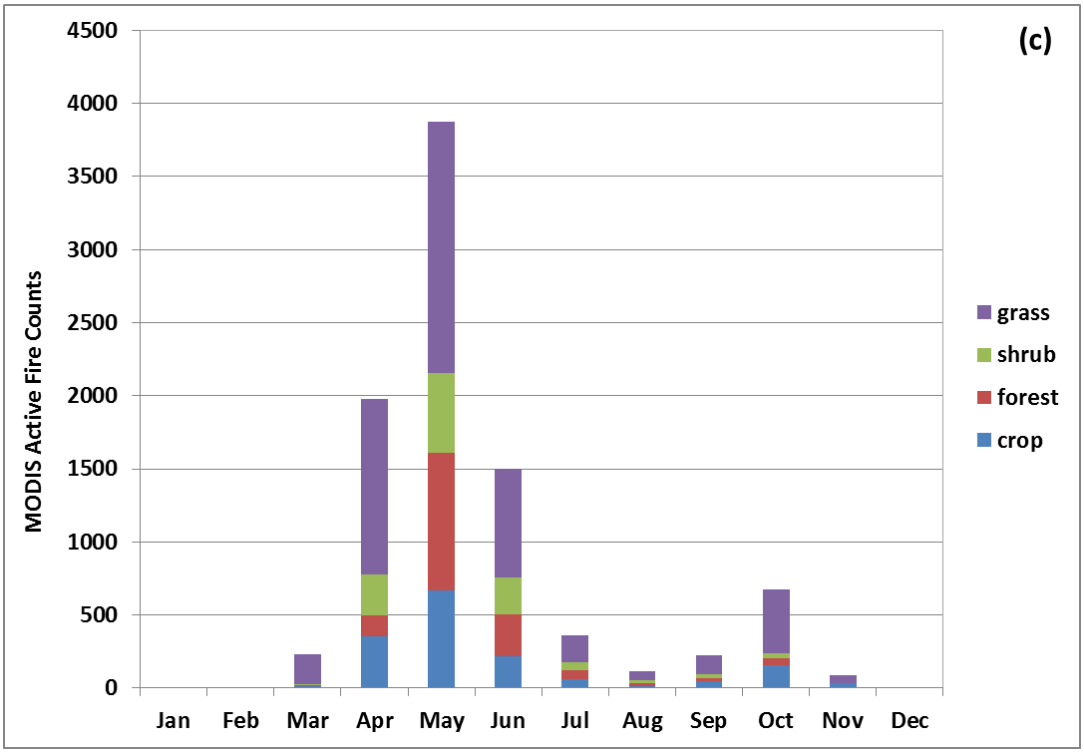
(c)
MODIS Active Fire Counts
4500
4000
3500
3000
2500
2000
1500
1000
500
0
Jan
Feb
Mar
Apr
May
Jun
Jul
Aug
Sep
Oct
Nov
Dec
grass
shrub
forest
crop

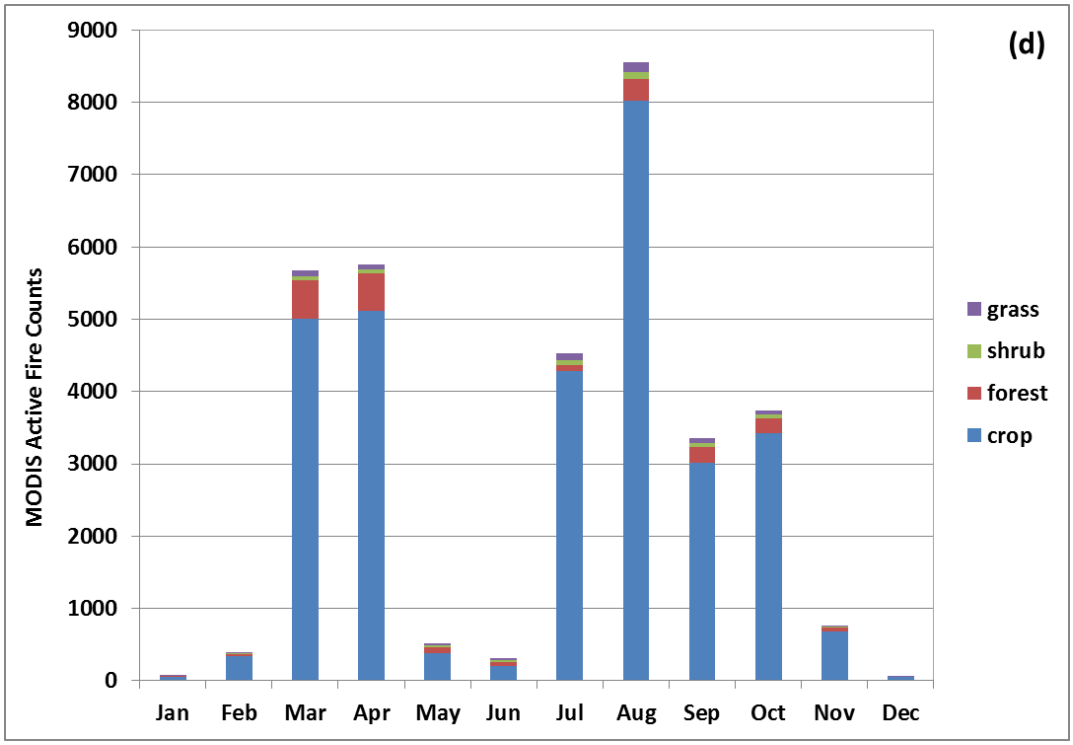

Figure S3: Average monthly MODIS active fire counts (2003 – 2015) within grassland, shrubland, forest and cropland as defined by the International Geosphere-Biosphere Programme (IGBP) land cover type data layer (MCD12Q1; Friedl et al., 2010) for the United States of America (a), Kazakhstan (b), Mongolia (c), and Ukraine (d). Note the differences in the y axis.

Supplementary Material Information

Supplementary S3

We analyzed the yearly changes over the 10 year period (2003 – 2012) corresponding to the CRAB product and found that more than 60% of the entire Russian cropland region was consistently mapped as croplands during the 10 year period, with most of the variability occurring in the eastern Russian MODIS tiles (h26v03, h26v04 and h27v04) which contain less than 5% of the Russian cropland region. Furthermore when focusing on the 4 main cropland MODIS tiles (h20v03, h20v04, h21v03 and h21v04) which contain approximately 65% of the Russian cropland region, our analysis revealed that 73% of that region was consistently mapped as croplands over the 10 year period. After analyzing the variability in the IGBP cropland and cropland/natural vegetation combined layers, we are satisfied with utilizing this product in the CRAB algorithm.

Supplementary Material Tables

Table S1: 1 km MODIS quality assessment (QA) data

	QA Bit	Accepted Values
Cloud State	0 – 1	0 = clear
Cloud Shadow	2	0 = no
Aerosol Quality	6 – 7	<2 = low
Cirrus Detected	8 – 9	<3 = less than average
Internal Cloud Algorithm	10	0 = no cloud
MOD35 Snow/Ice Flag	12	0 = no
Internal Snow Mask	15	0 = no snow

Table S2: Average burned area (km^2) between 2003 and 2012 and the average (2003 – 2012) percentage burned per oblast cropland area for summer and spring by oblast. The minimum and maximum burned area values are given in parentheses.

Oblast	**Cropland Area (km^2)**	**Summer: Average Burned Area (min, max) (km^2)**	**Spring: Average Burned Area (min, max) (km^2)**	**Summer: Average percentage of cropland areas burned**	**Spring: Average percentage of cropland areas burned**
Adygey	3659	63 (6, 138)	9 (2, 33)	1.73	0.26
Aginskiy Buryatskiy AO	5485	3 (0, 10)	64 (11, 185)	0.06	1.16
Altay	117552	1641 (861, 2705)	948 (296, 1527)	1.40	0.81
Amur	83410	153 (3, 589)	1242 (352, 2606)	0.18	1.49
Astrakhan	5753	7 (0, 16)	57 (16, 111)	0.12	0.99
Bashkir	90531	161 (52, 644)	1212 (43, 3281)	0.18	1.34
Belgorod	25495	324 (30, 987)	58 (8, 202)	1.27	0.23
Bryansk	21967	11 (3, 21)	558 (15, 2040)	0.05	2.54
Buryat	18169	18 (5, 32)	190 (80, 293)	0.10	1.04
Chechnya	6688	48 (7, 238)	20 (5, 48)	0.72	0.30
Chelyabinsk	54470	297 (102, 511)	571 (34, 1111)	0.55	1.05
Chitin	59020	74 (10, 204)	687 (286, 1094)	0.13	1.16
Chuvash	12297	13 (0, 69)	186 (6, 443)	0.11	1.51
Dagestan	10682	8 (1, 25)	20 (6, 71)	0.07	0.19
Evenk AO	12	0 (0, 0)	0 (0, 2)	0.00	3.27
Gorno Altay	8216	0 (0, 1)	82 (42, 138)	0.01	0.99
Ingush	1995	28 (1, 76)	5 (1, 11)	1.41	0.25
Irkutsk	23973	9 (3, 18)	244 (76, 492)	0.04	1.02
Ivanova	7974	0 (0, 1)	220 (6, 907)	0.00	2.76
Kabardino Balkar	6060	61 (20, 101)	6 (1, 16)	1.01	0.10
Kaliningrad	9637	0 (0, 0)	99 (2, 568)	0.00	1.03
Kalmyk	4089	328 (223, 530)	11 (2, 38)	8.01	0.27
Kaluga	14588	0 (0, 1)	563 (2, 2476)	0.00	3.86
Kamchatka	453	0 (0, 0)	13 (0, 49)	0.00	2.82
Karachayevo Cherkeskaya	5090	10 (2, 35)	12 (0, 27)	0.20	0.23
Kemerova	30807	14 (1, 41)	297 (118, 484)	0.05	0.96
Khabarovsk	38185	3 (0, 12)	351 (120, 1307)	0.01	0.92
Khakasiya	15700	8 (0, 21)	200 (70, 363)	0.05	1.27
Khanty	330	0 (0, 0)	2 (0, 5)	0.01	0.64

Mansiyskiy AP					
Kirov	25739	0 (0, 1)	632 (26, 2446)	0.00	2.45
Komi Permyatskiy AO	1661	0 (0, 0)	40 (1, 109)	0.00	2.39
Komi	81	0 (0, 0)	1 (0, 5)	0.00	1.08
Koryakskiy AO	226	0 (0, 0)	6 (0, 23)	0.00	2.60
Kostroma	6199	0 (0, 0)	212 (0, 1082)	0.00	3.42
Krasnodar	52305	1992 (714, 3706)	77 (17, 153)	3.81	0.15
Krasnoyarsk	53416	149 (84, 314)	661 (170, 1487)	0.28	1.24
Kurgan	58168	138 (58, 305)	641 (66, 2905)	0.24	1.10
Kursk	28826	574 (55, 1557)	76 (14, 241)	1.99	0.26
Leningrad	4586	0 (0, 0)	123 (3, 302)	0.00	2.68
Lipetsk	22596	322 (57, 735)	52 (6, 114)	1.42	0.23
Magadan	52	0 (0, 0)	0 (0, 0)	0.00	0.29
Mari El	8646	0 (0, 1)	198 (7, 661)	0.00	2.29
Mordva	19120	47 (7, 240)	161 (6, 444)	0.25	0.84
Moscow	18713	3 (0, 7)	340 (15, 998)	0.01	1.82
Nizhegorod	32668	26 (4, 90)	655 (56, 1405)	0.08	2.01
Novgorod	5122	0 (0, 0)	171 (0, 437)	0.00	3.34
Novosibirsk	116816	281 (156, 496)	1348 (157, 2789)	0.24	1.15
Omsk	91650	561 (205, 1589)	947 (36, 1900)	0.61	1.03
Orel	23710	277 (26, 998)	143 (7, 714)	1.17	0.60
Orenburg	70806	3073 (702, 7437)	398 (25, 1026)	4.34	0.56
Penza	34881	247 (52, 1403)	166 (24, 426)	0.71	0.48
Perm	18608	1 (0, 3)	322 (6, 821)	0.00	1.73
Primorsk	27598	1 (0, 9)	220 (51, 535)	0.00	0.80
Pskov	12235	0 (0, 0)	357 (2, 800)	0.00	2.92
Rostov	82996	7529 (3151, 13085)	239 (52, 784)	9.07	0.29
Ryazan	28166	129 (26, 338)	327 (109, 638)	0.46	1.16
Sakhalin	2771	0 (0, 0)	6 (1, 12)	0.00	0.22
Samara	45639	1396 (390, 3418)	208 (20, 534)	3.06	0.46
Saratov	68951	5139 (1777, 9465)	188 (55, 371)	7.45	0.27
Severnaya Osetin	3574	34 (3, 100)	7 (2, 16)	0.96	0.18
Smolensk	23897	0 (0, 0)	768 (3, 2266)	0.00	3.21
Stavropol	50836	6718 (4232, 9144)	58 (23, 105)	13.21	0.11
Sverdlovsk	22971	5 (0, 14)	294 (22, 1137)	0.02	1.28
Tambov	30749	390 (75, 1318)	97 (33, 191)	1.27	0.32
Tatar	55374	188 (37, 780)	560 (113, 1469)	0.34	1.01
Tomsk	13305	4 (1, 13)	191 (90, 340)	0.03	1.42
Tula	23082	93 (12, 204)	309 (45, 1223)	0.40	1.34
Tver	19045	0 (0, 0)	404 (2, 1524)	0.00	2.12

Tyumen	54745	29 (8, 68)	473 (46, 1195)	0.05	0.84
Tyva	4719	1 (0, 11)	44 (7, 105)	0.03	0.91
Udmurt	17974	0 (0, 1)	401 (13, 918)	0.00	2.23
Ulyanovsk	24708	390 (113, 1303)	129 (25, 342)	1.58	0.52
Ust Ordynskiy Buryatskiy	9446	6 (2, 13)	121 (43, 227)	0.06	1.28
Vladimir	10148	0 (0, 1)	248 (26, 820)	0.00	2.45
Volgograd	51135	4644 (1746, 7965)	153 (55, 322)	9.08	0.30
Vologoda	4950	0 (0, 0)	117 (0, 554)	0.00	2.37
Voronezh	48583	814 (115, 2376)	130 (38, 356)	1.68	0.27
Yakutsk	64	0 (0, 0)	0 (0, 2)	0.00	0.64
Yaroslavl	10409	0 (0, 0)	295 (2, 954)	0.00	2.84
Yevreyskaya AO	15177	0 (0, 0)	102 (10, 453)	0.00	0.67

Table S3: Monthly burned area (km^2) between 2003 and 2012 divided by Federal Districts.

Okrug	**Year**	**Cropland Area (km^2)**	**Burned Area (km^2)**						
			March	**April**	**May**	**June**	**July**	**August**	**Sept**
North Caucasus	2003	84927	60	105	17	2	519	2275	1534
	2004	84927	95	54	4	1	1101	1478	3849
	2005	84927	39	111	9	3	1397	2244	2379
	2006	84927	61	4	8	1	1084	3234	4345
	2007	84927	39	3	17	3	2521	2868	4131
	2008	84927	55	0	1	1	718	3548	1738
	2009	84927	69	16	5	0	744	2920	1776
	2010	84927	161	9	3	0	1105	2845	2914
	2011	84927	80	1	2	1	89	2296	4916
	2012	84927	94	135	2	9	1238	1566	5714
Southern	2003	209137	169	1075	237	12	687	2783	2586
	2004	209137	160	111	141	14	854	1918	5999
	2005	209137	65	688	291	28	1526	5507	5432
	2006	209137	145	18	140	53	914	3275	7941
	2007	209137	651	76	220	16	2144	7121	8215
	2008	209137	84	46	208	44	1368	6686	5227
	2009	209137	55	534	86	49	2319	5089	11056
	2010	209137	208	171	147	38	2401	7449	8166

	2011	209137	34	187	128	1	1534	5122	8973
	2012	209137	36	214	68	42	3608	5196	14614
Central	2003	363960	5	1025	456	0	40	146	237
	2004	363960	86	5927	56	12	29	276	500
	2005	363960	0	867	103	4	62	503	1427
	2006	363960	0	8527	994	123	90	281	571
	2007	363960	14438	252	315	11	168	1367	659
	2008	363960	1439	972	23	72	181	1267	3104
	2009	363960	1	4577	620	38	259	1171	4423
	2010	363960	0	3438	75	53	1221	3073	4231
	2011	363960	46	2527	289	1	246	699	991
	2012	363960	0	526	71	40	351	740	1092
Volga	2003	525942	0	1046	1023	3	367	951	1953
	2004	525942	25	2402	5728	82	580	2026	1910
	2005	525942	0	879	361	23	1230	3289	5992
	2006	525942	0	6899	5012	145	1105	1648	5504
	2007	525942	1661	308	375	37	961	3447	3220
	2008	525942	1078	9776	746	36	1729	3409	3170
	2009	525942	14	3137	1280	92	3452	3799	9058
	2010	525942	0	1201	3012	106	7636	6860	9603
	2011	525942	0	1459	2492	2	2369	3360	1841
	2012	525942	0	3403	285	55	3269	5099	8008
Northwest	2003	38265	524	1203	53	1	0	0	0
	2004	38265	77	1391	128	0	0	0	0
	2005	38265	11	80	3	0	0	0	0
	2006	38265	0	1702	270	1	0	0	0
	2007	38265	1586	30	2	2	0	0	0
	2008	38265	19	269	15	0	0	0	0
	2009	38265	0	539	121	0	0	0	0
	2010	38265	0	387	3	0	0	0	0
	2011	38265	0	534	60	4	0	0	0
	2012	38265	2	65	4	2	0	0	0
Urals	2003	190684	0	211	132	105	15	107	173
	2004	190684	0	226	2308	22	92	144	158
	2005	190684	0	968	186	30	82	160	356
	2006	190684	0	172	840	44	49	72	304
	2007	190684	0	118	49	47	33	88	111
	2008	190684	0	1417	342	86	75	198	79
	2009	190684	5	51	1554	31	96	189	246
	2010	190684	0	883	1406	13	182	136	406
	2011	190684	0	279	5823	9	41	67	139
	2012	190684	0	2413	103	27	243	352	302
Siberia	2003	558840	348	1141	5513	127	259	1010	582
	2004	558840	0	318	6607	96	316	750	1268
	2005	558840	98	2764	5066	149	218	659	1611
	2006	558840	1	306	4799	288	271	490	2420
	2007	558840	4	4232	683	75	188	450	1371

	2008	558840	259	474	4381	186	433	561	1849
	2009	558840	2	1297	3987	74	262	473	1187
	2010	558840	0	1695	3563	185	217	674	1389
	2011	558840	18	2454	2372	14	459	427	3281
	2012	558840	6	3450	1783	188	559	1216	2811
Far East	2003	167785	746	3548	126	80	19	1	5
	2004	167785	28	472	313	36	3	17	73
	2005	167785	35	398	218	65	1	38	204
	2006	167785	10	707	595	15	2	18	103
	2007	167785	1	1408	345	14	10	26	108
	2008	167785	292	420	307	26	3	55	531
	2009	167785	5	2444	1021	1	0	1	18
	2010	167785	0	1069	698	14	0	0	77
	2011	167785	30	2552	449	17	1	7	102
	2012	167785	26	642	231	17	4	24	121

Table S4: Monthly (2003 – 2015) successfully transported and total active fire counts within the Russian cropland.

		All Active Fires	Successful Active Fire Counts				
		Total	900mb	925mb	950mb	975mb	1000mb
2003	Jan	102	0	0	0	0	0
	Feb	487	0	0	0	0	0
	Mar	20450	143	196	69	60	201
	Apr	77325	605	481	560	368	253
	May	115731	3379	3233	2666	1975	1083
	Jun	25899	286	239	148	42	24
	Jul	16471	0	0	0	0	0
	Aug	8038	0	0	0	0	0
	Sep	22924	2	0	4	0	0
	Oct	25819	995	1114	768	1366	1117
	Nov	1038	1	1	3	5	4
	Dec	173	0	1	2	1	0
2004	Jan	141	0	0	0	0	0
	Feb	121	15	9	5	2	2
	Mar	3682	130	66	37	40	10
	Apr	49320	4597	5006	4977	3368	2332
	May	58511	11053	9474	9241	8835	5110
	Jun	3099	154	167	88	36	35
	Jul	10266	0	0	0	0	0
	Aug	24151	0	0	0	0	0
	Sep	14594	17	26	12	3	1
	Oct	15892	34	31	25	8	0
	Nov	1747	35	5	4	6	1
	Dec	120	0	0	0	0	0
2005	Jan	272	0	0	0	0	0
	Feb	1405	23	16	13	0	0
	Mar	7471	22	19	6	3	0
	Apr	39921	2926	3243	2524	2147	1160
	May	27721	1741	1544	1135	692	287
	Jun	1806	0	0	0	0	0
	Jul	13385	0	0	0	0	0
	Aug	27774	43	33	7	1	0
	Sep	24752	0	0	0	0	0
	Oct	45523	95	154	161	84	24
	Nov	3459	50	51	87	99	48
	Dec	169	0	0	0	0	0
2006	Jan	23	1	1	1	0	0
	Feb	109	0	0	0	0	0

	Mar	5779	322	283	230	3	4
	Apr	68179	16888	18157	18783	17483	11341
	May	108986	7072	7346	6788	5537	2445
	Jun	4337	3	1	1	0	0
	Jul	12555	0	1	0	0	0
	Aug	17265	0	0	0	1	0
	Sep	18937	0	0	0	0	0
	Oct	10965	23	25	19	13	4
	Nov	2379	50	45	37	44	13
	Dec	236	2	3	3	5	5
2007	**Jan**	243	0	0	0	0	0
	Feb	1582	6	14	4	1	0
	Mar	27910	3913	3528	3589	3015	558
	Apr	49619	7343	6800	6219	4777	2001
	May	18023	19	17	21	17	8
	Jun	3517	25	25	15	4	2
	Jul	19678	0	0	0	0	0
	Aug	26908	0	0	0	0	0
	Sep	15511	0	0	0	0	0
	Oct	20143	805	698	460	69	9
	Nov	3584	47	43	43	36	23
	Dec	508	0	0	0	0	0
2008	**Jan**	266	40	42	32	15	1
	Feb	972	0	0	0	0	0
	Mar	19811	2832	2705	2666	2517	1772
	Apr	148137	18167	18935	19477	19163	11335
	May	43602	10404	10078	8411	5470	1820
	Jun	4897	2	0	1	0	0
	Jul	9780	0	1	0	0	0
	Aug	41773	0	0	0	0	0
	Sep	16986	0	0	0	0	0
	Oct	19091	61	115	53	61	40
	Nov	3924	94	84	53	56	96
	Dec	493	48	23	5	4	0
2009	**Jan**	119	19	2	0	0	0
	Feb	431	1	1	0	0	0
	Mar	3181	148	95	17	8	7
	Apr	111064	9225	8811	7415	5716	2498
	May	53317	3328	3720	3974	4022	1077
	Jun	2922	8	18	8	0	2
	Jul	9090	0	0	0	0	0

	Aug	14537	0	0	0	0	0
	Sep	12052	0	0	0	0	0
	Oct	10970	4	5	3	5	4
	Nov	1585	44	47	46	41	15
	Dec	54	0	0	0	0	0
2010	**Jan**	47	5	5	0	0	0
	Feb	325	2	11	9	0	0
	Mar	3741	163	237	174	385	5
	Apr	63303	18233	18245	15494	11993	8030
	May	31375	1385	1130	701	283	62
	Jun	5119	6	1	1	1	0
	Jul	14970	0	0	0	0	0
	Aug	16529	0	0	0	0	0
	Sep	11179	37	15	5	0	0
	Oct	11041	1602	1595	1493	988	273
	Nov	3985	1	1	3	2	2
	Dec	238	0	0	0	0	0
2011	**Jan**	38	0	0	0	0	0
	Feb	607	277	277	209	38	0
	Mar	3736	96	21	15	10	9
	Apr	46267	8487	8225	7594	5478	2784
	May	33695	2907	2640	1853	851	170
	Jun	3293	1	0	0	0	0
	Jul	6001	0	0	0	0	0
	Aug	8625	0	0	0	0	0
	Sep	9420	105	0	0	0	2
	Oct	14645	5	11	7	0	0
	Nov	1645	0	0	5	1	0
	Dec	90	0	0	0	0	0
2012	**Jan**	41	0	0	0	0	0
	Feb	122	0	0	0	0	0
	Mar	8552	175	163	151	144	134
	Apr	64012	2449	2869	2759	2237	383
	May	25565	968	1399	1068	728	132
	Jun	11212	15	16	11	10	0
	Jul	8935	0	0	0	0	0
	Aug	6043	0	0	0	0	0
	Sep	6739	0	2	0	0	0
	Oct	4036	44	21	13	40	51
	Nov	570	3	2	1	1	0
	Dec	101	0	0	1	0	0

2013	**Jan**	27	0	0	0	0	0
	Feb	1247	1	0	0	0	0
	Mar	3291	20	14	39	23	0
	Apr	33366	834	774	769	577	195
	May	17111	403	377	304	166	112
	Jun	1742	0	0	0	0	0
	Jul	2968	0	0	0	0	0
	Aug	5615	0	0	0	0	0
	Sep	1008	5	0	0	0	0
	Oct	3275	85	60	31	19	12
	Nov	2356	53	77	30	22	11
	Dec	88	2	4	9	5	1
2014	**Jan**	68	0	0	0	0	0
	Feb	919	152	192	198	180	43
	Mar	28561	480	335	198	128	170
	Apr	73779	9435	10753	8576	7255	5123
	May	29284	6471	6772	6105	4938	1959
	Jun	1949	97	91	52	34	2
	Jul	5824	0	0	0	0	0
	Aug	8706	0	0	0	0	0
	Sep	11533	196	142	96	0	0
	Oct	16646	15	9	15	40	7
	Nov	1725	11	24	10	51	7
	Dec	102	0	0	1	1	1
2015	**Jan**	29	0	2	2	0	0
	Feb	1595	551	590	526	460	371
	Mar	17758	4056	3303	2869	2345	2192
	Apr	38064	2731	1260	984	1138	366
	May	21996	3862	3665	3137	2038	736
	Jun	2297	46	62	37	13	0
	Jul	8152	0	0	0	0	0
	Aug	9366	1	0	0	0	0
	Sep	11467	0	1	0	0	0
	Oct	10299	76	62	40	20	9
	Nov	3006	1	2	2	2	2
	Dec	87	1	1	1	1	0

Bibliography

Akagi, S., Yokelson, R.J., Wiedinmyer, C., Alvarado, M., Reid, J., Karl, T., Crounse, J., & Wennberg, P. (2011). Emission factors for open and domestic biomass burning for use in atmospheric models. Atmospheric Chemistry and Physics, 11, 4039-4072

AMAP. (2015). AMAP Assessment 2015: Black carbon and ozone as Arctic climate forcers. Arctic Monitoring and Assessment Programme (AMAP). Oslo, Norway, vii + 116

Allaby, M. (2015). The Gardener's Guide to Weather and Climate: How to Understand the Weather and Make It Work for You. Timber Press, 1-336

Amstrup, S.C., DeWeaver, E.T., Douglas, D.C., Marcot, B.G., Durner, G.M., Bitz, C.M., & Bailey, D.A. (2010). Greenhouse gas mitigation can reduce sea-ice loss and increase polar bear persistence. Nature, 468, 955-958

Andreae, M.O., & Merlet, P. (2001). Emission of trace gases and aerosols from biomass burning. Global biogeochemical cycles, 15, 955-966

Arctic Council. (2017). http://www.arctic-council.org/index.php/en/about-us. Last accessed 3/11/2017

Ardyna, M., Babin, M., Gosselin, M., Devred, E., Rainville, L., & Tremblay, J.-É. (2014). Recent Arctic Ocean sea ice loss triggers novel fall phytoplankton blooms. Geophysical Research Letters, 41, 6207-6212

Arnold, S., Law, K., Thomas, J., Starckweather, S., von Salzen, K., Stohl, A., Sharma, S., Lund, M., Flanner, M., & Petäjä, T. (2016). Arctic air pollution. Elementa: Science of the Anthropocene, 1-17

Barnes, E.A., Slingo, J., & Woollings, T. (2012). A methodology for the comparison of blocking climatologies across indices, models and climate scenarios. Climate Dynamics, 38, 2467-2481

Barnes, E. A., & Screen, J. A. (2015). The impact of Arctic warming on the midlatitude jet-stream: Can it? Has it? Will it?. Wiley Interdisciplinary Reviews: Climate Change, 6(3), 277-286

Barrie, L.A. (1986). Arctic air pollution: an overview of current knowledge. Atmospheric Environment (1967), 20, 643-663

Barriopedro, D., García-Herrera, R., Lupo, A.R., & Hernández, E. (2006). A Climatology of Northern Hemisphere Blocking. Journal of Climate, 19, 1042-1063

Berrisford, P., Dee, D., Poli, P., Brugge, R., Fielding, K., Fuentes, M., Kallberg, P., Kobayashi, S., Uppala, S., & Simmons, A. (2011). The ERA-Interim archive Version 2.0, ERA Report Series 1, ECMWF, Shinfield Park. Reading, UK, 13177

Bjerknes, J., & Solberg, H. (1922). Life cycle of cyclones and the polar front theory of atmospheric circulation: Grondahl, 3-18

Bond, T.C., Doherty, S.J., Fahey, D.W., Forster, P.M., Berntsen, T., DeAngelo, B.J., Flanner, M.G., Ghan, S., Karcher, B., Koch, D., Kinne, S., Kondo, Y., Quinn, P.K., Sarofim, M.C., Schultz, M.G., Schulz, M., Venkataraman, C., Zhang, H., Zhang, S., Bellouin, N., Guttikunda, S.K., Hopke, P.K., Jacobson, M.Z., Kaiser, J.W., Klimont, Z., Lohmann, U., Schwarz, J.P., Shindell, D., Storelvmo, T., Warren, S.G., & Zender, C.S. (2013). Bounding the role of black carbon in the climate system: A scientific assessment. Journal of Geophysical Research-Atmospheres, 118, 5380-5552. doi: 10.1002/jgrd.50171

Bondur, V.G. (2011). Satellite monitoring of wildfires during the anomalous heat wave of 2010 in Russia. Izvestiya Atmospheric and Oceanic Physics, 47, 1039-1048

Cape, J.N., Coyle, M., & Dumitrean, P. (2012). The atmospheric lifetime of black carbon. Atmospheric Environment, 59, 256-263

Carroll, M.L., Townshend, J.R., DiMiceli, C.M., Noojipady, P., & Sohlberg, R.A. (2009). A new global raster water mask at 250 m resolution. International Journal of Digital Earth, 2, 291-308. doi: 10.1080/17538940902951401

Cheng, M.-D. (2014). Geolocating Russian sources for Arctic black carbon. Atmospheric Environment, 92, 398-410

Chuvieco, E., Opazo, S., Sione, W., Valle, H. D., Anaya, J., Bella, C. D., Cruz, I., Manzo, L., López, G., Mari, N., & González-Alonso, F. (2008). Global burned-land estimation in Latin America using MODIS composite data. Ecological Applications, 18(1), 64-79

Cohen, J., Screen, J.A., Furtado, J.C., Barlow, M., Whittleston, D., Coumou, D., Francis, J., Dethloff, K., Entekhabi, D., Overland, J. and Jones, J. (2014). Recent Arctic amplification and extreme mid-latitude weather. Nature Geoscience, 7(9), 627-637

Cooke, W., Liousse, C., Cachier, H., & Feichter, J. (1999). Construction of a 1× 1 fossil fuel emission data set for carbonaceous aerosol and implementation and radiative impact in the ECHAM4 model. Journal of Geophysical Research: Atmospheres, 104, 22137-22162

Diao, Y., Li, J., & Luo, D. (2006). A New Blocking Index and Its Application: Blocking Action in the Northern Hemisphere. Journal of Climate, 19, 4819-4839

Doherty, S.J., Steele, M., Rigor, I., & Warren, S.G. (2015). Interannual variations of light-absorbing particles in snow on Arctic sea ice. Journal of Geophysical Research: Atmospheres, 120, 11, 391-311

Dole, R., Hoerling, M., Perlwitz, J., Eischeid, J., Pegion, P., Zhang, T., Quan, X.W., Xu, T.Y., & Murray, D. (2011). Was there a basis for anticipating the 2010 Russian heat wave? Geophysical Research Letters, 38, 6

Elmquist, M., Semiletov, I., Guo, L., & Gustafsson, Ö. (2008). Pan-Arctic patterns in black carbon sources and fluvial discharges deduced from radiocarbon and PAH source apportionment markers in estuarine surface sediments. Global biogeochemical cycles, 22, 2, 1-13

EPA, US Environmental Protection Agency's Agricultural Center. (2012). Agricultural Burning. http://www.epa.gov/agriculture/tburn.html. Last accessed 8/22/2015

EPA, US Environmental Protection Agency. (2016). Methane and Black Carbon Impacts on the Arctic: Communicating the Science

EPA, US Environmental Protection Agency. (2017). https://www.epa.gov/air-research/black-carbon-research. Last accessed 3/11/2017

Evangeliou, N., Balkanski, Y., Hao, W., Petkov, A., Silverstein, R.P., Corley, R., Nordgren, B.L., Urbanski, S.P., Eckhardt, S., & Stohl, A. (2016). Wildfires in northern Eurasia affect the budget of black carbon in the Arctic–a 12-year retrospective synopsis (2002–2013). Atmospheric Chemistry and Physics, 16, 7587-7604

Fang, Z., Yang, W., Chen, M., Zheng, M., & Hu, W. (2016). Abundance and sinking of particulate black carbon in the western Arctic and Subarctic Oceans. Scientific Reports, 6, 1-11

FAOSTAT. (2015). http://faostat3.fao.org/browse/E/EL/E. Last accessed 8/22/2015

FAOSTAT. (2015b). http://faostat3.fao.org/browse/T/TP/E. Last accessed 8/22/2015

Francis, J. A., & Vavrus, S. J. (2012). Evidence linking Arctic amplification to extreme weather in mid-latitudes. Geophysical Research Letters, 39, 6, 1-6

Foley, J.A., DeFries, R., Asner, G.P., Barford, C., Bonan, G., Carpenter, S.R., Chapin, F.S., Coe, M.T., Daily, G.C., Gibbs, H.K., Helkowski, J.H., Holloway, T., Howard, E.A., Kucharik, C.J., Monfreda, C., Patz, J.A., Prentice, I.C., Ramankutty, N., & Snyder, P.K. (2005). Global consequences of land use. Science, 309, 570-574. doi: 10.1126/science.1111772

Friedl, M.A., Sulla-Menashe, D., Tan, B., Schneider, A., Ramankutty, N., Sibley, A., & Huang, X. (2010). MODIS Collection 5 global land cover: Algorithm refinements and characterization of new datasets. Remote Sensing of Environment, 114, 168-182

Galvao, L.S., Roberts, D.A., Formaggio, A.R., Numata, I., & Breunig, F.M. (2009). View angle effects on the discrimination of soybean varieties and on the relationships between vegetation indices and yield using off-nadir Hyperion data. Remote Sensing of Environment, 113, 846-856. doi: 10.1016/j.rse.2008.12.010

Gao, B. C. (1996). NDWI—A normalized difference water index for remote sensing of vegetation liquid water from space. Remote sensing of environment, 58(3), 257-266

Giglio, L., Descloitres, J., Justice, C.O., & Kaufman, Y.J. (2003). An enhanced contextual fire detection algorithm for MODIS. Remote Sensing of Environment, 87, 273-282

Giglio, L., Loboda, T., Roy, D.P., Quayle, B., & Justice, C.O. (2009). An active-fire based burned area mapping algorithm for the MODIS sensor. Remote Sensing of Environment, 113, 408-420. doi: 10.1016/j.rse.2008.10.006

Giglio, L., Randerson, J.T., & van der Werf, G.R. (2013). Analysis of daily, monthly, and annual burned area using the fourth-generation global fire emissions database (GFED4). Journal of Geophysical Research: Biogeosciences, 118, 317-328

Gillett, N.P., Stone, D.A., Stott, P.A., Nozawa, T., Karpechko, A.Y., Hegerl, G.C., Wehner, M.F., & Jones, P.D. (2008). Attribution of polar warming to human influence. Nature Geoscience, 1, 750-754

Giovanni. (2013). Giovanni, Interactive Visualization and Analysis. GES DISC: Goddard Earth Sciences, Data and Information Services Center. http://disc.sci.gsfc.nasa.gov/giovanni. Last accessed, 10th February 2014

Groisman, P.Y., Sherstyukov, B.G., Razuvaev, V.N., Knight, R.W., Enloe, J.G., Stroumentova, N.S., Whitfield, P.H., Førland, E., Hannsen-Bauer, I., Tuomenvirta, H., Aleksandersson, H., Mescherskaya, A.V., & Karl, T.R. (2007). Potential forest fire danger over Northern Eurasia: Changes during the 20th century. Global and Planetary Change, 56, 371-386

Grumm, R.H. (2011). The Central European and Russian Heat Event of July-August 2010. Bulletin of the American Meteorological Society, 92, 1285-1296

Grunwald, S. (2015). Mollisols. University of Florida, Soil and Water Science Department. https://soils.ifas.ufl.edu/faculty/grunwald/teaching/eSoilScience/mollisols.shtml. Last accessed 8/22/2015

Guha-Sapir, D. 2010. Disaster Numbers – Presentation. EM-DAT: The International Disaster Database, Centre for Research on the Epidemiology of Disasters – CRED, http://cred.be/sites/default/files/Disaster_numbers_presentation_2010.pdf, last accessed February 6th, 2014

Hall, D., Salomonson, V., & Riggs, G. (2016). MODIS/Terra snow cover daily L3 global 0.05 Deg CMG, version 6. National Snow and Ice Data Center, Boulder, CO, digital media

Hall, J.V., Loboda, T.V., Giglio, L., & McCarty, G.W. (2016). A MODIS-based burned area assessment for Russian croplands: Mapping requirements and challenges. Remote Sensing of Environment, 184, 506-521

Hamman, S.T., Burke, I.C., & Stromberger, M.E. (2007). Relationships between microbial community structure and soil environmental conditions in a recently burned system. Soil Biology and Biochemistry, 39, 1703-1711

Hansen, J., & Nazarenko, L. (2004). Soot climate forcing via snow and ice albedos. Proceedings of the National Academy of Sciences of the United States of America, 101, 423-428. doi: 10.1073/pnas.2237157100

Hao, W.M., Petkov, A., Nordgren, B.L., Corley, R.E., Silverstein, R.P., Urbanski, S.P., Evangeliou, N., Balkanski, Y., & Kinder, B.L. (2016). Daily black carbon emissions from fires in northern Eurasia for 2002-2015. Geoscientific Model Development, 9, 4461-4474

Hare, F.K. (1968). The Arctic. Quarterly Journal of the Royal Meteorological Society, 94, 439-459

Hayasaka, H., Tanaka, H.L., & Bieniek, P.A. (2016). Synoptic-scale fire weather conditions in Alaska. Polar Science, 10, 217-226

Hegg, D.A., Warren, S.G., Grenfell, T.C., Doherty, S.J., Larson, T.V., & Clarke, A.D. (2009). Source Attribution of Black Carbon in Arctic Snow. Environmental Science & Technology, 43, 4016-4021. doi: 10.1021/es803623f

Hirdman, D., Sodemann, H., Eckhardt, S., Burkhart, J.F., Jefferson, A., Mefford, T., Quinn, P.K., Sharma, S., Ström, J., & Stohl, A. (2010). Source identification of short-lived air pollutants in the Arctic using statistical analysis of measurement data and particle dispersion model output. Atmos. Chem. Phys, 10, 669-693

Huang, L., Gong, S., Sharma, S., Lavoué, D., & Jia, C. (2010). A trajectory analysis of atmospheric transport of black carbon aerosols to Canadian high Arctic in winter and spring (1990–2005). Atmospheric Chemistry and Physics, 10, 5065-5073

Hubanks, PA, et al. (2008). MODIS Atmospheric L3 Gridded Product Algorithm Theoretical Basis Document. ATBD Reference Number: ATBD-MOD-30. http://modis-atmos.gsfc.nasa.gov/_docs/L3_ATBD_2008_12_04.pdf

Ichoku, C., & Kaufman, Y.J. (2005). A method to derive smoke emission rates from MODIS fire radiative energy measurements. Ieee Transactions on Geoscience and Remote Sensing, 43, 2636-2649

Iversen, T., & Joranger, E. (1985). Arctic air pollution and large scale atmospheric flows. Atmospheric Environment (1967), 19, 2099-2108

Jacobson, M.Z. (2001). Strong radiative heating due to the mixing state of black carbon in atmospheric aerosols. Nature, 409, 695-697

Jacobson, M.Z. (2004). The short-term cooling but long-term global warming due to biomass burning. Journal of Climate, 17, 2909-2926

Jacobson, M.Z., Bond, T.C., Ramanathan, V., Zender, C., and Schwartz, J. (2007). Hearing examines Black Carbon and Global Warming, House Committee on Oversight and Government Reform Testimony, http://tinyurl.com/yz2jesv. Last accessed 8/22/2015

Johnson, E.A., & Wowchuk, D. (1993). Wildfires in the southern Canadian Rocky Mountains and their relationship to mid-tropospheric anomalies. Canadian Journal of Forest Research, 23, 1213-1222

Jurado, E., Dachs, J., Duarte, C.M., & Simó, R. (2008). Atmospheric deposition of organic and black carbon to the global oceans. Atmospheric Environment, 42, 7931-7939

Kalnay, E., Kanamitsu, M., Kistler, R., Collins, W., Deaven, D., Gandin, L., Iredell, M., Saha, S., White, G., Woollen, J., Zhu, Y., Chelliah, M., Ebisuzaki, W., Higgins, W., Janowiak, J., Mo, K.C., Ropelewski, C., Wang, J., Leetmaa, A., Reynolds, R., Jenne, R., & Joseph, D. (1996). The NCEP/NCAR 40-year reanalysis project. Bulletin of the American Meteorological Society, 77, 437-471

Key, C. H., & Benson, N. C. (1999). Measuring and remote sensing of burn severity. In Proceedings joint fire science conference and workshop (Vol. 2, p. 284)

Klonecki, A., Hess, P., Emmons, L., Smith, L., Orlando, J., & Blake, D. (2003). Seasonal changes in the transport of pollutants into the Arctic troposphere-model study. Journal of Geophysical Research: Atmospheres, 108, 1-21

Kramer, A.E. (2010). Drought in Russia ripples beyond the wheat fields. The New York Times: Global Business. Last accessed 08/26/2015

Koch, D., & Hansen, J. (2005). Distant origins of Arctic black carbon: A Goddard Institute for Space Studies ModelE experiment. Journal of Geophysical Research-Atmospheres, 110, 1-14. doi: 10.1029/2004jd005296

Korontzi, S., McCarty, J., & Justice, C. (2008). Monitoring agricultural burning in the Mississippi River Valley Region from the moderate resolution imaging spectroradiometer (MODIS). Journal of the Air & Waste Management Association, 58(9), 1235-1239

Korontzi, S., McCarty J., Loboda, T., Kumar, S., & Justice, C. (2006). Global distribution of agricultural fires in croplands from 3 years of Moderate Resolution Imaging Spectroradiometer (MODIS) data. Global Biogeochem. Cycles, 20, GB2021, 1-15. doi:10.1029/2005GB002529

Laliberté, F., Howell, S.E.L., & Kushner, P.J. (2016). Regional variability of a projected sea ice-free Arctic during the summer months. Geophysical Research Letters, 43, 256-263

Larkin, N.K., DeWinter, J.L., Strand, T.M., Brown, S.G., Brown, S.M., Raffuse, S.M., Callahan, J., Craig, K.J., Solomon, R.C., & Hafner, H.R. (2012). Identification of Necessary Conditions for Arctic Transport of Smoke from United States Fires. JFSP Research Project Reports. Paper 93.

Law, K.S., & Stohl, A. (2007). Arctic air pollution: Origins and impacts. Science, 315, 1537-1540. doi: 10.1126/science.1137695

Lebedeva, M.G., Krymskaya, O.V., Lupo, A.R., Chendev, Y.G., Petin, A.N., & Solovyov, A.B. (2015). Trends in summer season climate for Eastern Europe and Southern Russia in the Early 21st Century. Advances in Meteorology, 2016, 1-10

Lejenäs, H., & Økland, H. (1983). Characteristics of Northern Hemisphere blocking as determined from a long time series of observational data. Tellus A: Dynamic Meteorology and Oceanography, 35, 350-362

Lenton, T.M. (2012). Arctic Climate Tipping Points. Ambio, 41, 10-22

Lin, H.W., Jin, Y.F., Giglio, L., Foley, J.A., & Randerson, J.T. (2012). Evaluating greenhouse gas emissions inventories for agricultural burning using satellite observations of active fires. Ecological Applications, 22, 1345-1364

Lindsay, R., & Zhang, J. (2005). The thinning of Arctic sea ice, 1988–2003: Have we passed a tipping point? Journal of Climate, 18, 4879-4894

Liu, D., Quennehen, B., Darbyshire, E., Allan, J.D., Williams, P.I., Taylor, J.W., Bauguitte, S.-B., Flynn, M.J., Lowe, D., & Gallagher, M. (2015). The importance of

Asia as a source of black carbon to the European Arctic during springtime 2013. Atmospheric Chemistry and Physics, 15, 11537-11555

Liu, J., Curry, J.A., Wang, H., Song, M., & Horton, R.M. (2012). Impact of declining Arctic sea ice on winter snowfall. Proceedings of the National Academy of Sciences, 109, 4074-4079

Loboda, T., O'Neal, K.J., & Csiszar, I. (2007). Regionally adaptable dNBR-based algorithm for burned area mapping from MODIS data. Remote Sensing of Environment, 109, 429-442

Loboda, T.V., Hoy, E.E., Giglio, L., & Kasischke, E.S. (2011). Mapping burned area in Alaska using MODIS data: a data limitations-driven modification to the regional burned area algorithm. International Journal of Wildland Fire, 20, 487-496. doi: 10.1071/wf10017

Lupo, A.R., Clark, J.V., Hendin, A., Kelly, A., Mihalka, K., Perrin, B., Puricelli, K., & Kelley, A. (2008). The global increase in blocking occurrences. In, Proceedings of the 20th Conference on Global Climate Change: American Meteorological Society. 19-24

Lupo, A.R., & Smith, P.J. (1995). Climatological features of blocking anticyclones in the Northern Hemisphere. Tellus A, 47, 439-456

Mari, X., Lefèvre, J., Torréton, J.P., Bettarel, Y., Pringault, O., Rochelle-Newall, E., Marchesiello, P., Menkes, C., Rodier, M., & Migon, C. (2014). Effects of soot deposition on particle dynamics and microbial processes in marine surface waters. Global biogeochemical cycles, 28, 662-678

Martin, M.V., Logan, J.A., Kahn, R.A., Leung, F.-Y., Nelson, D.L., & Diner, D.J. (2010). Smoke injection heights from fires in North America: analysis of 5 years of satellite observations. Atmos. Chem. Phys, 10, 1491-1510

McCarty, J.L., Ellicott, E.A., Romanenkov, V., Rukhovitch, D., & Koroleva, P. (2012). Multi-year black carbon emissions from cropland burning in the Russian Federation. Atmospheric Environment, 63, 223-238. doi: 10.1016/j.atmosenv.2012.08.053

McCarty, J.L., Korontzi, S., Justice, C.O., & Loboda, T. (2009). The spatial and temporal distribution of crop residue burning in the contiguous United States. Science of the Total Environment, 407, 5701-5712. doi: 10.1016/j.scitotenv.2009.07.009

McCarty, J.L., Loboda, T., & Trigg, S. (2008). A hybrid remote sensing approach to quantifying crop residue burning in the United States. Applied Engineering in Agriculture, 24, 515-527

McNairn, H., Shang, J., Champagne, C., & Jiao, X. (2009, July). TerraSAR-X and RADARSAT-2 for crop classification and acreage estimation. In Geoscience and Remote Sensing Symposium, 2009 IEEE International, IGARSS 2009 (Vol. 2, pp. II-898). IEEE.

Meyfroidt, P., Schierhorn, F., Prishchepov, A.V., Müller, D., & Kuemmerle, T. (2016). Drivers, constraints and trade-offs associated with recultivating abandoned cropland in Russia, Ukraine and Kazakhstan. Global Environmental Change, 37, 1-15

Monks, S., Arnold, S., Emmons, L., Law, K.S., Turquety, S., Duncan, B., Flemming, J., Huijnen, V., Tilmes, S., & Langner, J. (2015). Multi-model study of chemical and physical controls on transport of anthropogenic and biomass burning pollution to the Arctic. Atmospheric Chemistry and Physics, 15, 3575-3603

Najafi, M.R., Zwiers, F.W., & Gillett, N.P. (2015). Attribution of Arctic temperature change to greenhouse-gas and aerosol influences. Nature Climate Change, 5, 246-249

Nakamura, H., Nakamura, M., & Anderson, J.L. (1997). The role of high-and low-frequency dynamics in blocking formation. Monthly Weather Review, 125, 2074-2093

NASA, Arctic Boreal Vulnerability Experiment. (2017). http://above.nasa.gov/about.html?#about. Last accessed 3/11/2017

NOAA. 2005. http://www.cpc.ncep.noaa.gov. Last accessed 02/06/2014

NOAA. (2017). Arctic Report Card. http://arctic.noaa.gov/Report-Card. Last accessed 3/12/17

NSIDC. (2017). https://nsidc.org/cryosphere/arctic-meteorology/index.html. Last accessed 3/11/2017

NSDIC. (2017b). http://nsidc.org/cryosphere/seaice/index.html. Last accessed 3/11/2017

Overland, J.E., & Wang, M. (2013). When will the summer Arctic be nearly sea ice free? Geophysical Research Letters, 40, 2097-2101

Pelly, J.L., & Hoskins, B.J. (2003). A New Perspective on Blocking. Journal of the Atmospheric Sciences, 60, 743-755

Pettus, A. (2009). Agricultural Fires and Arctic Climate Change: A Special CATF Report. In: Clean Air Task Force, 1-33

Polychronaki, A., Gitas, I. Z., Veraverbeke, S., & Debien, A. (2013). Evaluation of ALOS PALSAR imagery for burned area mapping in Greece using object-based classification. Remote Sensing, 5(11), 5680-5701.

Qi, L., Li, Q., Li, Y., & He, C. (2017). Factors controlling black carbon distribution in the Arctic. Atmospheric Chemistry and Physics, 17, 1037-1059

Quinn, P.K., Bates, T.S., Baum, E., Doubleday, N., Fiore, A.M., Flanner, M., Fridlind, A., Garrett, T.J., Koch, D., Menon, S., Shindell, D., Stohl, A., & Warren, S.G. (2008). Short-lived pollutants in the Arctic: their climate impact and possible mitigation strategies. Atmospheric Chemistry and Physics, 8, 1723-1735. doi: 10.5194/acp-8-1723-2008

Quinn, P.K., Stohl, A., Arneth, A., Berntsen, T., Burkhart, J.F., Christensen, J., Flanner, M., Kupiainen, K., Lihavainen, H., Shepherd, M., Shevchenko, V., Skov, H., & Vestreng, V. (2011). The Impact of Black Carbon on Arctic Climate. AMAP Technical Report No. 4. Arctic Monitoring and Assessment Programme (AMAP), Oslo.

Raatz, W. E. (1989). An anticyclonic point of view on low-level tropospheric long-range transport. Atmospheric Environment (1967), 23(11), 2501-2504

Raatz, W.E., & Shaw, G.E. (1984). Long-Range Tropospheric Transport of Pollution Aerosols into the Alaskan Arctic. Journal of Climate and Applied Meteorology, 23, 1052-1064

Rahman, H., Quadir, D., Zahedul Islam, A., & Dutta, S. (1999). Viewing Angle Effect on the Remote Sensing Monitoring of Wheat and Rice Crops In, Geocarto International, 74-79

Ramanathan, V., & Carmichael, G. (2008). Global and regional climate changes due to black carbon. Nature Geoscience, 1, 221-227. doi: 10.1038/ngeo156

Ramankutty, N., Evan, A.T., Monfreda, C., & Foley, J.A. (2008). Farming the planet: 1. Geographic distribution of global agricultural lands in the year 2000. Global biogeochemical cycles, 22, 1-19

Randerson, J. T., Chen, Y., van derWerf, G.R., Rogers, B.M., & Morton, D.C. (2012). Global burned area and biomass burning emissions from small fires, J. Geophys. Res., 117, G04012, 1-23. doi:10.1029/2012JG002128

Ranson, K.J., Daughtry, C.S.T., Biehl, L.L., & Bauer, M.E. (1985). Sun-view angle effects on reflectance factors of corn canopies. Remote Sensing of Environment, 18, 147-161. doi: 10.1016/0034-4257(85)90045-8

Rex, D.F. (1950). Blocking action in the middle troposphere and its effect upon regional climate. Tellus, 2, 275-301

Ridley, J., Lowe, J., & Hewitt, H. (2012). How reversible is sea ice loss? The Cryosphere, 6, 193-198

Riggs, G.A., & Hall, D.K. (2015). MODIS Snow Products Collection 6 User Guide

Rouse Jr, J., Haas, R. H., Schell, J. A., & Deering, D. W. (1974). Monitoring vegetation systems in the Great Plains with ERTS. NASA special publication, 351, 309-317

Roy, D., Jin, Y., Lewis, P., & Justice, C. (2005). Prototyping a global algorithm for systematic fire-affected area mapping using MODIS time series data. Remote Sensing of Environment, 97, 137-162

Roy, D.P., Boschetti, L., Justice, C.O., & Ju, J. (2008). The collection 5 MODIS burned area product - Global evaluation by comparison with the MODIS active fire product. Remote Sensing of Environment, 112, 3690-3707. doi: 10.1016/j.rse.2008.05.013

Sahoo, R. (2013). Hyperspectral Remote Sensing. Indian Agricultural Statistics Research Institute, New Delhi 110 012. http://www.iasri.res.in/ebook/GIS_TA/M2_4_HYSRS.pdf. Last accessed 10/01/2015

Sato, M., Hansen, J., Koch, D., Lacis, A., Ruedy, R., Dubovik, O., ... & Novakov, T. (2003). Global atmospheric black carbon inferred from AERONET. Proceedings of the National Academy of Sciences, 100(11), 6319-6324.

Schaaf, C.B., Gao, F., Strahler, A.H., Lucht, W., Li, X.W., Tsang, T., Strugnell, N.C., Zhang, X.Y., Jin, Y.F., Muller, J.P., Lewis, P., Barnsley, M., Hobson, P., Disney, M., Roberts, G., Dunderdale, M., Doll, C., d'Entremont, R.P., Hu, B.X., Liang, S.L., Privette, J.L., & Roy, D. (2002). First operational BRDF, albedo nadir reflectance products from MODIS. Remote Sensing of Environment, 83, 135-148. doi: 10.1016/S0034-4257(02)00091-3

Scherrer, S.C., Croci-Maspoli, M., Schwierz, C., & Appenzeller, C. (2006). Two-dimensional indices of atmospheric blocking and their statistical relationship with winter climate patterns in the Euro-Atlantic region. International Journal of Climatology, 26, 233-250

Schierhorn, F., Müller, D., Prishchepov, A.V., Faramarzi, M., & Balmann, A. (2014). The potential of Russia to increase its wheat production through cropland expansion and intensification. Global Food Security, 3, 133-141

Schiffer, R., & Rossow, W.B. (1983). The International Satellite Cloud Climatology Project(ISCCP)- The first project of the World Climate Research Programme. American Meteorological Society, Bulletin, 64, 779-784

Schillinger, W.F., Young, D.L., Kennedy, A.C., & Paulitz, T.C. (2010). Diverse no-till irrigated crop rotations instead of burning and plowing continuous wheat. Field Crops Research, 115, 39-49

Screen, J.A., & Simmonds, I. (2010). The central role of diminishing sea ice in recent Arctic temperature amplification. Nature, 464, 1334-1337

Screen, J.A., & Simmonds, I. (2013). Exploring links between Arctic amplification and mid-latitude weather. Geophysical Research Letters, 40, 959-964

Seiler, W., & Crutzen, P.J. (1980). Estimates of gross and net fluxes of carbon between the biosphere and the atmosphere from biomass burning. Climatic Change, 2, 207-247

Shaposhnikov, D., Revich, B., Bellander, T., Bedada, G.B., Bottai, M., Kharkova, T., Kvasha, E., Lezina, E., Lind, T., & Semutnikova, E. (2014). Mortality related to air pollution with the Moscow heat wave and wildfire of 2010. Epidemiology, 25, 359-364

Sharma, S., Ishizawa, M., Chan, D., Lavoué, D., Andrews, E., Eleftheriadis, K., & Maksyutov, S. (2013). 16-year simulation of Arctic black carbon: Transport, source contribution, and sensitivity analysis on deposition. Journal of Geophysical Research: Atmospheres, 118, 943-964

Sharma, S., Lavoué, D., Cachier, H., Barrie, L., & Gong, S. (2004). Long-term trends of the black carbon concentrations in the Canadian Arctic. Journal of Geophysical Research: Atmospheres, 109, 1-10

Shindell, D.T., Chin, M., Dentener, F., Doherty, R.M., Faluvegi, G., Fiore, A.M., Hess, P., Koch, D.M., MacKenzie, I.A., Sanderson, M.G., & Schultz, M.G. (2008). A multi-model assessment of pollution transport to the Arctic. Atmospheric Chemistry and Physics, 8(17), 5353-5372

Shoyer, J., Peterson, D., Presely, D., DeWolf, E., & Whitworth, J. (2013). Pros and cons of burning wheat residue before planting. Kansas State University. http://www.agprofessional.com/resource-centers/wheat/disease/news/Pros-and-cons-of-burning-wheat-residue-before-planting-226956471.html. Last accessed 09/30/2015

Skinner, W., Stocks, B., Martell, D., Bonsal, B., & Shabbar, A. (1999). The association between circulation anomaliesin the mid-troposphere and area burnedby wildland fire in Canada. Theoretical and Applied Climatology, 63, 89-105

Soja, A.J., Fairlie, T.D., Westberg, M.D.J., & Pouliot, G. (2012). Biomass burning plume injection height using CALIOP, MODIS and the NASA Langley Trajectory Model. https://www3.epa.gov/ttn/chief/conference/ei20/session7/asoja.pdf, 1-17

Stubbins, A., Spencer, R.G., Mann, P.J., Holmes, R.M., McClelland, J.W., Niggemann, J., & Dittmar, T. (2015). Utilizing colored dissolved organic matter to derive dissolved black carbon export by arctic rivers. Frontiers in Earth Science, 3, 63, 1-11

Sovecon. (2013). Agricultural Burning Survey Report prepared for US Forest Service. Personal communication with Dr. Wei Min Hao – Missoula Fire Lab

Stein, A., Draxler, R., Rolph, G., Stunder, B., Cohen, M., & Ngan, F. (2015). NOAA's HYSPLIT atmospheric transport and dispersion modeling system. Bulletin of the American Meteorological Society, 96, 2059-2077

Stocker, T.F., Qin, D., Plattner, G.K., Alexander, L.V., Allen, S.K., Bindoff, N.L., Bréon, F.M., Church, J.A., Cubash, U., Emori, S., Forster, P., Friedlingstein, P., Gillett, N., Gregory, J.M., Hartmann, D.L., Jansen, E., Kirtman, B., Knutti, R., Krishna Kumar, K., Lemke, P., Marotzke, J., Masson-Delmotte, V., Meehl, G.A., Mokhov, I.I., Piao, S., Ramaswamy, V., Randall, D., Rhein, M., Rojas, M., Sabine, C., Shindell, D., Talley, L.D., Vaughan, D.G., & Xie, S.P. (2013). Technical Summary: The Physical Science Basis. Contribution of Working Group I to the Fifth Assessment Report of the Intergovernmental Panel on Climate Change. Cambridge University Press, Cambridge, United Kingdom and New York, NY, USA

Stohl, A. (2006). Characteristics of atmospheric transport into the Arctic troposphere. Journal of Geophysical Research-Atmospheres, 111, 1-17

Stohl, A., Andrews, E., Burkhart, J.F., Forster, C., Herber, A., Hoch, S.W., Kowal, D., Lunder, C., Mefford, T., Ogren, J.A., Sharma, S., Spichtinger, N., Stebel, K., Stone, R., Strom, J., Torseth, K., Wehrli, C., & Yttri, K.E. (2006). Pan-Arctic enhancements of light absorbing aerosol concentrations due to North American boreal forest fires during summer 2004. Journal of Geophysical Research-Atmospheres, 111, 1-20. doi: 10.1029/2006jd007216

Stohl, A., Berg, T., Burkhart, J.F., Fjaeraa, A.M., Forster, C., Herber, A., Hov, O., Lunder, C., McMillan, W.W., Oltmans, S., Shiobara, M., Simpson, D., Solberg, S., Stebel, K., Strom, J., Torseth, K., Treffeisen, R., Virkkunen, K., & Yttri, K.E. (2007). Arctic smoke - record high air pollution levels in the European Arctic due to agricultural fires in Eastern Europe in spring 2006. Atmospheric Chemistry and Physics, 7, 511-534

Stubbins, A., Spencer, R.G.M., Mann, P.J., Holmes, R.M., McClelland, J.W., Niggemann, J., & Dittmar, T. (2015). Utilizing colored dissolved organic matter to

derive dissolved black carbon export by arctic rivers. Frontiers in Earth Science, 3, 1-11

Swingedouw, D., Braconnot, P., & Marti, O. (2006). Sensitivity of the Atlantic Meridional Overturning Circulation to the melting from northern glaciers in climate change experiments. Geophysical Research Letters, 33, 1-4

Tibaldi, S., & Molteni, F. (1990). On the operational predictability of blocking. Tellus A, 42, 343-365

Treffeisen, R., Tunved, P., Ström, J., Herber, A., Bareiss, J., Helbig, A., Stone, R., Hoyningen-Huene, W., Krejci, R., & Stohl, A. (2007). Arctic smoke–aerosol characteristics during a record smoke event in the European Arctic and its radiative impact. Atmospheric Chemistry and Physics, 7, 3035-3053

Trigg, S., & Flasse, S. (2000). Characterizing the spectral-temporal response of burned savannah using in situ spectroradiometry and infrared thermometry. International Journal of Remote Sensing, 21(16), 3161-3168

Tsou, C. H., & Smith, P. J. (1990). The role of synoptic/planetary–scale interactions during the development of a blocking anticyclone. Tellus A, 42, 1, 174-193

Tyrlis, E., & Hoskins, B. (2015). Aspects of a Northern Hemisphere atmospheric blocking climatology. Journal of the Atmospheric Sciences, 72, 1638-1652

USDA FAS (Foreign Agricultural Service). 2012. Russian Wheat Prospects Continue to Deteriorate.
http://www.pecad.fas.usda.gov/highlights/2012/08/Russia_15aug2012/, last accessed February 4th 2014

USDA FAS (Foreign Agricultural Service). (2013). Russia: Agricultural Overview. Production Estimates and Crop Assessment Division.
http://www.fas.usda.gov/pecad2/highlights/2005/03/Russia_Ag/. Last accessed 02/06/2014

USDA FAS, (Foreign Agricultural Service). (2013b). Russian Federation Grain and Feed Update. Gain Report number RS1364.
http://www.thefarmsite.com/reports/contents/RussiaFeed1Oct2013.pdf. Last accessed 06/06/2014

USDA FAS, (Foreign Agricultural Service). (2016). Russian Federation Grain and Feed Annual. Gain Report number RS1617.
https://gain.fas.usda.gov/Recent%20GAIN%20Publications/Grain%20and%20Feed%20Annual_Moscow_Russian%20Federation_4-18-2016.pdf. Last accessed 03/11/2017

Vargin, P.N., Luk'yanov, A.N., & Gan'shin, A.V. (2012). Investigation of dynamic processes in the period of formation and development of the blocking anticyclone over European Russia in summer 2010. Izvestiya Atmospheric and Oceanic Physics, 48, 476-495

Vermote, E.F., Kotchenova, S.Y., & Ray, J.P. (2011). MODIS Surface Reflectance (MOD/MYD09) User's Guide. Version 1.3. http://modis-sr.ltdri.org/guide/MOD09_UserGuide_v1_3.pdf. Last accessed 8/26/2015

Wang, M., & Overland, J.E. (2012). A sea ice free summer Arctic within 30 years: An update from CMIP5 models. Geophysical Research Letters, 39, 1-6

Warneke, C., Froyd, K.D., Brioude, J., Bahreini, R., Brock, C.A., Cozic, J., de Gouw, J.A., Fahey, D.W., Ferrare, R., Holloway, J.S., Middlebrook, A.M., Miller, L., Montzka, S., Schwarz, J.P., Sodemann, H., Spackman, J.R., & Stohl, A. (2010). An important contribution to springtime Arctic aerosol from biomass burning in Russia. Geophysical Research Letters, 37, 1-5. doi: L01801 10.1029/2009gl041816

Wiedenmann, J.M., Lupo, A.R., Mokhov, I.I., & Tikhonova, E.A. (2002). The Climatology of Blocking Anticyclones for the Northern and Southern Hemispheres: Block Intensity as a Diagnostic. Journal of Climate, 15, 3459-3473

Wiedinmyer, C., Akagi, S., Yokelson, R.J., Emmons, L., Al-Saadi, J., Orlando, J., & Soja, A. (2011). The Fire INventory from NCAR (FINN): a high resolution global model to estimate the emissions from open burning. Geoscientific Model Development, 4, 625-241

Winton, M. (2006). Does the Arctic sea ice have a tipping point? Geophysical Research Letters, 33, 1-5

Witham, C., & Manning, A. (2007). Impacts of Russian biomass burning on UK air quality. Atmospheric Environment, 41, 8075-8090. doi: 10.1016/j.atinosenv.2007.06.058

Witte, J., Douglass, A., Silva, A.d., Torres, O., Levy, R., & Duncan, B. (2011). NASA A-Train and Terra observations of the 2010 Russian wildfires. Atmospheric Chemistry and Physics, 11, 9287-9301

Wu, M., Knorr, W., Thonicke, K., Schurgers, G., Camia, A., & Arneth., A. (2015). Sensitivity of burned area in Europe to climate change, atmospheric CO2 levels, and demography: A comparison of two fire-vegetation models, J. Geophys. Res. Biogeosci., 120, 2256–2272, doi:10.1002/2015JG003036

Wu, Y., Ting, M., Seager, R., Huang, H. P., & Cane, M. A. (2011). Changes in storm tracks and energy transports in a warmer climate simulated by the GFDL CM2. 1 model. Climate dynamics, 37(1-2), 53-72

Yan, L., Roy, D.P., Zhang, H., Li, J., & Huang, H. (2016). An automated approach for sub-pixel registration of Landsat-8 Operational Land Imager (OLI) and Sentinel-2 Multi Spectral Instrument (MSI) imagery. Remote Sensing, 8, 520, 1-23

Yttri, K.E., Lund Myhre, C., Eckhardt, S., Fiebig, M., Dye, C., Hirdman, D., Ström, J., Klimont, Z., & Stohl, A. (2014). Quantifying black carbon from biomass burning by means of levoglucosan–a one-year time series at the Arctic observatory Zeppelin. Atmospheric Chemistry and Physics, 14, 6427-6442

Zender, C. S. (2007). Arctic climate effects of black carbon. http://dust.ess.uci.edu/ppr/ppr_hogrc_wrt.pdf. Last accessed 02/27/2016

Zhang, Y.H., Wooster, M.J., Tutubalina, O., & Perry, G.L.W. (2003). Monthly burned area and forest fire carbon emission estimates for the Russian Federation from SPOT VGT. Remote Sensing of Environment, 87, 1-15. doi: 10.1016/s0034-4257(03)00141-x